January 2015

Artificial Magnetic Conductor Integrated Textile Monopole Antenna

Ala Alemaryeen

ARTIFICIAL MAGNETIC CONDUCTOR INTEGRATED TEXTILE MONOPOLE ANTENNA

by

Ala Ali Alemaryeen
Bachelor of Electrical Engineering, Mutah University, 2012

A Thesis
Submitted to the Graduate Faculty

of the

University of North Dakota

In partial fulfillment of the requirements

for the degree of

Master of Science

Grand Forks, North Dakota
May
2015

This thesis, submitted by Ala Alemaryeen in partial fulfillment of the requirements for the Degree of Master of Science from the University of North Dakota, has been read by the Faculty Advisory Committee under whom the work has been done, and is hereby approved.

Sima Noghanian

Reza Fazel-Rezai

Isacc Chang

This thesis is being submitted by the appointed advisory committee as having met all of the requirements of the Graduate School at the University of North Dakota and is hereby approved.

Wayne Swisher
Dean of the Graduate School

Date

PERMISSION

Title Artificial Magnetic Conductor Integrated Textile Monopole Antenna

Department Electrical Engineering

Degree Master of Science

In presenting this thesis in partial fulfillment of the requirements for a graduate degree from the University of North Dakota, I agree that the library of this University shall make it freely available for inspection. I further agree that permission for extensive copying for scholarly purposes may be granted by the professor who supervised my thesis work or, in her absence, by the Chairperson of the department or the dean of the Graduate School. It is understood that any copying or publication or other use of this thesis or part thereof for financial gain shall not be allowed without my written permission. It is also understood that due recognition shall be given to me and to the University of North Dakota in any scholarly use which may be made of any material in my thesis.

Ala Alemaryeen
DATE: May 2015

TABLE OF CONTENTS

LIST OF FIGURES

LIST OF TABLES

ABBREVIATIONS

ISM	Industrial Scientific and Medical
HIS	High Impedance Surface
CPW	Coplanar Waveguide
SAR	Specific Absorption Rate
FBR	Front to Back Ratio
AMC	Artificial Magnetic Conductor
PEC	Perfect Electric Conductor
PMC	Perfect Magnetic Conductor
CP	Circularly Polarized
AR	Axial Ratio
EBG	Electromagnetic Band Gap
PBG	Photonic Band Gap
UWB	Ultra Wide Band
1D	One Dimensional
2D	Two Dimensional
3D	Three Dimensional
UC-HIS	Uniplanar Compact-High Impedance Surface
DTV	Digital TeleVision
UHF	Ultra High Frequency
FSS	Frequency Selective Surface
PIFA	Planar Inverted-F Antenna
MIMO	Multiple Input Multiple Output
WLAN	Wireless Local Area Network
GPS	Global Positioning System
PCB	Printed Circuit Board
ICNIRP	International Commission on Non-Ionizing Radiation Protection
GSM	Global System of Mobile
MBAN	Medical Body Area Network
EVA	Extra Vehicular Activity
WBAN	Wireless Body Area Network
PBC	Periodic Boundary Condition

ACKNOWLEDGEMENTS

I wish to express my sincere appreciation for many individuals who have helped to complete the research and edit this thesis. First, I would like to thank my advisor, Professor Sima Noghanian and the members of my advisory committee, Professor Reza Fazel-Rezai and Professor Isaac Chang, for their guidance and support during the course of this study. Also, I would like to thank Tyler Przybylski, Milad Mirzaee, Patrick Froehle, and Tahmid Rashid for their help in fabrication.

Additionally, I would like to express my appreciation to North Dakota Experiment Program to Stimulate Competitive Research (ND NASA EPSCoR), and University of North Dakota for the financial support of this project.

Lastly, I would like to thank my family and friends for their love and support.

To my parents,

Ali and Najah Alemaryeen

and my brother

Khalid Alemaryeen

ABSTRACT

Wearable antenna is a fast growing field in application-oriented research, which introduced a new generation of garments capable of monitoring wear health as well as environmental states. This thesis is concerned with the design and fabrication of a compact textile wearable antenna at operating frequency within the Industrial, Scientific and Medical (ISM) band, intended for integration into a flight jacket of the astronaut inside the habitat. The antenna is integrated with artificial material known as High Impedance Surface (HIS) for performance enhancement. The purpose of the system is to constantly monitor vital signals of the astronauts.

The entire design cycle of wearable Co-Planar Waveguide (CPW) fed monopole antenna, starting from simulation-based design to fabricated prototype and antenna testing under different conditions was carried out in this thesis. Because of the lossy nature of human body tissues, the radiation efficiency of the antenna will be reduced due to the absorption of the radiated energy. Hence, changes in the radiation characteristics of the wearable antenna like operating frequency, gain and impedance bandwidth will take place. To overcome these challenges, HIS has been suggested and integrated with the monopole antenna to isolate the antenna from the ambient environments. This wearable antenna was tested under real operating conditions such as bending and crumpling conditions.

Moreover, as the antenna operates near human body tissues, Specific Absorption Rate (SAR) assessment is required to consider the safety concerns of the antenna system. SAR analysis based on simulation results has been carried out in this thesis to show a significant reduction in SAR with the usage of HIS in the antenna system.

CHAPTER 1

INTRODUCTION

A growing interest in the field of on body centric wireless communication has been noticed in the recent years, specially with the advent of wearable communication technology. In general, the wearable antenna is considered as a crucial component in the body centric wireless communication systems, which should satisfy the wide criteria of causing a minimum efficiency degradation when integrated onto human body. The key part of this thesis is to design a textile wearable antenna integrated on HIS for future applications in space suits. In the following section, the motivations behind the research work in this thesis will be highlighted.

1.1 Motivation

In general, there is an increasing need for integrating antennas into clothing for wireless body centric communications for user convenience. Therefore, antenna with properties, such as being light-weight and low-profile characteristics, while they can be easily worn and conformed to the body are necessary in wearable antenna design. Also, with the ever growing miniaturization of electronic devices in electronic industry, many challenges are imposed on antenna designers to come up with compact antennas occupying small physical spaces. Hence, there is a significant progress in mobile, portable and wearable antennas. Conventional antennas based on rigid materials are not suitable for

wearable applications. Extensive research has been carried out on the usage of several fabric types as dielectric and conductive materials [1-3] in the antenna design, which is a preferred solution as the textile materials meet the requirements of wearable antenna.

In wearable antenna applications, it is necessary to consider the interaction between the human body and the antenna. Human body is lossy, dispersive material, and possesses high dielectric constant ($\varepsilon_r \approx 35$). Consequently, large amount of the radiated electromagnetic power from the antenna is absorbed by the human body, which may cause unwanted, adverse biological effects. Also, the gain of the antenna significantly decreases and frequency detuning occurs when the antenna operates close to the human body, which results in a deterioration of the communication range of the radio system [4]. Therefore, there is a need for methods to isolate the antenna from the human body.

Integrating periodic structures known as High Impedance Surfaces (HISs) with wearable antennas not only the physical characteristics, such as low profile and compact in size will be achieved but also the radiation characteristics of the antennas can be greatly enhanced in terms of impedance bandwidth, radiation pattern, gain, and Front to Back Ratio (FBR) [5-8].

Effects of the HIS on the resonance frequency, matching properties, impedance bandwidth, antenna gain, and Front to Back Ratio (FBR) of a Coplanar Waveguide (CPW) fed monopole antenna are of interest. Mainly, this thesis focuses on antenna gain enhancement. Moreover, for on body environment it is difficult to keep the antenna in a flat condition spatially for textile antenna. Antenna bending and crumpling effects on the

wearable antenna have been investigated. Moreover, SAR evaluation of the wearable antenna system has been studied.

1.2 Thesis Outlines

The important previous work and ideas that motivate and introduce the need behind the research in this thesis are summarized in Chapter 2. The literature review will introduce the reader to the subject of wearable antennas and their applications into different disciplines. It will also provide the relevant theory of the HISs. Their unique electromagnetic properties of in-phase reflection and surface wave suppression will be discussed as well.

In Chapter 3, the design of a fully textile CPW-fed monopole antenna is introduced. Geometry, simulation set up, and in phase reflection characteristic of the proposed HIS cell will be presented. The antenna was integrated on HIS for performance enhancement. The simulated as well as measured results will be presented for reflection coefficient and radiation patterns. SAR analysis in a layered human body model due to a body worn CPW-fed monopole antenna and the antenna integrated on HIS will be discussed in this chapter.

In order to validate the proposed design for wearable antenna application, performance characteristics of the monopole antenna and the antenna integrated on HIS structure under bending and crumpling conditions will be discussed in Chapter 4 and Chapter 5, respectively. Bending and crumpling in different planes of the antenna structure for different cases, approximating real life situations, will be presented.

Finally Chapter 6 addresses the conclusions of the key findings of this research. Also, it gives guidelines and suggestions for further work.

CHAPTER 2

LITERATURE REVIEW

2.1 High Impedance Surfaces (HIS)

2.1.1 Introduction

In 1999 [9], it was shown that by integrating a periodic pattern on a conducting surface, it is possible to change its radio frequency properties. Such structures have attracted significant attention by researchers in many antenna applications due to their beneficial features that arise from the interaction of these engineered elements with the electromagnetic waves, which can't be obtained using the materials in nature. These structures have been named High Impedance Surfaces (HIS).

2.1.2 Characterizations of HIS

2.1.2.1 In-phase reflection or Artificial Magnetic Conductor (AMC) behavior

Before launching in-phase reflection feature of HIS, it is important to introduce the use of Perfect Electric Conductor (PEC) and Perfect Magnetic Conductor (PMC) as a ground plane in the antenna design and their effects on the overall performance of the antenna. In general, the use of the ground plane in the antenna design has two advantages. One, is it redirects one half of the radiation into the desired beam, which improves the antenna gain by a factor of 2 to 3dB, given the correct position of the antenna's radiating

element; and two, it shields the body underneath the ground plane from the electromagnetic radiation.

Although a simple conducting surface has these needed features, it also shows one undesirable property of inverting the phase of the reflected wave to satisfy the boundary conditions at the metal/air boundary. The disadvantage of this phenomena in antenna applications can be explained by considering the phase shift that occurs in a sequence of operation when the incident wave impinges the PEC ground plane, and it is reflected back, experiencing an 180° phase shift and, finally, adding with the original waves emitted directly by the radiating element to form a destructive interference pattern on the front side of the antenna, which results in reduced radiation efficiency.

This problem can be solved by separating the radiating element from the PEC ground plane by at least one quarter of the operating wavelength. When the electromagnetic wave travels a distance of $\lambda/4$, it undergoes a phase change of 90°. Additionally, the reflected wave experiences a further 180° phase change, which results of a phase shift equal to one complete cycle for the total round trip. Therefore, both original waves and reflected waves will be in phase and will interfere constructively. This constructive interference phenomenon is shown in Figure 1. However, a minimum required thickness of $\lambda/4$ of such an antenna structure doesn't meet the low profile antenna designs requirements that limited the overall height of the antenna structure to be less than one tenth of a wavelength at the operating frequency [10].

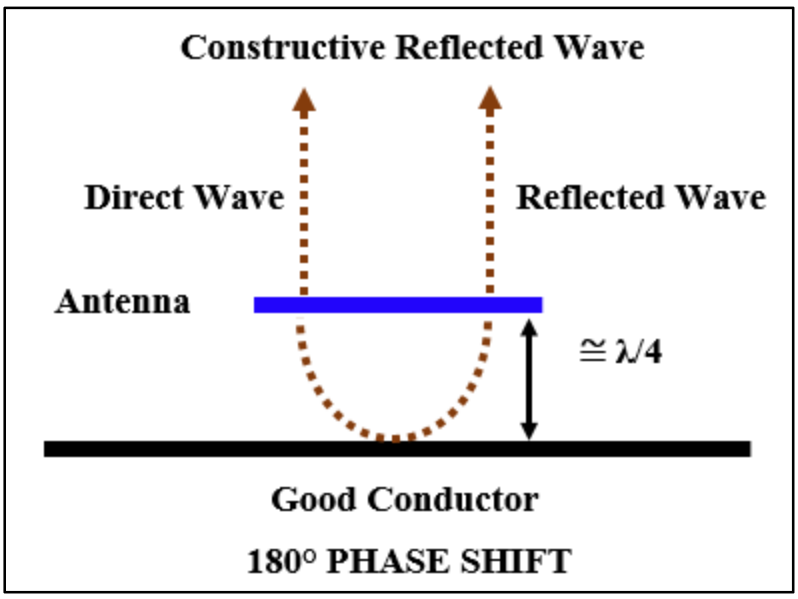

Figure 1: Antenna separated by λ/4 from electric conductor.

In contrast, using PMC surface as a ground plane, results in a reflected wave that has no phase shift on reflection from PMC surface. Consequently, this property of PMC helps to reduce the antenna profile since the λ/4 minimum distance is no longer needed, and the reflected wave will, constructively, interfere with the radiated wave. This constructive interference phenomenon is shown in Figure 2. Much effort was dedicated to realize a PMC-like surface artificially, since no natural material has been found to realize such a magnetic conductive surface.

However, the reflection phase of an HIS varies from -180° to 180° with frequency. In the range of -90° to 90° of the reflection phase, the reflected wave back from an HIS is more in phase than out of phase with the original radiated wave. This means HIS behaves as PMC in a certain frequency band, as shown in Figure 3. HIS showing such characteristics, has been called Artificial Magnetic Conductor (AMC), and used as a ground plane for low profile antenna design [11].

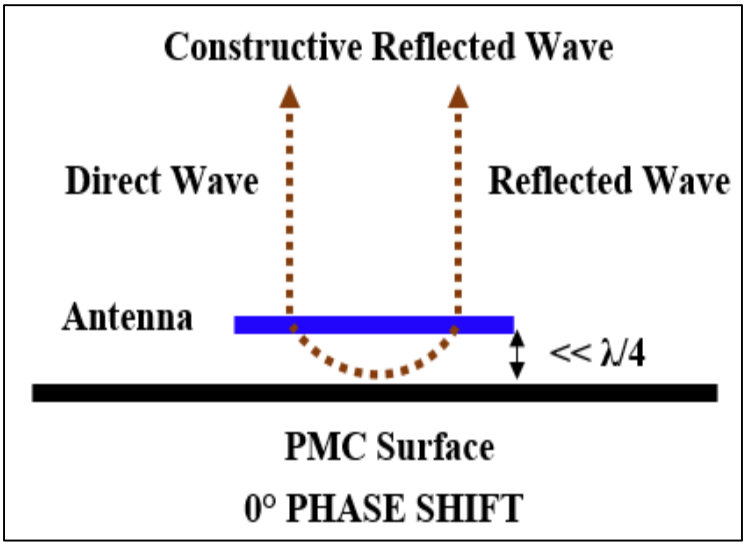

Figure 2: Antenna laying above PMC ground plane.

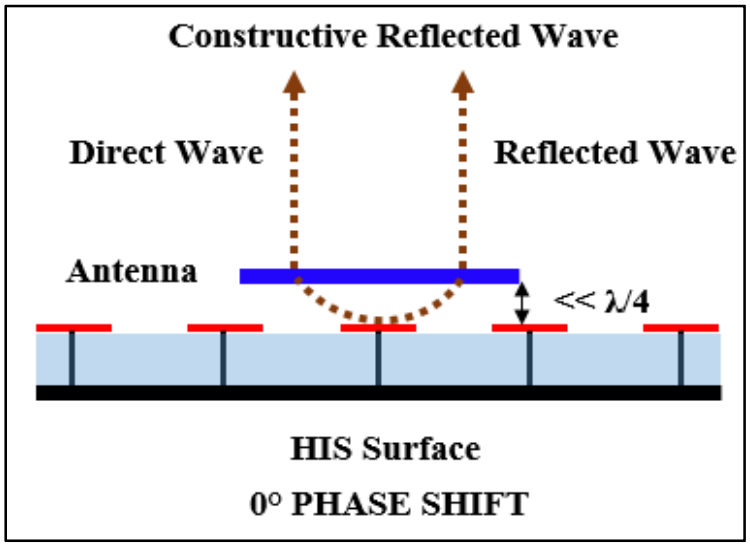

Figure 3: Antenna laying above HIS ground plane.

As an example, curl antenna was one of the earliest proposed low profile and Circularly Polarized (CP) antenna, which was suffering from the low radiation efficiency because of the reversed image current due to the conventional PEC ground plane [12]. In

order to improve the radiation efficiency, the conventional PEC ground plane was replaced by an AMC ground plane as shown in Figure 4 [13].

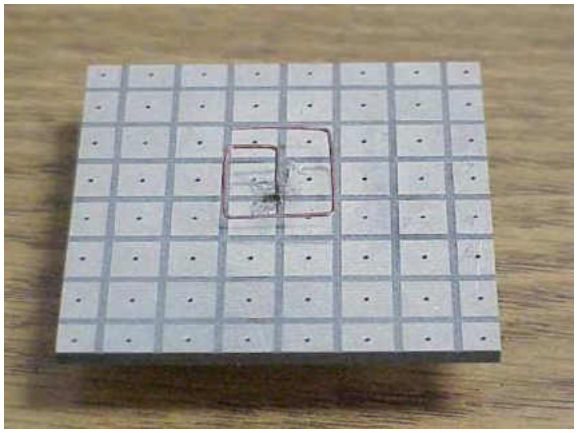

Figure 4: Photograph of CP curl antenna over AMC ground plane [13].

In Figure 5 (a) results of the reflection coefficient show the curl antenna over PEC ground plane isn't matched well. In contrast, the curl antenna over AMC ground plane experience a good matching in the frequency range from 6 to 8.5 GHz because of the in-phase reflection property. In addition, as illustrated in Figure 5 (b) the Axial Ratio (AR) results show a good CP, where AR value of 0.9 dB was achieved at 7.18 GHz. 8.4 % CP bandwidth (AR < 3 dB) was achieved, using AMC as a ground plane in the design [13].

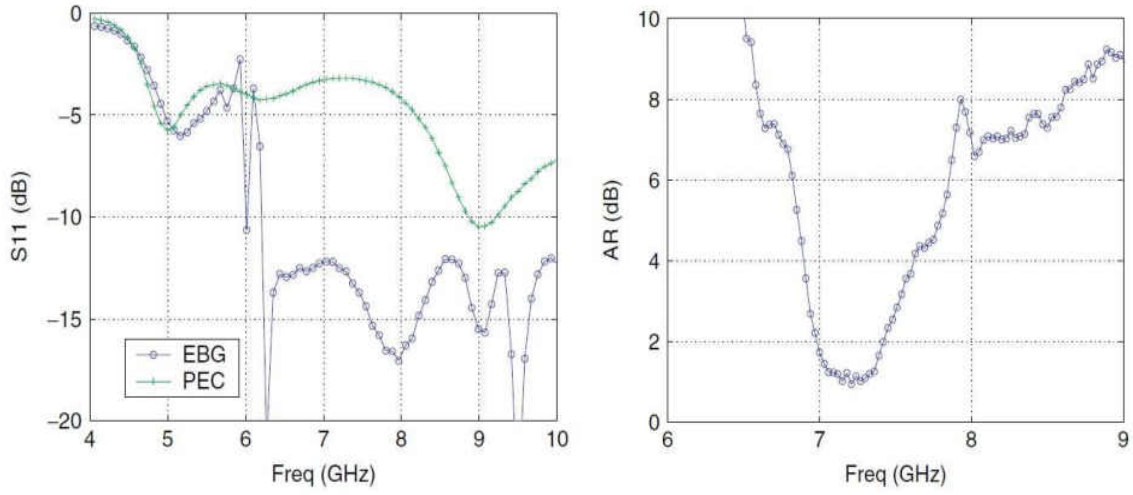

Figure 5: Measured results of CP curl antenna: (a) reflection coefficient (S_{11}), and (b) AR [13].

2.1.2.2 Surface wave suppression or Electromagnetic Band Gap (EBG) behavior

Another property of conductor surfaces is that they support surface waves [14]. To understand the effect of surface waves on the performance of the antenna, it is important to introduce the concept of these waves. Surface waves are bound to the interface between two different materials, for example, metal and freespace. When an antenna operates close to a metal sheet, it will radiate planewaves into freespace; however, it will also induce surface currents that will propagate along the conducting sheet. If the conductive ground plane is smooth and infinite in extent, the effect of the surface waves would be seen as a slight reduction in radiation efficiency. However, in reality, due to the finite size of the ground plane, the surface waves can propagate until they reach the dielectric to air boundary and then radiate into freespace in a cylindrical fashion, which causes a kind of multipath interference with the space wave [9, 15] as illustrated in Figure 6.

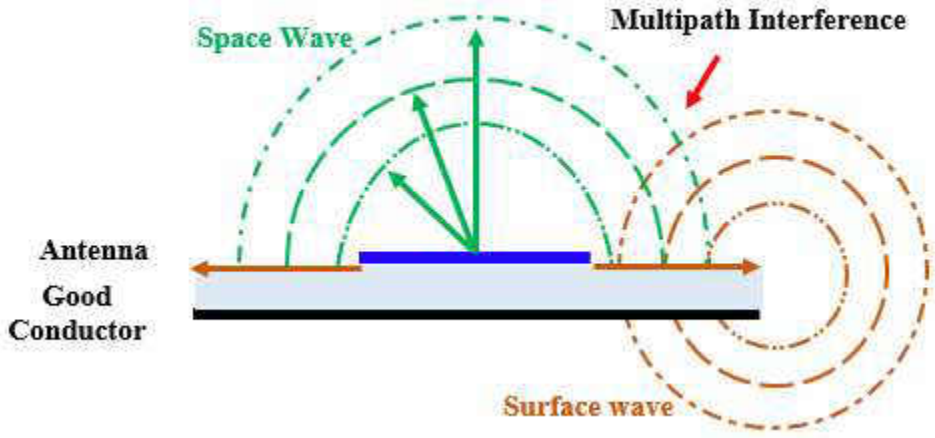

(a)

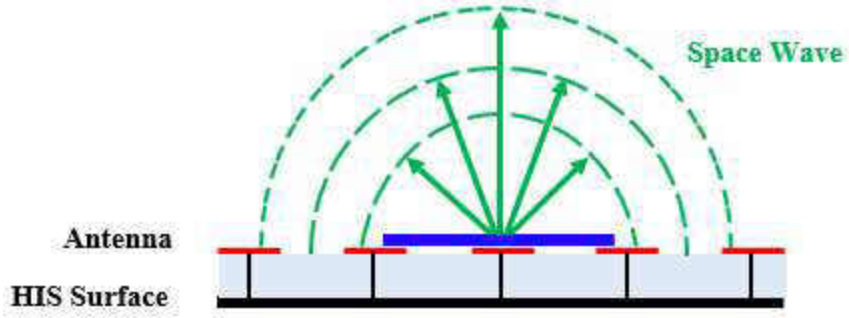

(b)

Figure 6: Multipath interference due to the surface waves on (a) normal ground plane, and (b) alternative ground plane with HIS structure.

As a result, the combined radiation from the antenna and different parts of the conducting ground plane will form a series of lobes and nulls at various angles, which will be seen as ripples in the far-field radiation pattern [9]. In addition, part of the energy of the signal will be blocked from radiating in the desired beam, decreasing FBR. Moreover, when multiple antennas share the same ground plane to form an array, unwanted mutual coupling among them might take place.

In order to decrease the energy coupled to the surface waves and their effects on the performance of the antenna, one of the suggested solutions is to increase the dielectric permittivity and thickness. However, a low permittivity substrate results in large antenna size while using high thickness substrate results in a reduction in the antenna efficiency [9, 15].

HIS exhibits a novel ability to control the propagation of the surface waves within a frequency band due to the high surface impedance property, hence, they are named Electromagnetic Band Gap (EBG) structures. The concept of EBG structures started in the optical domain, where the light emissions were prohibited within a certain bandgap in the photonic crystals. As a result, Photonic Band Gap (PBG) structures were extensively used in the early days. Although the PBG properties are scalable and applicable for wide range of frequencies, including microwave, the researchers in electromagnetic and antenna community are focusing to produce electromagnetic structures for radio frequency and microwaves applications. The first band gap feature was realized and practically applied in the early 1990s, using a periodic dielectric structures [10].

In fact, the unwanted effects of surface waves are expeditiously suppressed in many antenna designs, using EBG structures. EBG structures have been successfully utilized to improve the radiation pattern in the forward direction, reduce backward radiation and, hence, increase in the gain, and improve the FBR. For example, the integration of EBG structures with microstrip antenna arrays has been explored to reduce the mutual coupling between elements. Figure 7 shows a photograph of a fabricated two pairs of antenna with 2×5 EBG lattice, which reduced the coupling level by 11 dB without any adverse effect

on the radiation performances [16]. In [17], a double layer EBG structure has been used for broadband mutual coupling reduction between Ultra Wide Band (UWB) monopoles.

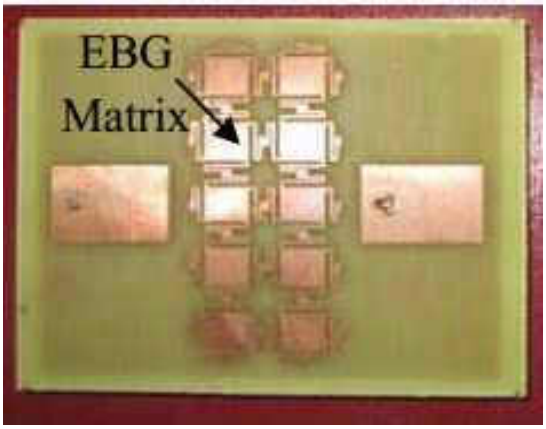

Figure 7: Microstrip antennas separated by EBG structure for mutual coupling reduction [16].

It is worth mentioning that there are some structures, which show both EBG and AMC characteristics. For example, the mushroom-like HIS [9] and the uni-planar HIS [18] belong to both groups. Initially, it was proposed that if there are no vias in the mushroom-like HIS, it does not show EBG behavior [19]. However in [20], it was experimentally proved that when via is removed from the mushroom-like HIS, the EBG phenomenon still exists, but the spectral position moves to the higher frequency band while the AMC band remains at the same position as in mushroom-like HIS. It was then proposed that by varying the periodicity of the HIS structure and keeping the patch size fixed, the AMC and EBG bands can be tailored independently and designed to overlap for simultaneous EBG and AMC operation.

2.1.3 Classifications of HIS

After their introduction, a wide variety of HIS structures have been proposed and studied in the microwave and antenna community. Because of their diverse shapes, it is important to classify them. In general, EBG structures can be classified, based on their geometry into three categories, that is, one dimensional (1D), two dimensional (2D), and three dimensional periodic structures (3D).

Three dimensional volumetric HIS structures have the periodicity along all the three dimensions. The beneficial feature of these structures is the complete band gaps, which means the propagation is prohibited in all directions. However, integration and fabrication of these structures are difficult. Figure 8 shows the woodpile structure consisting of square dielectric bars. This was a successful attempt made in Iowa State University to obtain 3D HIS structure [10, 21].

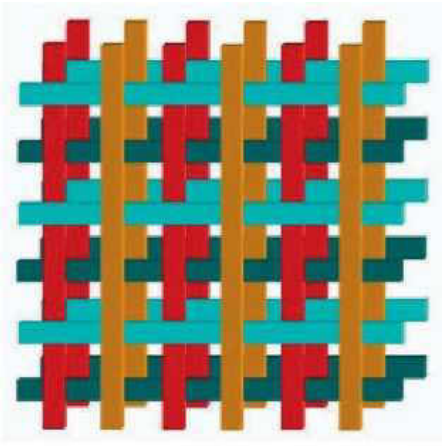

Figure 8: 3D woodpile HIS structure [22].

In two dimensional HIS planar surfaces, because of the periodicity in two directions, the propagation is allowed in one direction. These 2D structures have the

advantages of stability, light weight, and low cost of fabrication, which make them widely used in microwave devices. Two representative 2D HIS structures, mushroom-like surface Sievenpiper's structure and Itoh's Uniplanner Compact (UC-HIS) structure are shown in Figure 9 and Figure 10, respectively [10, 23].

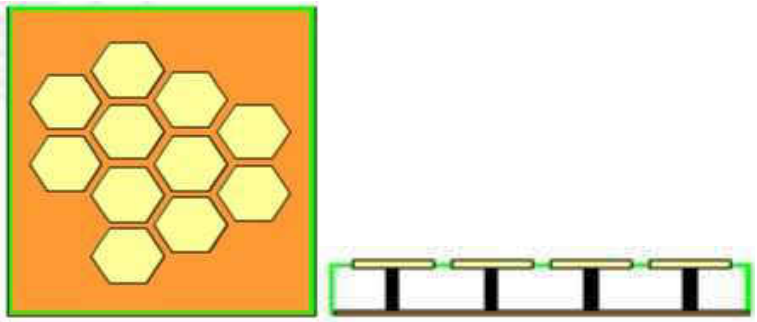

Figure 9: 2D HIS structure: a mushroom-like HIS structure [11].

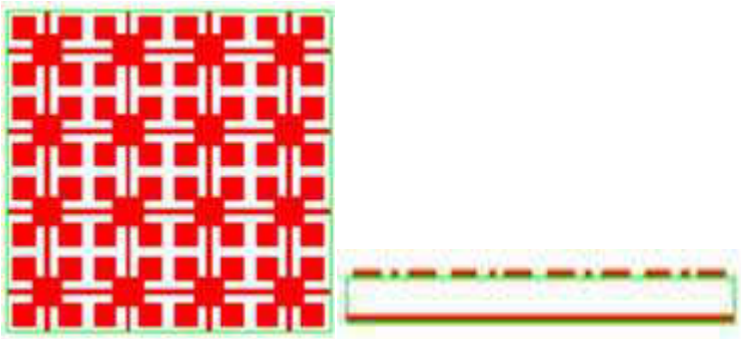

Figure 10: 2D HIS structure: a uniplanar compact HIS structure [11].

Finally, in one dimensional HIS structures, the periodicity is along one axis only. Figure 11 shows the one dimensional HIS structure implemented in microstrip line, which consists of periodic holes in the ground plane [10].

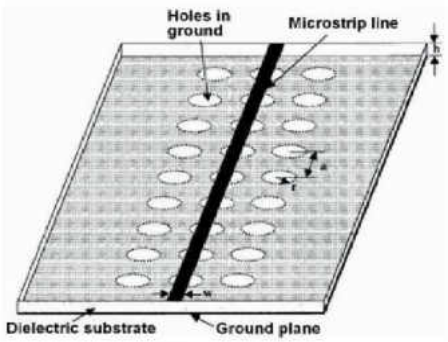

Figure 11: 1D microstrip line [24].

2.1.4 Applications of HIS Structures in Antenna Design

In this section the application of different HIS structures in antenna design will be discussed.

2.1.4.1 Mushroom-like HIS Structure

Mushroom-like HIS is a type of two-dimensional planer metallic electromagnetic structure, which has been characterized by high surface impedance. The geometry consists of periodic metallic patches on the top of dielectric substrate connected to the ground plane via short and vertical pins. The width of the patches and the gap between the metallic patches determine the periodicity of the structure [25].

In [9], performance of a simple horizontal monopole on a flat metal ground plane has been compared with the same antenna placed on high impedance ground plane. It has been found that the signal level is about 10dB higher on the high impedance ground plane. In addition, the radiation pattern is smoother and has fewer ripples in case of the antenna placed on high impedance ground. In [26-28], different designs of UWB band notched microstrip-fed printed monople antennas have been proposed. These antennas are

integrated with a rectangular mushroom-type HIS structure to obtain band-notched charectrerstics.

A monopole antenna for Digital Television (DTV) applications in Ultra High Frequency (UHF) band has been proposed in [29]. An HIS plane, consisting of a Frequency Selective Surface (FSS), an air-gap and a groundplane, as shown in Figure 12, is used as a reflector for the antenna in order to obtain a high gain antenna with lightweight structure. The antenna prototype achieved 55.6% relative bandwidth, high gain of 10.25 dBi, and a radiation efficiency of 97%. In [30], a mushroom-like HIS structure was used in the design of semicircular microstrip monople antenna for bandwith enhancment purpose.

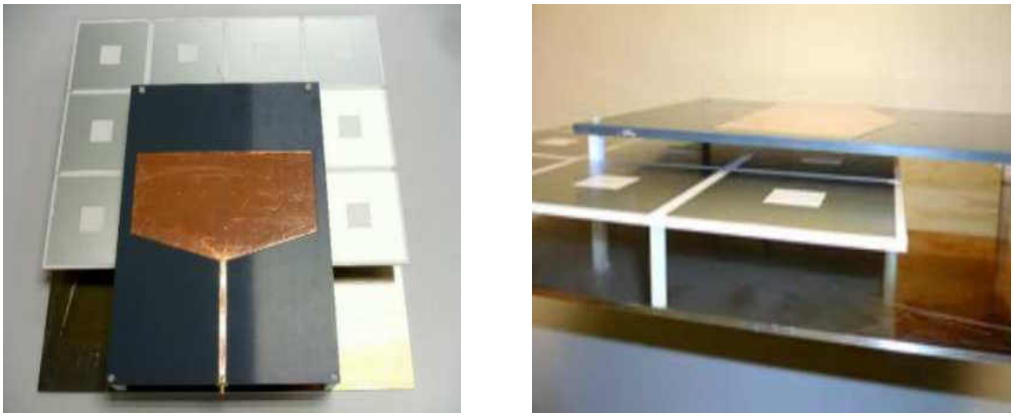

(a) (b)

Figure 12: Manufactured prototype of FSS in HIS: (a) top view, and (b) lateral view [29].

In [31], microstrip antenna surrounded by four rows of mushroom-like HIS structure have been designed in order to effectively suppress the surface waves at the resonance frequency. The performance of microstrip antenna, using HIS structure, is compared to the performance of two normal patches, built on thin and thick substrates used as a reference. Another patch antenna designed on a step-like substrate. It was found that

HIS antenna had the highest front radiation and the lowest back radiation among all these antennas and showed better radiation pattern [31].

2.1.4.2 Uniplanar-Compact HIS Structure (UC-HIS)

Elements in the periodic pattern of uniplanar HIS structure consist of a metal patch and four lines of metal in order to connect the patches together. In [32], the characteristics of a series of designs for uniplanar HISs, as shown in Figure 13, for antennas and microwave circuits were studied. The use of these designs was investigated in low profile antenna applications and mutual coupling reduction of planar radiating elements. An important feature of these UC-HISs is the ease of fabrication. Thus, standard planar fabrication techniques can be used without modifications, which result in low-cost manufacturing. In [33], three uniplanar shapes of HIS as T-shape, fractal shape, and interdigital capacitors are etched on the ground plane of Planar Inverted-F Antenna (PIFA) for laptop Multiple-Input Multiple-Output (MIMO) applications to improve the impedance bandwidth, reduce the antenna size, increase the gain, and improve the radiation pattern. Investigation of the application of several different UC-HISs, acting as AMC for bandwidth broadening, gain enhancement and beam shaping of monopole antennas are presented in [24].

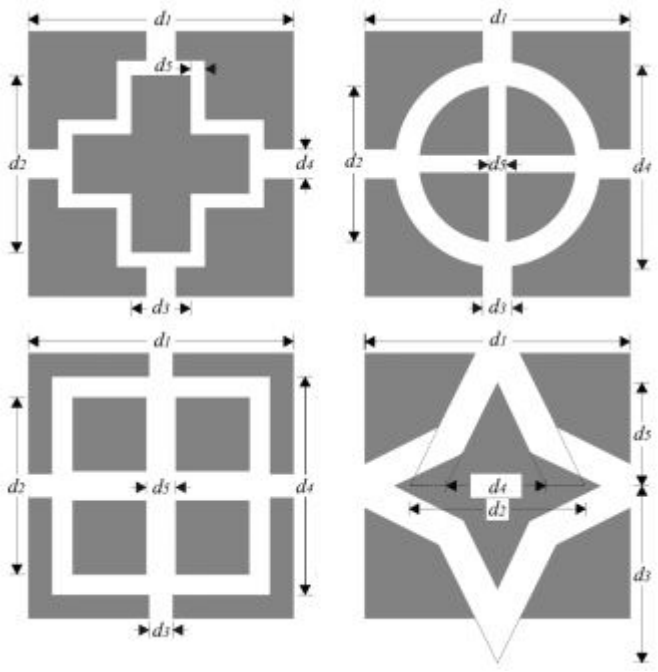

Figure 13: A series of UC-HISs: cross-HIS (left, top), circle-HIS (right, top), square-HIS (left, bottom), star-HIS (right, bottom) [32].

UC-EBGs have been used in microstrip antennas to enhance their performance since the propagation of the surfacewave is prohibited within the bandgap associated with the structure [10, 18]. For example, over a 3 dB gain enhancement and more focused radiated beam in the broadside direction of the antenna is achieved by surrounding a patch antenna, resonating at 12 GHz, with three rows of UC-EBGs [18].

2.1.4.3 Dielectric Electromagnetic Bandgap Structures

Dielectric EBG structures were obtained by drilling a periodic pattern of dielectric implications, which have a different dielectric property from the host dielectric substrate. These configurations of EBG have been used widely in microstip antennas to enhance their performance by improving the radiation pattern and increasing the efficiency and gain [34, 35].

For example, an array of air holes were drilled through the substrate in order to enhance the patch antenna performance, as shown in Figure 14. The FBR in the conventional patch was 17 dB at a resonance frequency of 2.14 GHz. In contrast, the EBG antenna presents FBR of 24 dB, indicating a lower back plane radiation was achieved by using EBG structure [34].

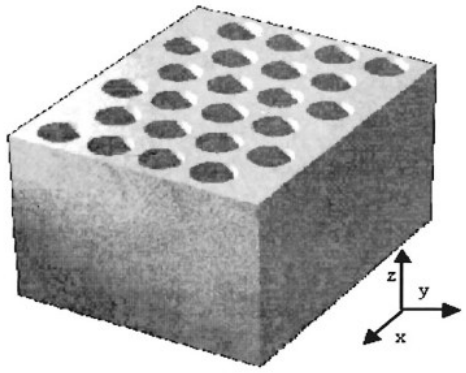

Figure 14: Dielectric EBG formed by an array of air columns drilled in a dielectric substrate [34].

2.1.4.4 Photonic Bandgap Structures (PBG)

Similar to the semiconductor devices, which can exhibit an electronic bandgap where the electrons cannot exist, the photonic crystal of PBG structure doesn't allow the propagation of the electromagnetic waves within a certain range of frequencies defined as photonic bandgap [36]. Research on photonic crystals started in 1887. However, the first photonic bandgap was introduced by Yablonvitch in 1987 [37]. In general, the basic PBG structure can be realized using two different materials. These materials can be metal and dielectric materials, or two different dielectric materials with different periodicities 1D, 2D, and 3D structures as shown in Figure 15 [38].

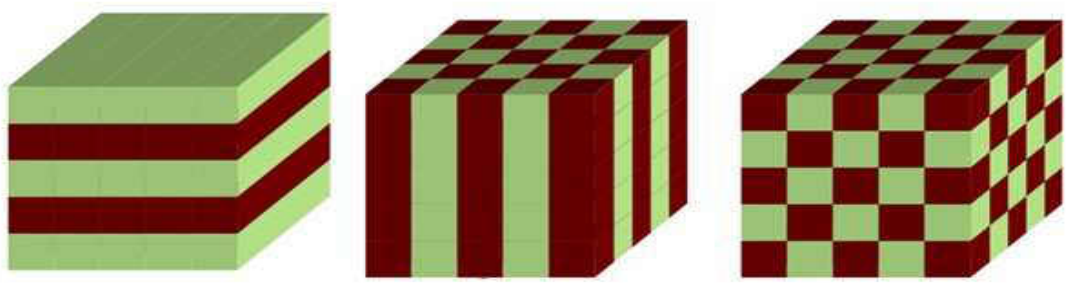

(a) (b) (c)

Figure 15: Configurations of PBG: (a) 1D, (b) 2D, and (c) 3D [39].

A significant improvement in the directivity of microstrip antenna, operating at 1.95 GHz was achieved by using PBG substrate; the PBG substrate increased the directivity from 6.0 dBi (obtained by the conventional patch antenna) to 6.7 dBi. Furthermore, a PBG cover on the top of the patch antenna, as shown in Figure 16, was used to increase the directivity to 17.1 dBi [40].

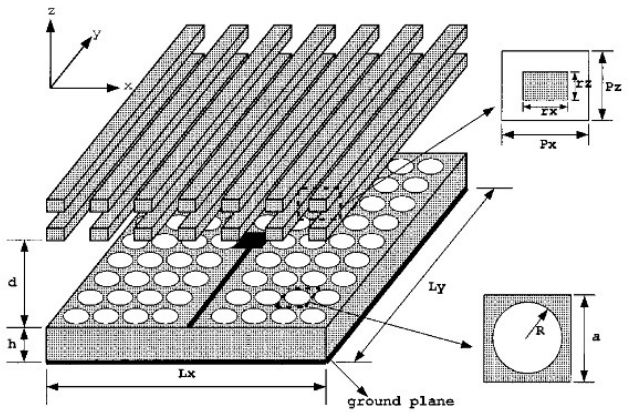

Figure 16: Geometry of patch antenna with both PBG substrate and cover [40].

2.2 Wearable Antenna

2.2.1 Introduction

Communication technology is progressively interposing in everyday life. The rapid progress in wireless communication besides the recent utilization of wearable antennas and electronics in many industrial and academic research makes the antenna as one of the key components in these systems. Consequently, there is a need for new design, fabrication and measurements techniques to build unconventional antennas and test them.

In general, wearable antennas can be defined as those that can be integrated into clothing. They might be a part of a system that provides information about the wearer's health and environmental states. Thereby, wearable antenna has been utilized in many applications, such as in-space applications, military domains, firefighting, personal communications, and health monitoring [41].

Depending on the application specifications, the requirements of wearable antenna can vary. However, wearable antenna possess some common features that can be addressed as follows [42, 43]:

1) Low profile,
2) Low fabrication and maintenance cost,
3) Flexible and withstand bending, damage from obstacles, and stretching,
4) Less disturbing, and not causing extra drag for the operating system,
5) Capable of providing shielding from the adverse effects on the human body

2.2.2 Classifications of Wearable Antennas

The research work done on wearable antennas domain can be categorized into different bases. One can be the antenna type used in wearable application, such as monopole antenna, microstrip patch antenna, PIFA, E-shaped and U-slot patch antennas, etc. Additionally, it can be categorized on their intended applications, such as cellular mobile communications, Wireless Local Area Network (WLAN), Global Positioning System (GPS), and UWB applications.

Based on the antenna material, wearable antennas can be mainly categorized into two types:

1. Hard dielectric substrate wearable antennas: In order to meet the requirements of wearable antennas, this type of antennas need to be designed in a small size or manufactured in a curved contoured shape, and be mounted on the human body. However, these restrictions on antenna area and form are often difficult to achieve, which makes this type of antennas impractical and not convenience to the user in many applications [44].
2. Flexible wearable antennas: Many flexible materials might be utilized, such as foam, polyimides, commercial papers, and flexible Printed Circuit Board (PCB). Although this type of antenna brings more flexibility as compared with hard dielectric substrate, it is still restricted by the limitations on the antenna size and the difficulty to be well integrated with clothing in many applications. Another type of flexible antenna is textile-based antenna, where the conductive material or/and non-conductive are based on fabrics. Consequently, the antenna can be well integrated with clothing, which can produce more freedom to design without restrictions on the antenna area. Designing textile antenna requires the knowledge of electromagnetic properties, such as permittivity and loss tangent

of the textile materials. Conductive textile materials, such as zelt, flectron and pure-copper-polyester-taffeta fabrics are regularly used as the radiating element while non-conductive textile, such as silk, felt and fleece are used as substrates [45].

2.2.3 Wearable Antennas: Critical Design Issues

In a wearable antenna system, there are many challenges that are imposed by the real system set up, which might cause a degradation in the antenna performance. Thus, they should be considered when analyzing the antenna performance. One of the serious challenges is the interaction between the human body and the antenna. As a result of the antenna working in close proximity to human body in wearable antenna applications, frequency-detuning problem might arise because of the high dielectric properties of the human body [4]. Furthermore, due to the lossy nature of human body tissues, some parts of the radiating power of the antenna will be absorbed, and it will result in lower gain [43].

Additionally, when the antenna is placed in close proximity to human body, the amount of power absorbed by the human body, which is defined by SAR, should be controlled to be at the safety levels of electromagnetic fields defined by the commonly used SAR standards, such as International Commission on Non-Ionizing Radiation Protection (ICNIRP) and IEEE. Thereby, measurements on real human body or with phantom should take place. Additionally, the antenna's performance characteristics under bent and crumpling conditions need to be investigated due to the human body movements and the irregularity in the human body shape.

In fabric-based wearable antennas, stretching and compression can easily deform the antenna structure and affect its performance. In addition, the antenna performance should be considered with different environmental conditions, such as high humidity to

represent perspiration or exposure to water, which might change the resonance frequency and the input impedance bandwidth. Consequently, it will be difficult to produce an antenna with the same radiation characteristics even using the same textile material.

In order to point out the area of wearable antenna that needs further research study, in the next section of the literature review the evolution of wearable antenna in many applications is explained with a focus on textile antennas.

2.2.4 Wearable Antennas: Review of the Literature

A large number of wearable antenna designs have been presented by researchers for different applications, using different kinds of materials. In 1999, the research work presented by Salonen in [46] is claimed to be the first published work on wearable antenna domain. Conventional PIFA, integrating a U shaped slot, is designed in order to achieve a dual band operation for wireless communication applications within the Global System of Mobile (GSM) 900 MHz and ISM-2.4 GHz bands. Although the antenna is designed, based on a conventional hard dielectric material, it is mounted on the sleeve of clothing to make a wearable antenna. In [47], the same PIFA design mentioned in [46] was used, using a flexible material with dielectric constant of 3.29, thickness of 0.236 mm, and loss tangent of 0.0004. The antenna was attached to a human arm for a Bluetooth-operated system.

Later, the interest in wearable antennas was significantly increased among academic and industry researchers. In [48], a circular patch wearable antenna was constructed using woven conductive and insulating felt fabrics. The antenna operating at 2.5 GHz was designed to monitor the location of elderly people. In [49], three types of antennas operating at 868 MHz: quarter-wavelength antenna with ground shield, a dipole

V antenna and a square dipole antenna, were designed, using glass epoxy as a substrate material for medical tele-monitoring applications. A flexible microstrip-fed monopole antenna was proposed in [50] for tracking and detection purposes.

Evaluation of a wearable hybrid textile antenna is outlined in [51] in order to validate PCB to textile transition. Three fabrication topologies with similar dimensions were used to design a rectangular microstrip antenna. A fully textile design, based on fleece fabric as a substrate and zelt conductive textile, a hybrid FR4-conductive textile, and a copper foil used with FR4 substrate designs were tested while placed on the human arm. All antennas suffered from loss in efficiency and gain, degrading by about half of their freespace values while the hybrid structure had the lowest degradation in terms of bandwidth and frequency shift.

As different textile materials start appearing in wearable antenna design, it was necessary to study the performance of wearable antenna using different textiles. The work in [52] demonstrated the characterization of five different fabrics suitable for circular polarized microstrip antennas for GPS application. The materials are fleece, V ellux, synthetic felt, U pholstery fabric and cordura. Cordura fabric-based antenna showed the best performance characteristics when stretched. In [53], performance of four rectangular patch antennas, employing different varieties of cotton and polyester clothing for on-body wireless communications in the 2.45 GHz WLAN band, was analyzed. Results from the paper demonstrated the suitability of these patch antennas for on body wireless communications under bending conditions. In [3] the effect of different conductive materials on the performance of WLAN antenna for wearable application were presented.

The effect of the structure of electro-textile materials, which are used to construct the conductive parts of the antenna, on the antenna's performance was studied in [2].

As mentioned in the previous section, it's necessary to consider the challenges of designing wearable antenna for proper assessment of the antenna performance characteristics. In [54], an experimental study was carried out by bending a rectangular patch antenna on surfaces with different radii (50.8mm, 63.5mm, 76.2mm and 88.9mm), which are typical for different parts of human body, such as arm, leg, and shoulder. The antenna was fabricated, using zelt conductive fabric and a Polyester fabric as a substrate material. It was observed that the more the antenna was bent, the more the resonance frequency of the antenna was shifted up due the reduction in the resonant length.

Additionally, since wearable antennas are intended to work in close proximity to human body, it is imperative to consider the presence of lossy tissues. Measurements on the real human body were carried out in [55, 56] and on human phantom in [57]. The impact of human body and clothing on the performance of a dual band textile antenna designed for DTV and many wireless standards were studied in [58]. Return loss measurements showed good performance of the antenna when worn at various positions on the body, and when further covered by common garments, including thick waterproof sportswear outfits. In addition, full three-dimensional radiation patterns have been measured when the antenna, being positioned on a phantom, was used to simulate human body. Backing the antenna by either AMC surfaces or more simply by a number of felt layers helped produce more efficient designs for wearable applications.

Exposing wearable antennas to harsh operational environments was investigated by many researchers. The first compact fabric antenna design for commercial smart clothing was presented in [59]. The rectangular microstrip patch antenna employed knitted copper fabric for conducting parts, and fleece fabric for the dielectric substrate was designed for WLAN band to use in sportswear and emergency worker outfits. The performance of multilayer textile microstrip patch antenna for integration into protective clothing for professional workers was presented in [60]. Different conditions were considered in the antenna's performance measurements, such as the presence of additional layers covering the antenna, different bending conditions, and on body measurements. It was noticed that neither covering nor bending the antenna had a significant influence on the antenna gain while the antenna gain was decreased for on-body measurements in comparison with off-body measurements. A circular polarized microstrip patch antenna, operating in the ISM-2.45 GHz band, was presented in [61] for integration into a fire-fighter's jacket. For a bandwidth enhancement purpose, the antenna was fabricated as a multilayer textile structure, which consisted of four aramid layers, using an adhesive sheet.

Wearable antennas are finding another potential demand in medical applications for medical treatments and health monitoring. In [62], a printed circular monopole antenna for healthcare applications was modeled with an FR4 substrate and used as a body-worn sensor antenna. The performance of this antenna was numerically investigated with the sensor placed on the chest of a human body. A slight detuning in the resonance frequency was noticed due to the presence of lossy human body tissues. The effect of the antenna body separation on the performance of a low profile microstip patch for wireless communications in Medical Body Area Networks (MBAN) was presented in [63]. A

monopole antenna was used in microwave imaging for detection of early cancer by processing the reflected wave to make a comparison between healthy tissues and abnormal tissues [64].

The large space available on the human body can be used for designing a high gain antenna array. This concept was explored in [65] for a body-worn electro-textile antenna array. A novel wideband antenna element, referred as a complementary-8 element because of its shape, was investigated for use in possible Extra Vehicular Activity (EVA) communication systems. A self-complementary antenna was designed for use above 2.1 GHz, using the Nora conductive fabric and a 0.635-cm Nomex substrate. Investigation of six complementary-8 antenna elements placed around the periphery of an EVA suit for navigation purposes was discussed in this work.

UWB is an emerging wireless technology, which offers a low power consumption in low/medium data rate over short distances applications, thus, being very attractive for body-worn battery operated devices. Performance deterioration of two flexible CPW-fed monopole UWB antennas, copper film antenna, and AgHT film antenna for wearable applications were studied based on simulation results in [66]. Both antennas were designed and simulated, employing polymer film substrate and flexed through various radii of curvatures to show that AgHT-8 material had less impact on the performance with bending. One of the first UWB antennas, based on textile materials, was proposed in [67] for a Wireless Body Area Network (WBAN). Two designs were investigated. The first was a CPW-fed disk monopole antenna, and the other one was a microstrip-fed annular slot antenna. Antennas were fabricated on acrylic fabric of 0.5mm thickness as a dielectric substrate, which made it easy to integrate antennas directly into clothing. A UWB

microstrip-fed monopole antenna, which provided 17 GHz bandwidth for medical monitoring applications was investigated in [68]. The antenna was fabricated, using two different textile conducting materials; one was a copper conducting sheet, and the other was a conducting thread, while a flannel fabric was used as a dielectric substrate material. Off-body measurements of UWB monopole antenna placed close to the human arm were presented in [69] and showed that the antenna design is suitable for WBAN applications.

The work in [70] is claimed to be the first constructed circular polarized textile patch antenna for WLAN wearable antenna applications. A microstrip patch antenna with truncated corners was designed, using dielectric polyamide spacer fabric and nickel plated woven textile for conductive parts.

A circular polarization wave radiates the energy in both horizontal and vertical planes, and all planes in between, which was necessary to ensure that the antenna was reliable in wearable antenna applications, specially when the wearer is mobile. Circularly polarized and low cost truncated patch antenna, based on zelt fabric as a conducting part and felt substrate, was proposed in [71] for off-body wireless sensor communications for monitoring patients at 915 MHz ISM band. A purely textile patch antenna for Bluetooth applications, using frequency range around 2.4 GHz, was proposed in [72]. Both linear, as well as circular polarized designs, were investigated. Researchers proposed four microstrip-fed antennas, using woolen felt and a polymides spacer as a substrate materials with a conductive textiles. Performance of the antennas was studied under different bending conditions, and it was observed that circular polarization can be affected if the bending radius is too small.

One of the first EBG based antenna design for wearable application was presented in [73]. Although a 2.45 GHz patch antenna was fabricated on the traditional rigid FR4 substrate, the antenna design was proposed to use for wearable applications. An EBG pattern was etched on the ground plane of the antenna to reduce the backward radiation, increase the antenna gain, and reduce the antenna size.

In [5], the design of flexible M-shaped printed monopole antenna, operating in the ISM 2.45 GHz band, was proposed for telemedicine communications. The antenna substrate was made of polyimide kapton flexible material, and AMC ground plane was used in the design of the antenna in order to isolate the user's body from undesired electromagnetic radiations in addition to minimizing the antenna's impedance mismatch, caused by the high permittivity human tissues. A design of a purely textile patch antenna on the top of EBG array, for bandwidth enhancement and size reduction, was presented in [6] for wearable applications. Fleece fabric was used as antenna substrate, and the conducting parts were made of copper tape.

In [74], on body measurements, flexibility test in terms of bending and crumpling to ensure the performance reliability, and SAR analysis were reported for fractal-based monopole antenna integrated with EBG structure. The fractal antenna and EBG cell were designed on jeans fabric. EBG structure acted as a band-reject filter at GSM 1800 MHz and ISM 2.45 GHz to show a significant reduction in SAR and back lobe in the operating bands.

Commercial 0.25 mm thick paper was used as a substrate for microstrip monopole antenna, backed with EBG array operating at ISM band, for wearable bio-monitoring

applications in [7]. Measurements on a human phantom show a superior performance in terms of gain enhancement and size reduction for the monopole antenna with EBG compared with the conventional microstrip monopole antennas. In [75] a dual-band coplanar patch antenna integrated with AMC and operating at 2.45 and 5 GHz was fabricated, using felt. On-body measurements were done for the antenna placed on a human arm, thigh, and back. EBG reduces the radiation into the body by over 10 dB and improve the antenna gain by 3 dB. In [8], the back radiation was reduced by 10 to 15 dB in a dual-band triangular textile patch antenna over an EBG structure.

A study on the EBG size effects on the antenna, obtained efficiency and size, was presented in [76] to address that more work on achieving higher efficiencies with smaller EBG needs to be performed since the miniaturization is a key concern in wearable antenna design.

CHAPTER 3

DESIGN AND SYNTHESIS OF TEXTILE MONOPOLE ANTENNA INTEGRATED ON AMC GROUND PLANE

3.1 Introduction

In this chapter, the design cycle of a textile monopole antenna and flexible AMC structure will be presented. The antenna key performance indicators such as reflection coefficient, impedance bandwidth, antenna gain, and FBR are studied and compared for the monopole antenna with and without AMC reflector. Moreover, SAR analysis using a three layered rectangular body model is also performed to validate the wearable antenna, so that it doesn't pose any safety issues.

The reflection coefficient or S_{11} describes the impedance mismatch between the feed line and the antenna feed point. It can be defined as the ratio of the power reflected back from the antenna at the feed point to the power fed to the antenna. If the power is completely reflected back at the feed point, S_{11} will equal to 1 or 0 dB. On the other hand, if the power is completely absorbed by the antenna, the value will equal to 0 or -: dB. A low S_{11} value corresponds to a good matching at a specific frequency [72]. Impedance bandwidth refers to the range of frequencies in which a certain level of reflection

coefficient can be maintained. Usually it is determined as the frequency range of -10 dB level of S_{11}, which is defined by the lower f_l and the upper frequency f_h band limits.

The realized antenna gain describes the amplification of the microwave signal at a specified frequency in a particular direction (usually direction of signal propagation) compared to the isotopically radiating antenna. The realized gain is not only determined by the antenna shape, but also by the material, input impedance matching, and the antenna surrounding environment. Antenna radiation patterns characterize the variation of the radiated far-field intensity of an antenna as an angular function at a specific frequency. Usually, they are shown as cuts along two orthogonal planes of the antenna, namely E-plane and H-plane. In this thesis the radiation patterns are defined in the same manner for all antennas investigations, so that, E-plane is YZ plane and H-plane is XZ plane. Also, these planes can be defined by the cut angle, so that, E-plane is defined at $\varphi=90°$ and H-plane is defined at $\varphi=0°$, where φ is the angle measured from x axis.

Antenna efficiency relates the power delivered to the antenna and the power radiated by the antenna, so it considers the losses associated within the antenna such as conduction and dielectric losses in addition to the mismatch loss of the antenna. FBR is used to relate the power in the direction of the main beam to that in the opposite direction, which is important parameter in wearable antenna design [77].

3.2 Characteristics of a CPW-Fed Monopole Textile Antenna

The monopole antenna is designed to cover the whole IEEE 802.15 frequency band of 2.4 ~ 2.5 GHz (ISM-band) for space biomedical application. The antenna configuration was based on the proposed design in [78] and optimized using commercial electromagnetic

simulation software CST Microwave Studio [79]. The antenna consists of a rectangular radiating element with two slots and fed by a CPW line, which offers a uniplanar antenna structure that can eliminate all problems associated with the alignment of different conducing layers [67]. The radiating element and the CPW feeding line are printed on the same side of a Pellon fabric substrate having a thickness of 1.8 mm, a dielectric constant ε_r = 1.08 and a loss tangent tanδ = 0.008. Figure 17 depicts the geometry and the fabricated prototype of the antenna. Dimensions of the antenna are given in mm and listed in Table 1. Pellon fabric is chosen as the antenna's substrate since it exhibits a low profile and flexible characteristics, which stacking multiple layers to control the thickness of the substrate.

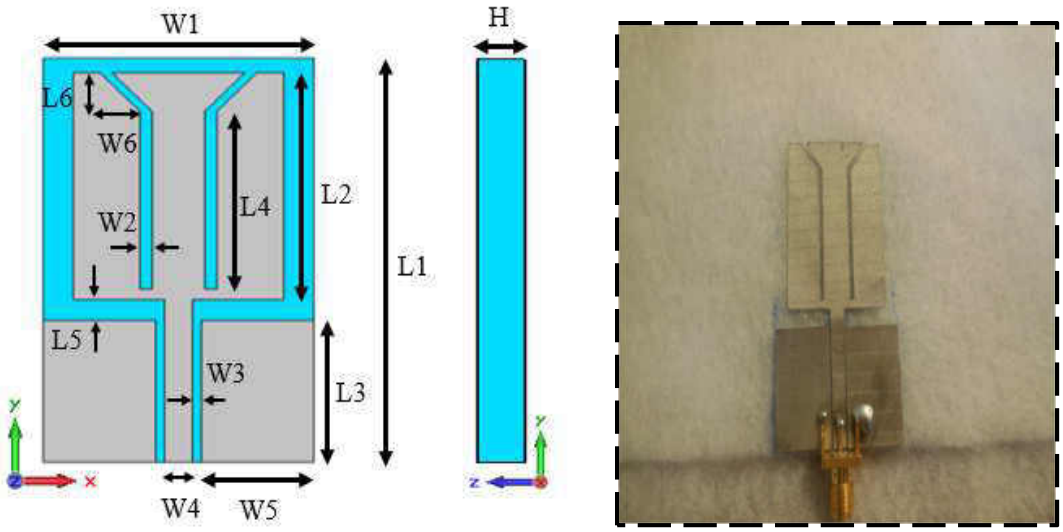

(a) (b)

Figure 17: CPW-fed monopole antenna, (a) geometry, and (b) fabricated prototype.

Table 1: Parameters of CPW-fed monopole antenna shown in Figure 17. Dimensions are in mm.

Parameter	Value
W1	32.10
W2	1.00
W3	0.30
W4	3.00
W5	14.00
W6	5.00
L1	57.00
L2	32.00
L3	20.00
L4	25.00
L5	3.00
L6	5.50
H	3.60

Figure 18 presents the simulated and measured reflection coefficient results of the monopole antenna. Reflection coefficient measurements have been carried out using Agilent E5071C Network Analyzer. Simulation result yields a -10 dB impedance bandwidth of 2.58 GHz (1.75 GHz - 4.33 GHz) with a good impedance matching at 2.45 GHz (S_{11}= -16.01 dB). On the other hand, measurement result shows a higher -10 impedance bandwidth of 3.58 GHz (1.28 GHz - 4.86 GHz) with a better matching characteristic at 2.45 GHz (S_{11}=-20.97 dB).

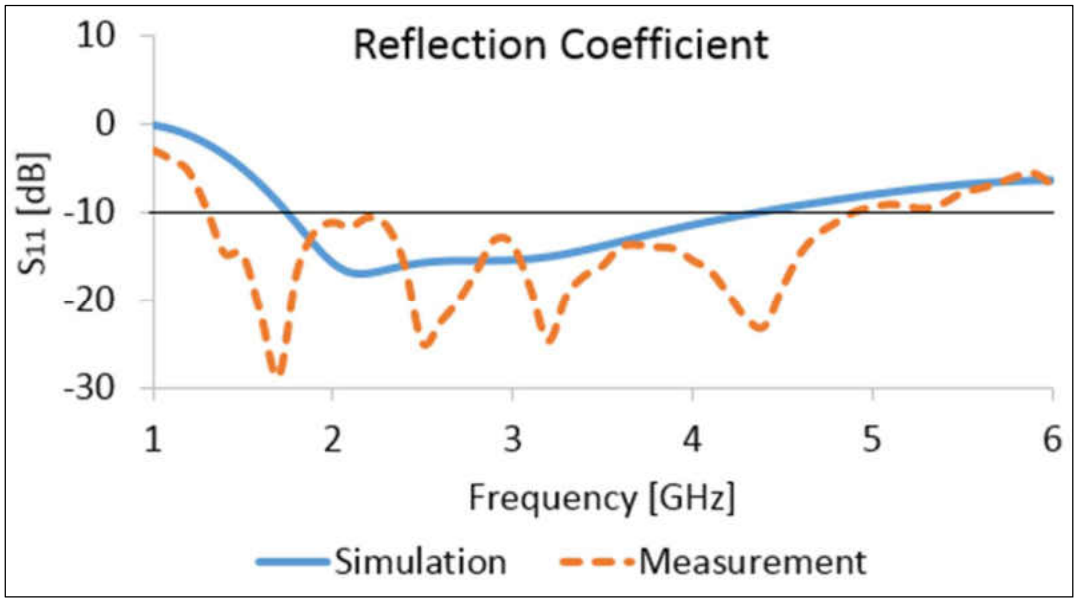

Figure 18: S_{11} results of CPW-fed monopole antenna.

Furthermore, radiation patterns measurements have been performed using the anechoic chamber in Antenna Measurements laboratory at University of North Dakota. Figure 18 shows the normalized E-plane radiation pattern of the monopole antenna at 2.45 GHz based on simulation and measurement results. It's worth mentioning that the simulated cross-pole component isn't shown in the figure since it has a low value that is less than -60 dB. The simulated antenna gain is 2.45 dBi while the measured value is 3.39 dBi, which means an improvement by 0.94 dBi. On the other hand, a reduction by 1 dB in the antenna gain is obtained from the measured radiation pattern in H-plane of the antenna as compared with simulated value (we need to repeat the measurement for this plane).

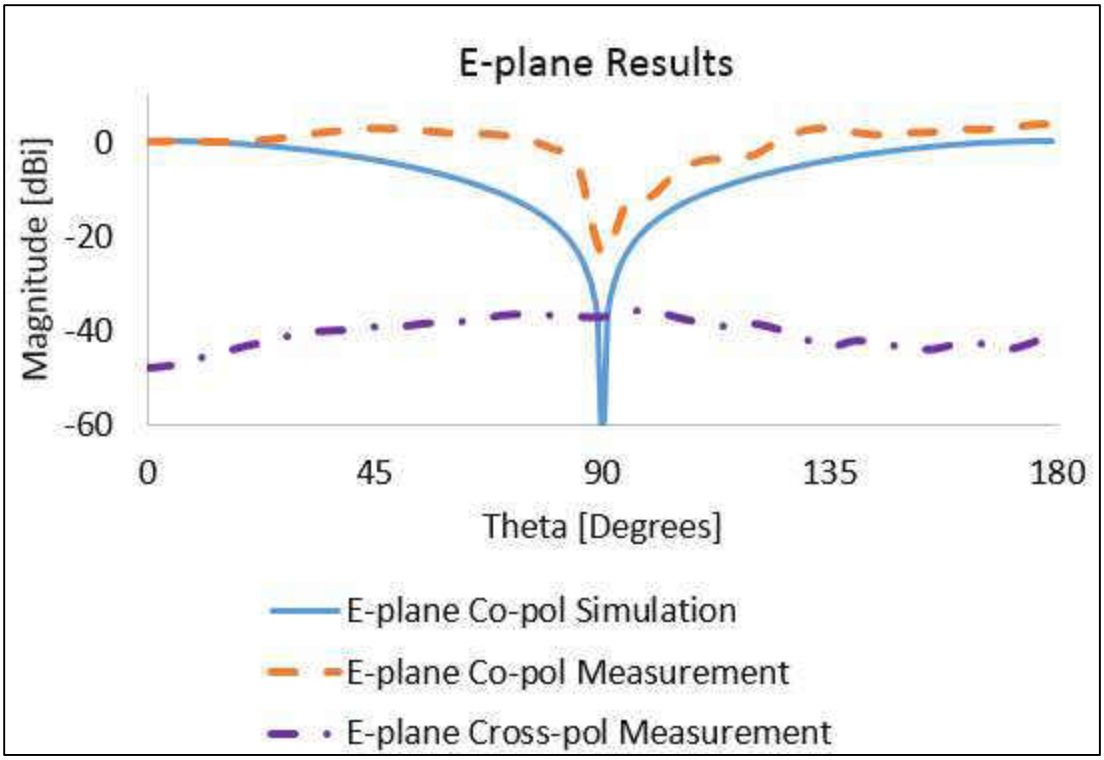

Figure 19: E-plane radiation pattern of CPW-fed monopole antenna at 2.45 GHz.

3.3 Characteristics of Monopole Antenna Integrated on AMC Ground Plane

3.3.1 HIS Unit Cell Geometry and Reflection Phase Characterization

This section presents the HIS unit cell, namely UC-HIS cell, which includes geometry and dimensions of the cell, and simulation results of reflection phase characteristic. The geometry of the HIS unit cell was based on the proposed design in [80] and optimized using CST Microwave Studio software. HIS cell measures 31 × 31 mm^2, and it is printed on 1.52 mm thick RO3003 flexible material with ε_r= 3 and tanδ = 0.0013. Figure 20 and Table 2 show the geometry and dimensions of the proposed HIS unit cell.

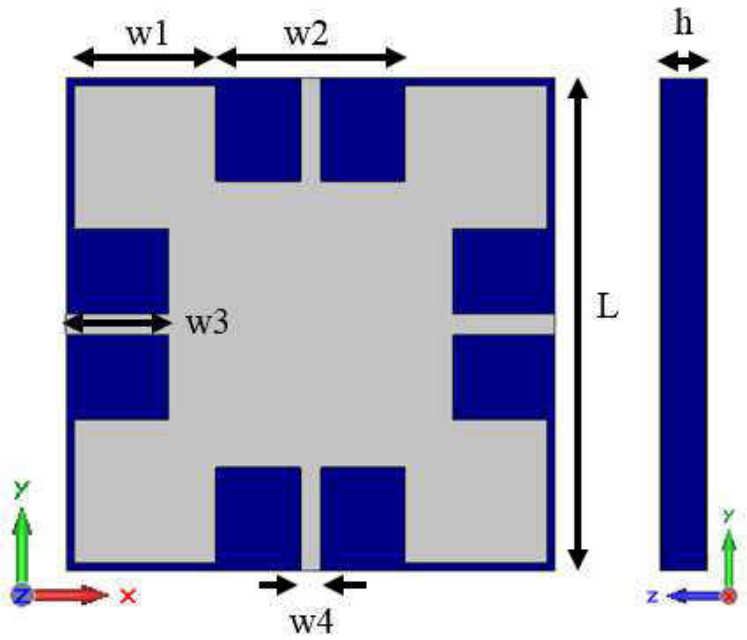

Figure 20: Geometry of the proposed HIS cell.

Table 2: Parameters of the HIS unit cell shown in Figure 20. Dimensions are in mm.

Parameter	Value
w1	9.00
w2	12.00
w3	5.50
w4	1.30
L	31.00
h	1.52

HIS is placed above a conductive layer, which forms AMC to improve the performance of the antenna and reduce the back radiation when it is placed on human body. The AMC reflector is designed by means of reflection phase characterization. The reflection phase is examined with the simulation model shown in Figure 21. The AMC reflection phase characterization procedure follows the same methodology applied in [11].

In order to search for the AMC in phase band, a single cell with Periodic Boundary Conditions (PBC) in *x* and *y* directions was simulated.

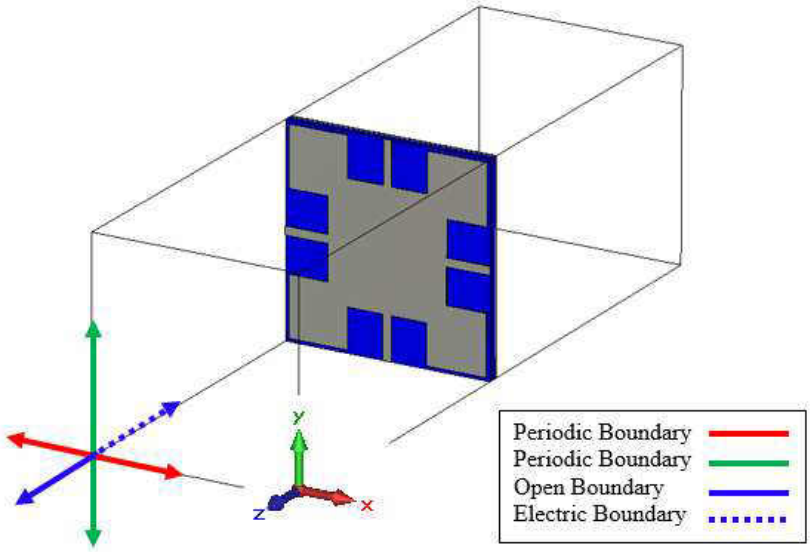

Figure 21: A unit cell simulation model set up for reflection phase analysis.

Figure 22 illustrates the calculated reflection phase of AMC structure. The phase decreases continuously from 180° to -180° as frequency increases. At low and high frequency regions, AMC structure shows a similar phase to a perfect electric conductor case, which is 180°. The AMC reflection phase is 0° at the resonance frequency, which resembles the unique property of AMC surface. The useful bandwidth of AMC surface has been defined by the range ± 90°. Within this range, image currents are almost in phase rather out of phase, thereby, the reflected wave makes constructive interference with the radiated wave [9]. In the proposed cell, the exact AMC point is located at 2.45 GHz, having a narrow bandwidth of 138 MHz (2.34 GHz to 2.48 GHz) within ±90 phase values.

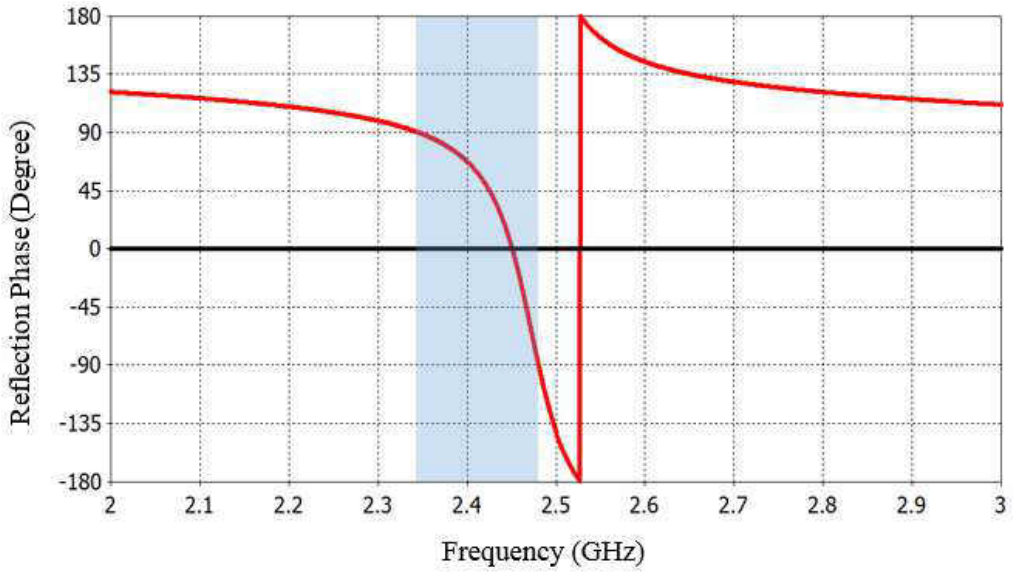

Figure 22: Reflection phase diagram of an AMC cell at normal incidence.

3.3.2 Monopole Antenna Integrated AMC Ground Plane

The proposed structure consists of a monopole antenna, backed with symmetric AMC array (4 rows by 4 columns) measuring 124 × 124 mm^2 as shown in Figure 23. The array size was increased by one row and one column at a time until satisfactory performance was achieved in terms of high gain within the frequency range of interest and relatively small size.

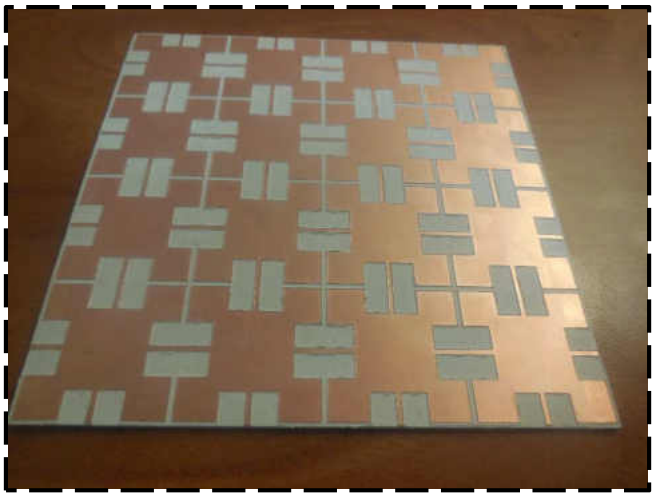

(a)

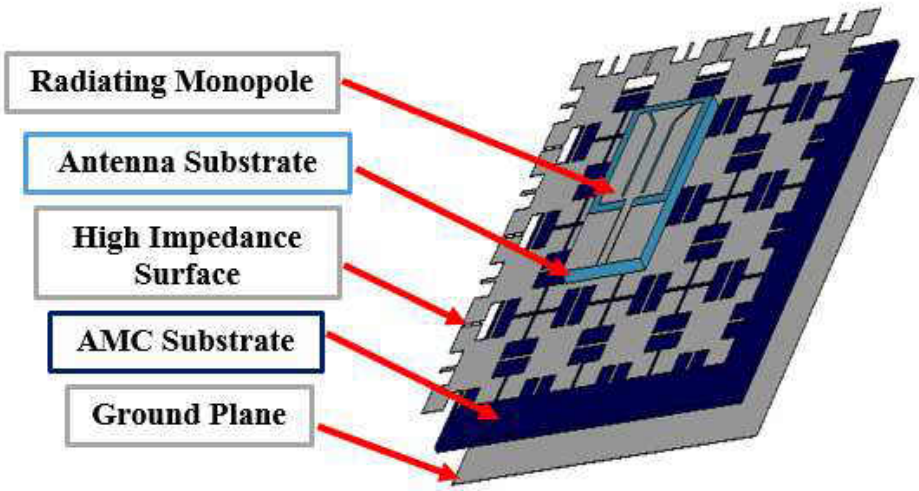

(b)

Figure 23: Monopole antenna on AMC ground plane, (a) proposed AMC ground plane, and (b) AMC antenna.

Normalized radiation patterns in E-plane and H-plane of AMC antenna based on simulation and measurement results at 2.45 GHz are shown in Figure 24 and Figure 25, respectively. However, the simulated cross-pole component in both planes isn't shown in

the figures since it has low value that is less than -40 dB in both planes. The measured AMC antenna gain is 6 dBi while the simulation-based value is 8.41 dBi, which means a reduction in the antenna gain by 2.41 dB. This reduction in the AMC antenna gain might be due to the accuracy of the fabrication process of both monopole antenna and AMC reflector.

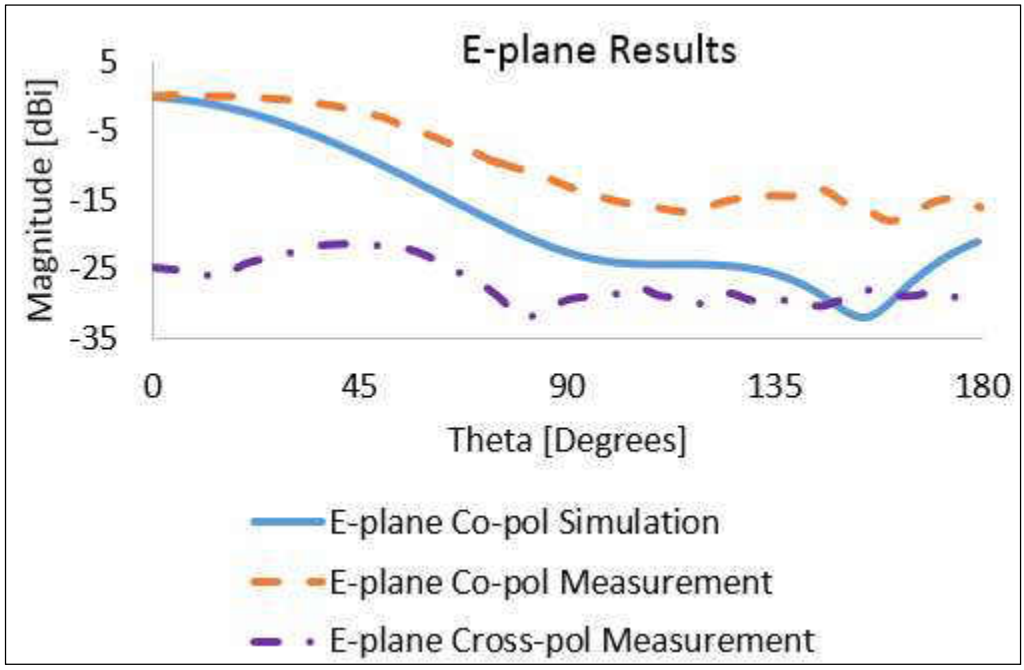

Figure 24: E-plane radiation pattern of AMC antenna at 2.45 GHz.

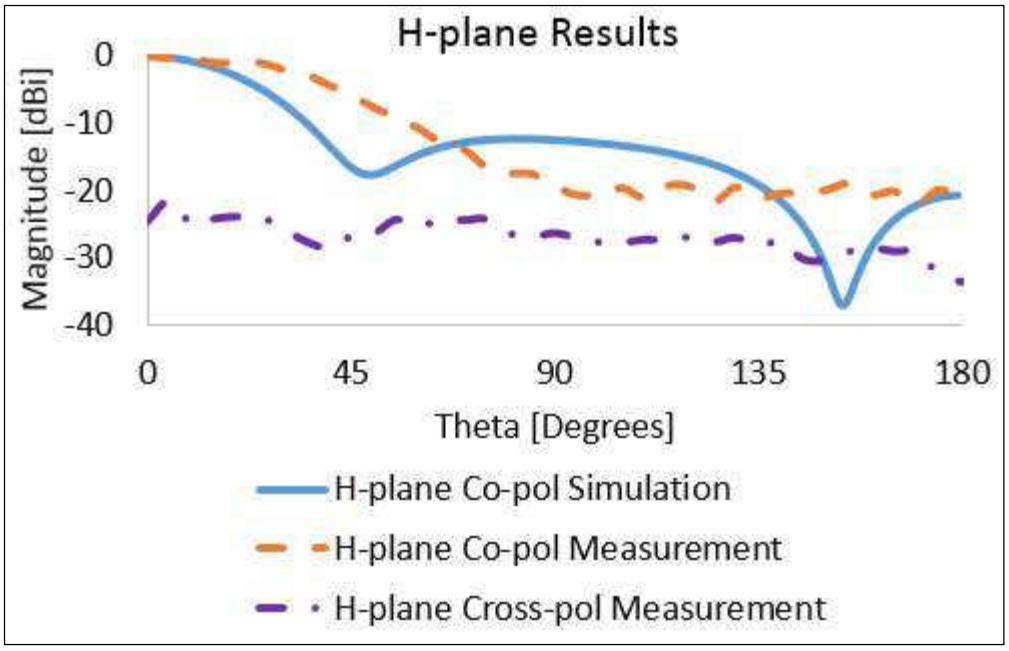

Figure 25: H-plane radiation pattern of AMC antenna at 2.45 GHz.

The effectiveness and usefulness of the AMC ground plane can be assessed by comparing the antenna gain with and without AMC reflector. A few important observations can be made from the results shown in Figure 26 and Figure 27. The 3D realized gain and the radiation patterns at 2.45 GHz for conventional monopole antenna and the antenna integrated on AMC based on the simulation results are shown in these figures. As it could be expected, the backward radiation of the antenna is reduced by AMC reflector, hence the gain is considerably improved. The antenna on AMC reflector has a realized gain of 8.41 dBi, while the conventional antenna shows 2.41 dBi gain. This means improvement of 75% in antenna gain using AMC reflector. Moreover, FBR is a critical factor in wearable antennas, which has been increased from 0.05 dB obtained value in the conventional monopole antenna to 16.15 dB using AMC ground plane. The radiation patterns at 2.45 GHz show the improvement in the antenna gain and directivity as well. Antenna directivity

has been increased from 2.67 dB to 10 dB using AMC ground plane. However, the power level of the cross pol components of the antenna's field has been increased using AMC reflector, which is usually undesirable.

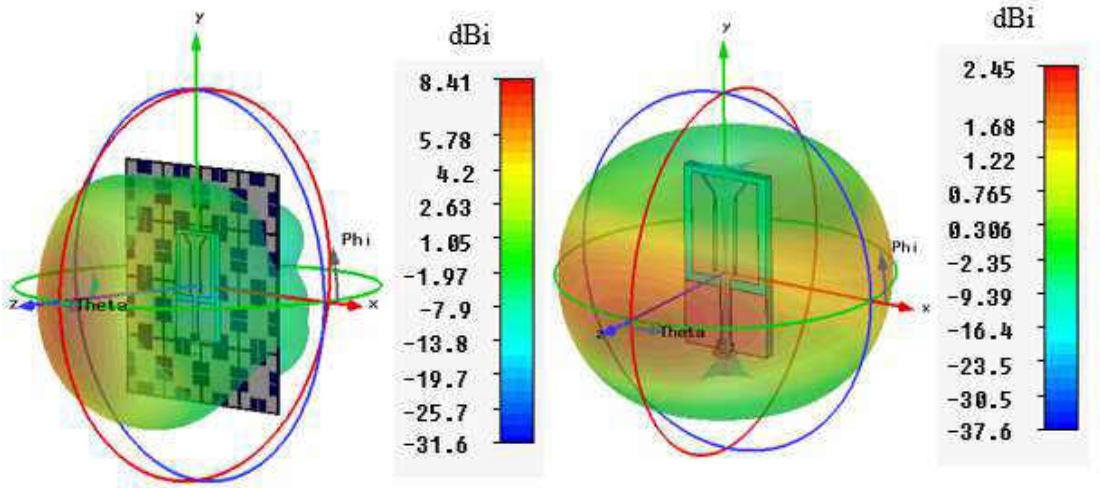

(a) (b)

Figure 26: 3D patterns at 2.45 GHz of (a) AMC antenna, and (b) monopole antenna.

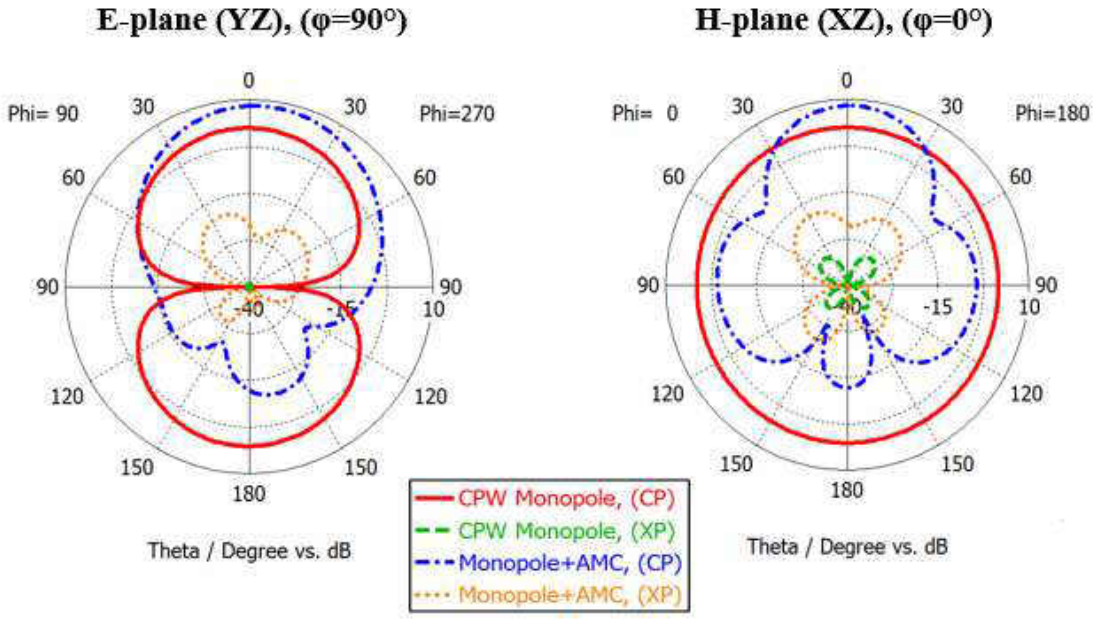

Figure 27: Simulated radiation patterns of monopole antenna with and without AMC reflector at 2.45 GHz: (left) E-plane and (right) H-plane; Co Polarization (CP) and Cross Polarization (XP).

Simulated reflection coefficient of the proposed AMC antenna is compared with the measured one as shown in Figure 28. It can be observed that there is an improvement in the impedance bandwidth based on the measurement results. The obtained -10 dB impedance bandwidth of AMC antenna based on simulation results is 47 MHz (2.433 GHz - 2.48 GHz) while the measured value is 1.05 GHz (2.3 GHz – 3.35 GHz).

On the other hand, a significant reduction in the impedance bandwidth of monopole antenna by about 2.53 GHz (based on measurements) due to the usage of AMC ground plane, which makes it hard to compare both results in the same figure. However, the obtained bandwidth of AMC antenna is obviously covering the ISM-2.45 GHz band with a good matching characteristics.

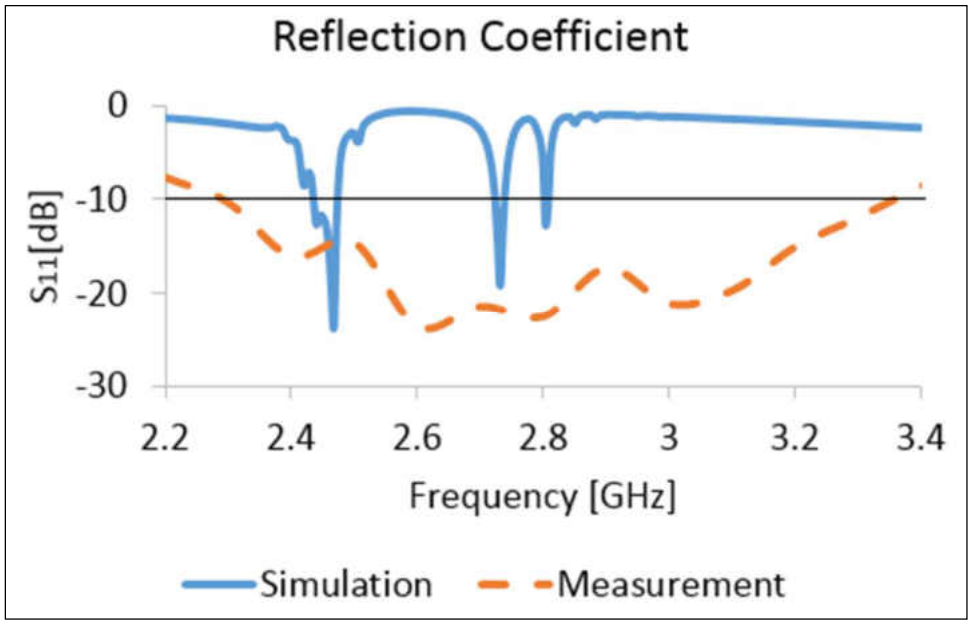

Figure 28: S_{11} results of AMC antenna.

Finally, results in terms of S_{11}, impedance bandwidth, antenna gain and FBR of monopole and AMC antennas are summarized and compared with those for microstrip

patch antenna based on simulation results in Table 3. Radiation patterns of E-plane and H-plane of the antennas are depicted in Figure 30. This gives a direct comparison of the performance of AMC antenna with that of a ground plane based antenna of the same dimensions. Microstrip antenna shown in Figure 29 is designed using a Pellon substrate of 3.6 mm thick. The results clearly demonstrate that AMC ground plane has effectively improved the antenna performance as compared with the conventional monopole antenna. Also, it is interesting to note that the antenna parameters for microstrip antenna are comparable to those for AMC antenna showing the significance of using AMC reflector as a ground plane.

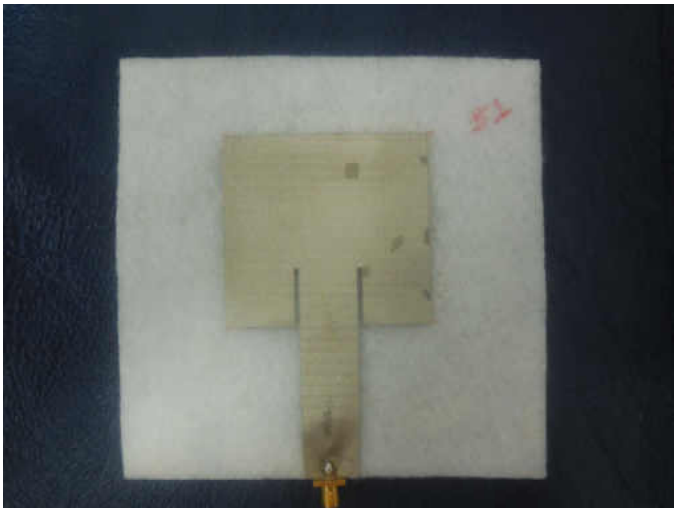

Figure 29: Geometry of microstrip antenna.

Table 3: Performance summary of monopole antenna with and without AMC ground plane and microstrip antenna based on simulation results.

Parameter	Monopole antenna	AMC antenna	Microstrip antenna
Size (L×W) (mm^2)	57×32	124×124	124×124
f_l (GHz)	1.76	2.43	2.42
f_h (GHz)	4.33	2.48	2.47
f_r (GHz)	2.16	2.46	2.46
Gain at f_r (dBi)	2.23	8.55	9.13
Gain at 2.45 GHz (dBi)	2.45	8.41	9.00
S_{11} at f_r (dB)	-16.92	-32.50	-19.99
S_{11} at 2.45 GHz (dB)	-15.80	-12.00	-16.34
FBR (dB)	0.05	16.15	18.00

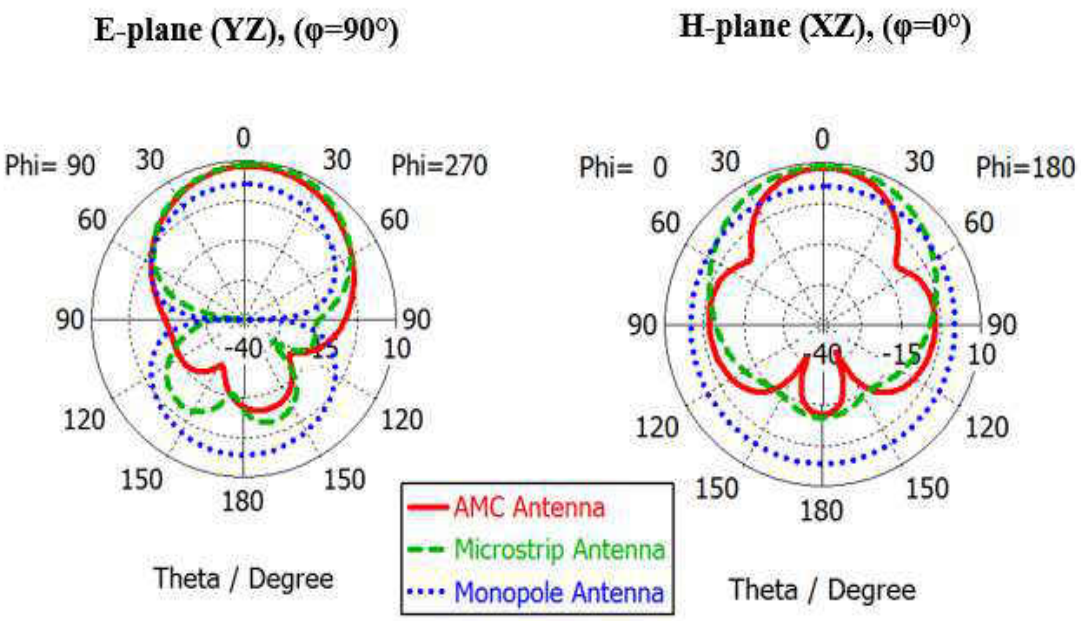

Figure 30: Simulated radiation patterns of monopole antenna, AMC antenna, and microstrip antenna at 2.45 GHz: (left) E-plane and (right) H-plane.

3.4 Specific Absorption Rate (SAR) Analysis

SAR is a measure of the rate at which the energy is absorbed by the human body when exposed to electromagnetic field. As the wearable antennas are designed for on body communications, which means that they are required to operate in the vicinity of the human body. Therefore, SAR analysis is an essential factor to evaluate the performance of the antenna (when it is working close to human body) and to consider the safety concerns and limits imposed by the most commonly used SAR standards. The maximum SAR limit according to IEEE standard is 1.6W/Kg for any 1g tissue, and for ICNIRP standard is 2W/kg for any 10g tissue. SAR of monopole and AMC antennas is analyzed using a three layered planar rectangular human body model, consisting of skin, fat and muscle tissue layers with overall surface size measures 200 × 200 mm^2, which is more than 3 times the surface area of the designed antenna.

This layered model can quite well represent most of the body regions, since the fat has similar properties to the bone tissue, and the electrical parameters of the muscle and many inner organs are alike [81]. A Pellon fabric layer ($\varepsilon_r = 1.08$, $\tan\delta = 0.008$) is located between the antenna and the body model during each simulation. The thickness and dielectric properties of the layers considered in the body model [82] are tabulated in Figure 31 and Table 4.

Figure 31: Three layered (skin-fat-muscle) human body model.

Table 4: Electrical properties of the body tissues at 2.45 GHz [82].

Parameter	Skin	Fat	Muscle
Relative Permittivity (ε_r)	38.01	5.28	52.73
Conductivity (σ) [S/m]	1.464	0.10452	1.7388
Thickness (*mm*)	3	7	60

Mass averaged SAR method (typically 1g and 10g) was used in the simulation for 1 Watt delivered power. For the considered input power, SAR values at 2.45 GHz for 1 g tissue are 16.46 W/Kg and 0.3327 W/Kg, for monopole antenna and AMC antenna, respectively. On the other hand, the obtained SAR for 10 g tissue are 9.39 W/Kg and 0.1663 W/Kg for monopole antenna and AMC antenna, respectively. These results are shown in Figure 32 and Figure 33, and summarized in Table 5. A significant reduction in SAR values has been achieved using AMC ground plane in compare to the original monopole antenna, also the obtained SAR values using AMC ground in the antenna design are above the specified rate allowed by the standards mentioned earlier.

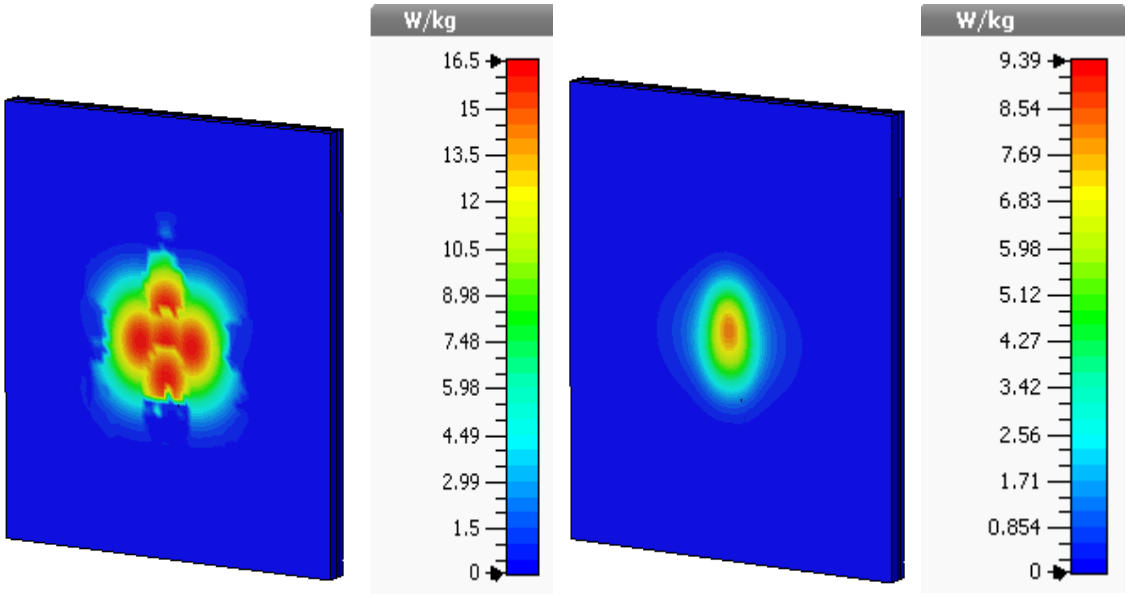

(a) (b)

Figure 32: Monopole antenna SAR [W/Kg] in the layered body model, (a) 1g and (b) 10g.

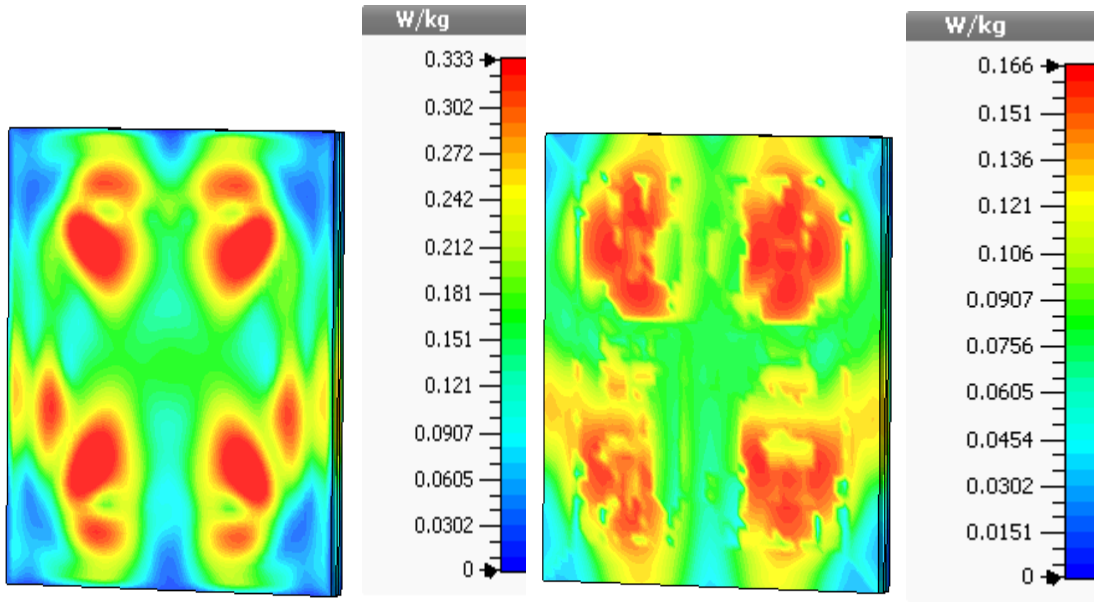

(a) (b)

Figure 33: AMC antenna SAR [W/Kg] in the layered body model, (a) 1g and (b) 10g.

Table 5: Simulated SAR of wearable antennas on the rectangular human body model at 2.45 GHz.

	Size (mm^2)	Distance from antenna to the body model (mm)	1 g tissue (W/Kg)	10 g tissue (W/Kg)	Point SAR (W)
Monopole Antenna	32.1×57	3.6	16.4600	9.3900	56.620
AMC Antenna	120×120	3.6	0.3327	0.1663	2.141

Mass averaged method is basically depending on the surface area of the human body model chosen for investigation, however this method is still valid to show the benefit of using AMC reflector in the antenna design of reducing the obtained SAR values. Maximum point SAR analysis is performed and the results are shown in Table 5 for monopole and AMC antennas to show a reduction in SAR value by 96% obtained in the AMC antenna.

CHAPTER 4

PERFORMANCE OF WEARABLE ANTENNAS UNDER BENDING CONDITIONS

4.1 Introduction

In wearable antenna systems, it is difficult to keep the antenna flat all the time, specially when the antenna is made out of textile material. Moreover, the wearable antenna is bent frequently due to the human body movements. Therefore, investigation of the antenna's performance on the dynamic body environment such under bending conditions due to the antenna conformability with the surface of the body is one of the important factors to be studied.

In this chapter, characteristics of the monopole antenna and AMC antenna under different bending conditions will be presented and compared with the conventional flat form of the antennas. Bending radii (R) chosen in our investigation are: 40 mm, 100 mm and 140 mm to approximate a human adult's arm, leg and thigh. Moreover, simulations were executed for two bending conditions: bending in YZ plane (E-plane of the antenna) and bending in XZ plane (H-plane of the antenna). Simulations were carried out in CST Microwave Studio software.

4.2 Performance of Monopole Antenna under Bending Conditions

Performance of monopole antenna was investigated in details in Section 2 of Chapter 3. However, the results assumed that the antenna was always in flat form. In this section antenna under different bending conditions will be investigated for their performance to observe the changes in the radiation performance and the limitations for any bending plane. Return loss and impedance bandwidth results for both E-plane and H-plane bending will be presented. Moreover, radiation characteristics and radiation pattern cuts at 2.45 GHz in the orthogonal planes of the antenna, namely E-plane and H-plane, will be presented as well. Geometry of the monopole antenna under bending conditions in H-plane and E-plane are shown in Figure 34.

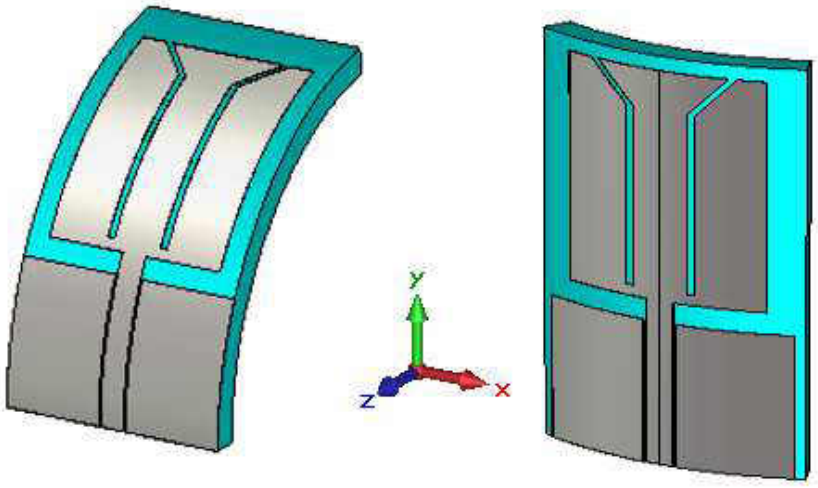

a b

Figure 34: Monopole antenna bent in (a) H-plane, and (b) E-plane.

4.2.1 Input Impedance Matching Results under Bending Conditions

Reflection coefficient results of monopole antenna under E-plane and H-plane bending conditions are depicted in Figure 35 and Figure 36, respectively. Moreover, the

deviations of the resonance frequency, input matching at 2.45 GHz and impedance bandwidth due to antenna bending are summarized in a graphical representations in Figure 37.

The antenna resonance frequency and impedance bandwidth under bending conditions in E-plane remain comparable with those obtained when the antenna is flat. Although the antenna bending in E-plane is performed at the center of the feeding line, a reduction in the reflection coefficient at 2.45 GHz is observed when the antenna is more and more bent (the bending radius is decreasing) to get to its maximum value of 3 dB when R= 40 mm.

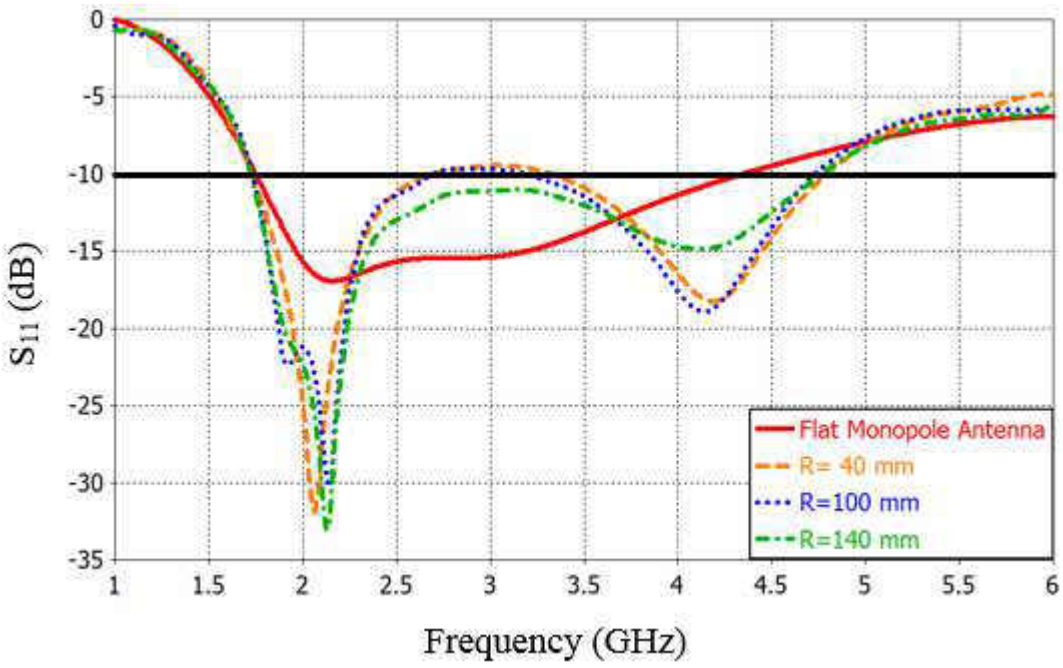

Figure 35: Simulated S_{11} of the monopole antenna bent with different radii in E-plane.

On the other hand, it can be observed that due to antenna bending in H-plane, the antenna resonant length get changed, and hence, the resonance frequency is shifted up. The

antenna resonance frequency is shifted from 2.16 GHz for flat condition to 2.87 GHz when R=140 mm, which represents the maximum observed shift in the resonance frequency. Considering the matching properties, the reflection coefficient at the resonance frequency and at 2.45 GHz has been improved compared to the obtained values when the antenna is flat. A reduction in the impedance bandwidth of about 500 MHz is observed due to H-plane bending conditions.

It is important to mention that there are no severe changes as the antenna is bent with different radii, thus, this antenna is still able to operate in the desired ISM-2.45 GHz band even under bending conditions.

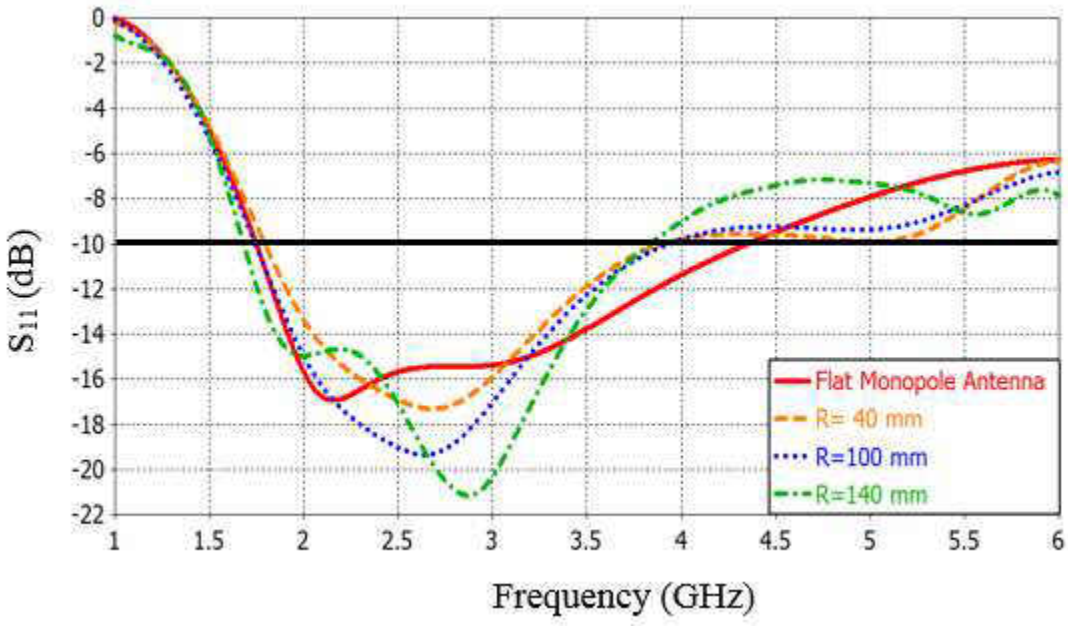

Figure 36: Simulated S_{11} of the monopole antenna bent with different radii in H-plane.

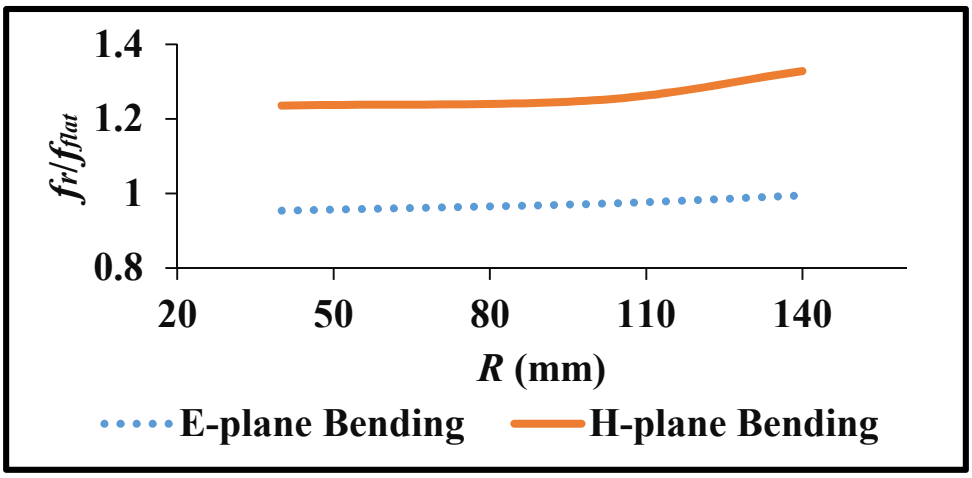

(a)

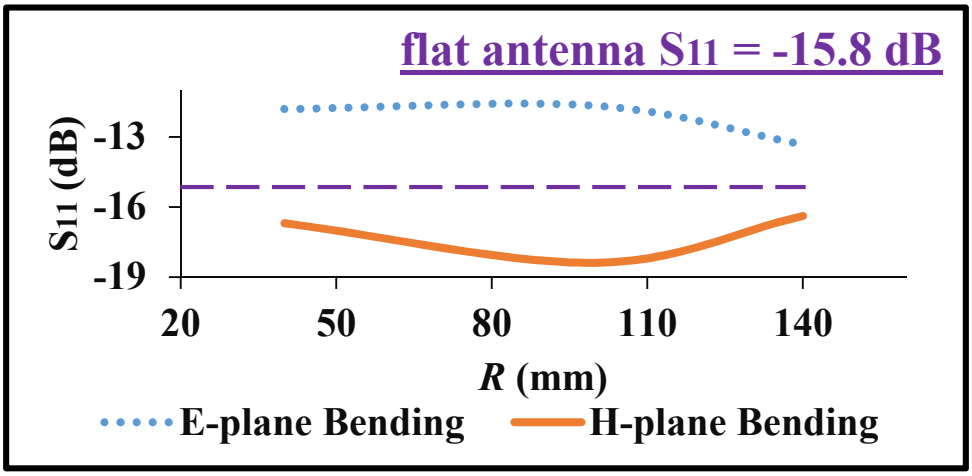

(b)

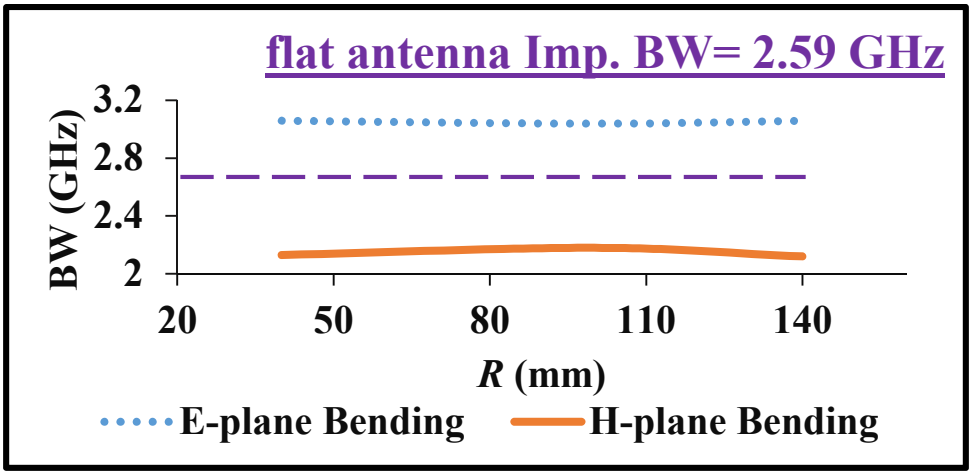

(c)

Figure 37: Effect of antenna bending on (a) resonance frequency, (b) reflection coefficient at 2.45GHz, and (c) impedance bandwidth.

4.2.2 Radiation Characteristics Results under Bending Conditions

The deviations of antenna gain, directivity, total efficiency, and FBR at 2.45 GHz due to antenna bending in both E-plane and H-plane are summarized in Figure 38 and Figure 39. Moreover, radiation patterns in E-plane and H-plane of the antenna at 2.45 GHz are presented in Figure 40 and Figure 41, respectively. The patterns for the unbending case are also observed to compare the variations in the pattern shape.

It is observed that the variations in the antenna gain and directivity due to antenna bending have an opposite trend in the bending planes. However, it is interesting to note that even the most bent antenna (R=40 mm) has got a moderate and acceptable gain and directivity at 2.45GHz. Considering the total efficiency, although the antenna efficiency got increased due to E-plane bending and decreased due to H-plane bending, it is noticed that in general as the antenna is bent more and more (the bending radius is decreased) the antenna efficiency is decreased. An improvement in the FBR is noticed due to bending in both planes.

Radiation patterns at 2.45GHz for E-plane bent antenna show less deviation in pattern shape in compare to the flat case. However, antenna bending in H-plane has remarkable effect on the radiation pattern shape. It is intuitively clear that antenna bending with R=40 mm and R=140 mm radii has a significant effect on increasing the cross polarization power level for H-plane patterns comparable with the planar case.

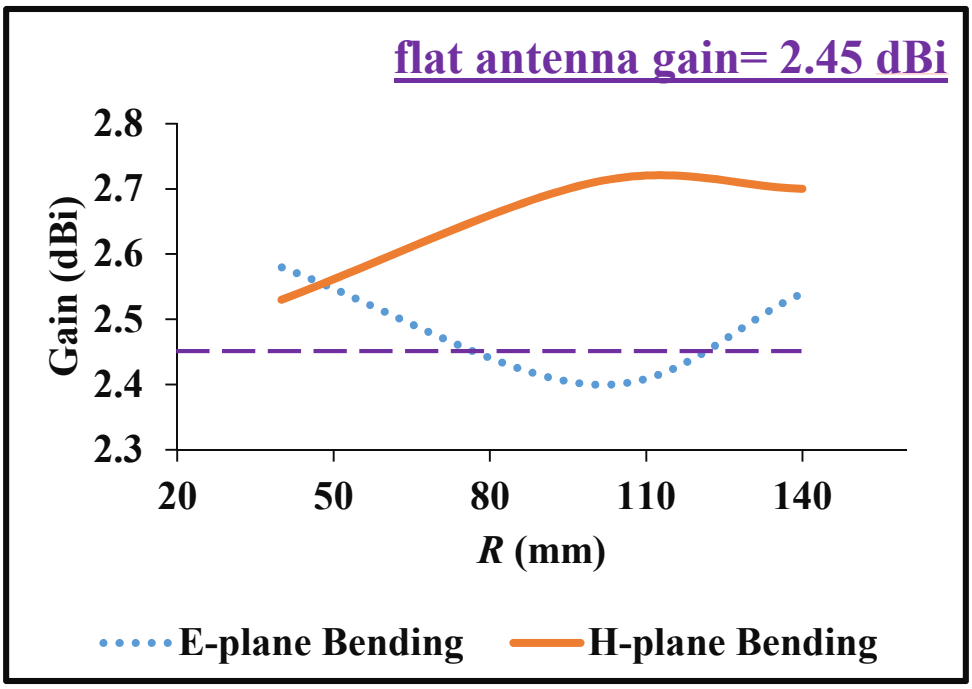

(a)

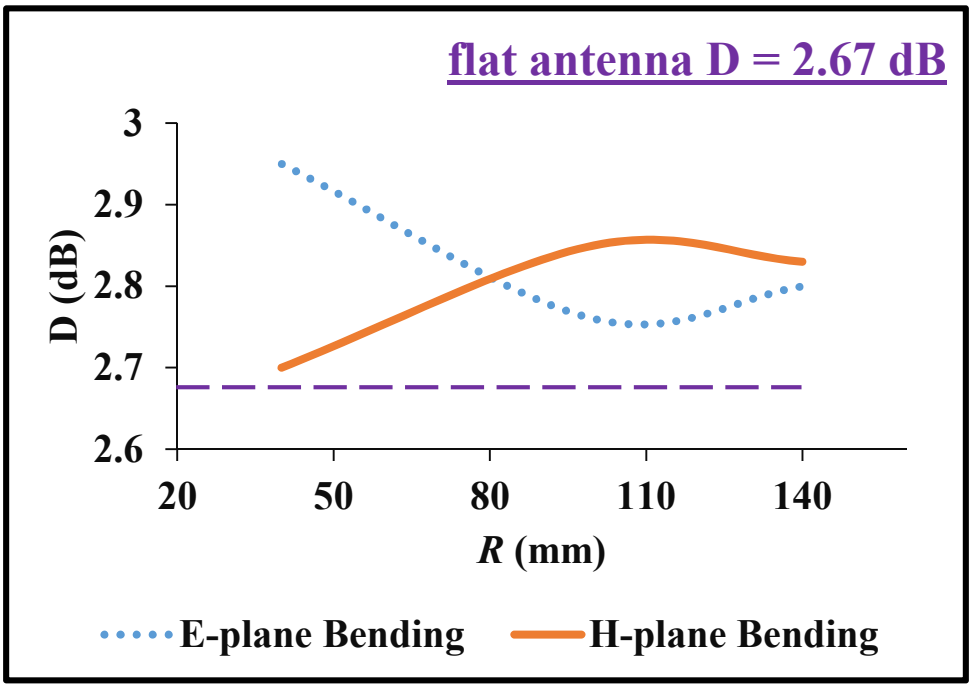

(b)

Figure 38: Effect of antenna bending on antenna (a) gain, and (b) directivity at 2.45 GHz.

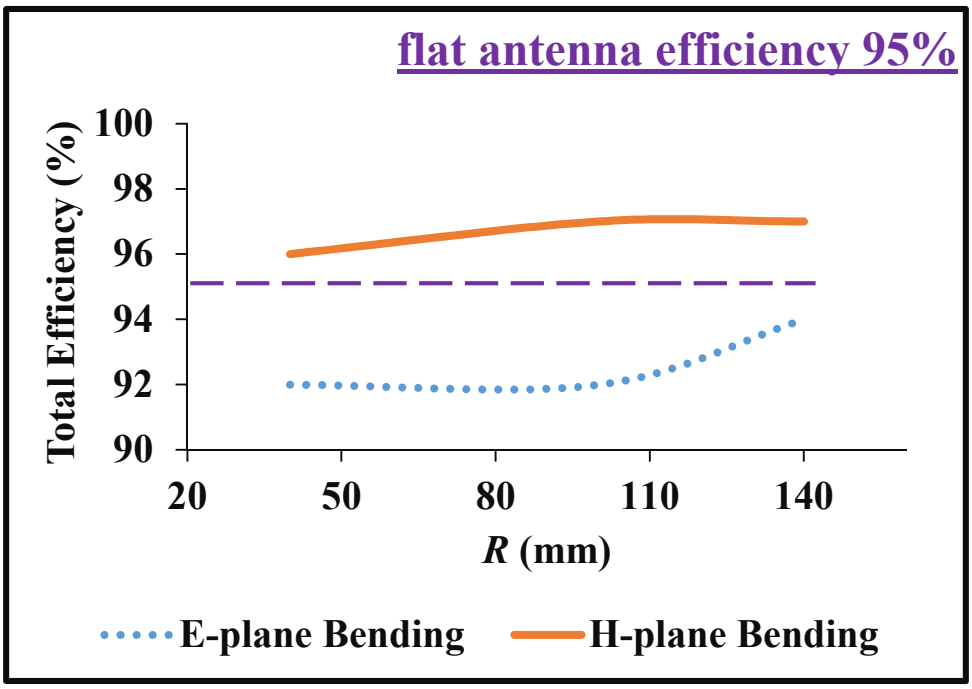

(a)

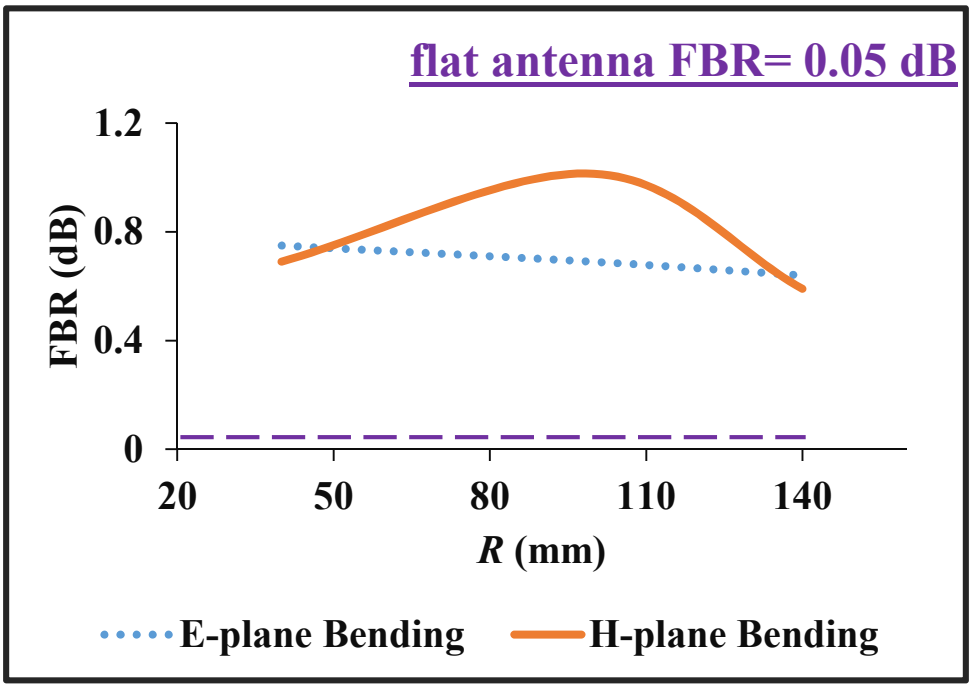

(b)

Figure 39: Effect of antenna bending on antenna (a) efficiency, and (b) FBR at 2.45 GHz.

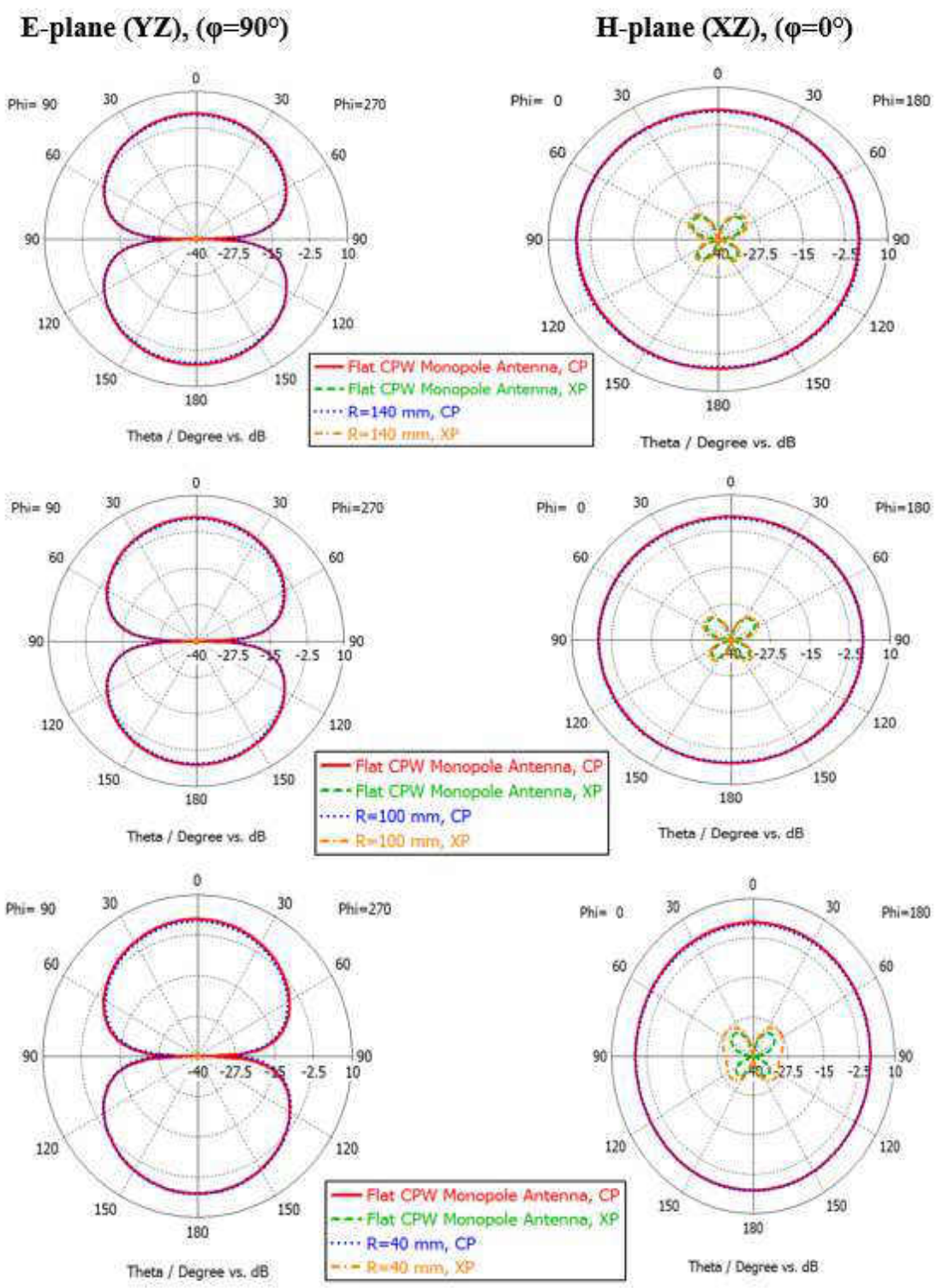

Figure 40: Simulated radiation patterns of monopole antenna bent along Y-axis at 2.45 GHz: (left) E-plane and (right) H-plane; Co Polarization (CP) and Cross Polarization (XP).

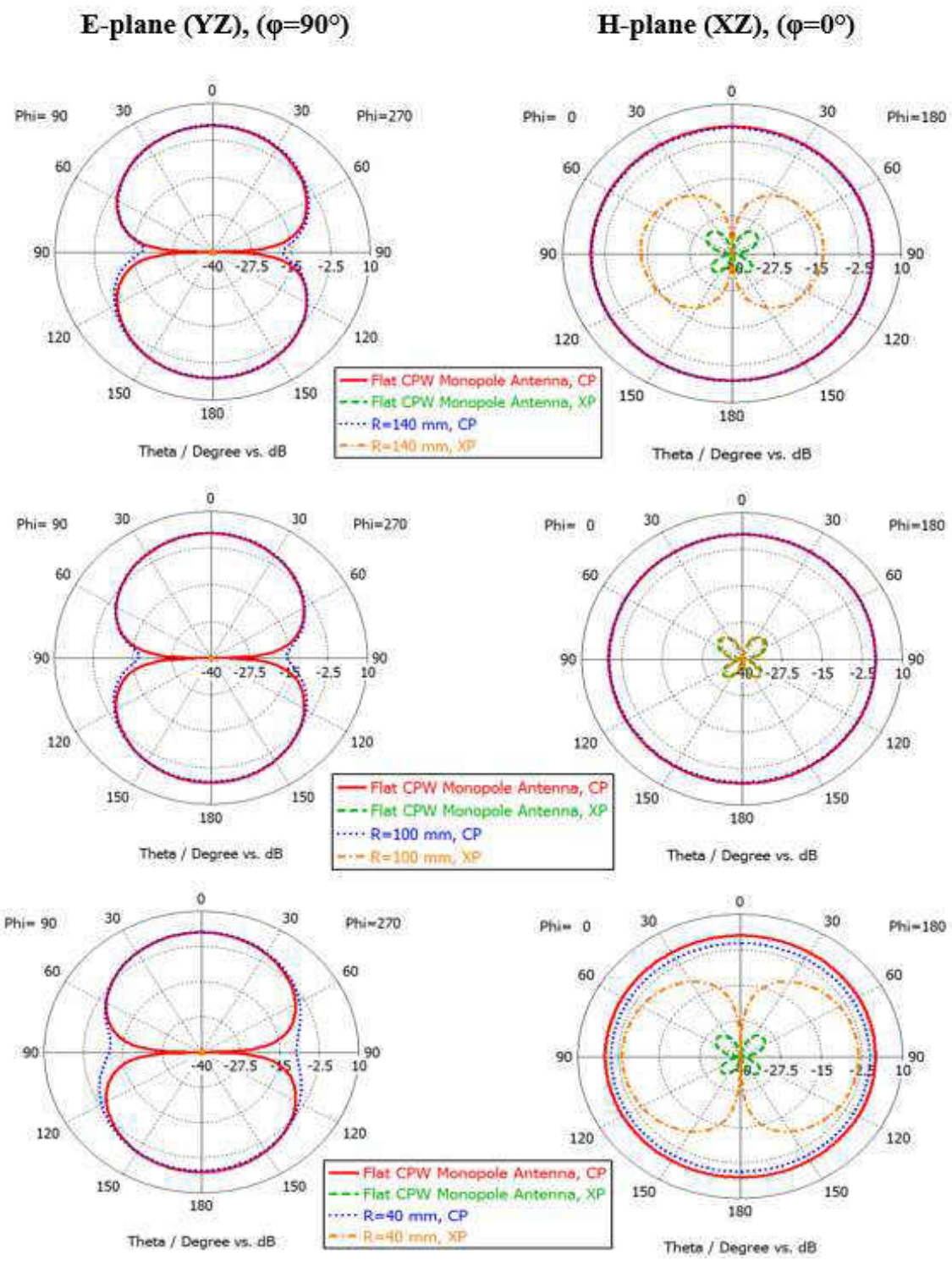

Figure 41: Simulated radiation patterns of monopole antenna bent along X-axis at 2.45 GHz: (left) E-plane and (right) H-plane; Co Polarization (CP) and Cross Polarization (XP).

4.3 Performance of AMC Antenna under Bending Conditions

Performance of AMC antenna was investigated in Section 3 of Chapter 3. However, the results assumed that AMC antenna was always in flat form. The following investigation aims to study the performance of AMC antenna under different bending conditions in both E-plane and H-plane. Input impedance matching and radiation characteristics in addition to the radiation patterns at the resonance frequency of AMC antenna under bending conditions will be presented to observe the changes in the performance of AMC antenna. Geometry of AMC antenna under bending conditions in H-plane and E-plane are shown in Figure 42.

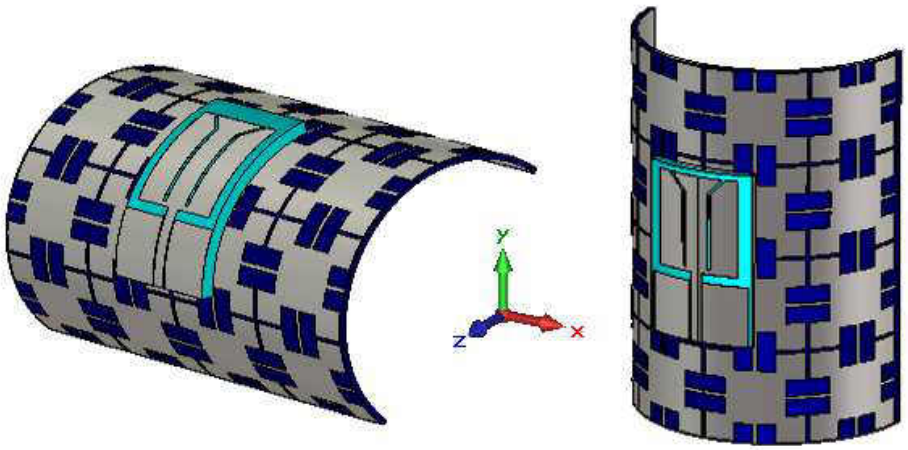

(a) (b)

Figure 42: AMC antenna bent in (a) H-plane, and (b) E-plane.

4.3.1 Input Impedance Matching Results under Bending Conditions

Reflection coefficient results of AMC antenna under bending conditions in both E-plane and H-plane are depicted in Figure 43 and Figure 44, respectively. Moreover, deviations of the resonance frequency, matching properties in terms of reflection

coefficient at the resonance of AMC antenna, and impedance bandwidth due to antenna bending in both E-plane and H-plane are summarized in Figure 45.

As can be seen the resonance frequency shifted toward lower values due to antenna bending in both planes, which is independent of bending radius since the resultant shift remains almost the same for all bending radii for both planes (E-plane and H-plane). AMC antenna bending effects on the matching properties have an opposite trend in the bending planes. However, the matching at the resonance frequency got improved compared to that obtained with the flat antenna.

Although, it is evident that there is no severe changes as the AMC antenna is bent with different radii in different planes, the observations suggest that when placing the AMC antenna on human body, it's better to align the antenna along the planar parts of the body surface in the E-plane, in order to avoid the reduction in the impedance bandwidth that might be insufficient for the communication in the ISM-2.45 GHz band.

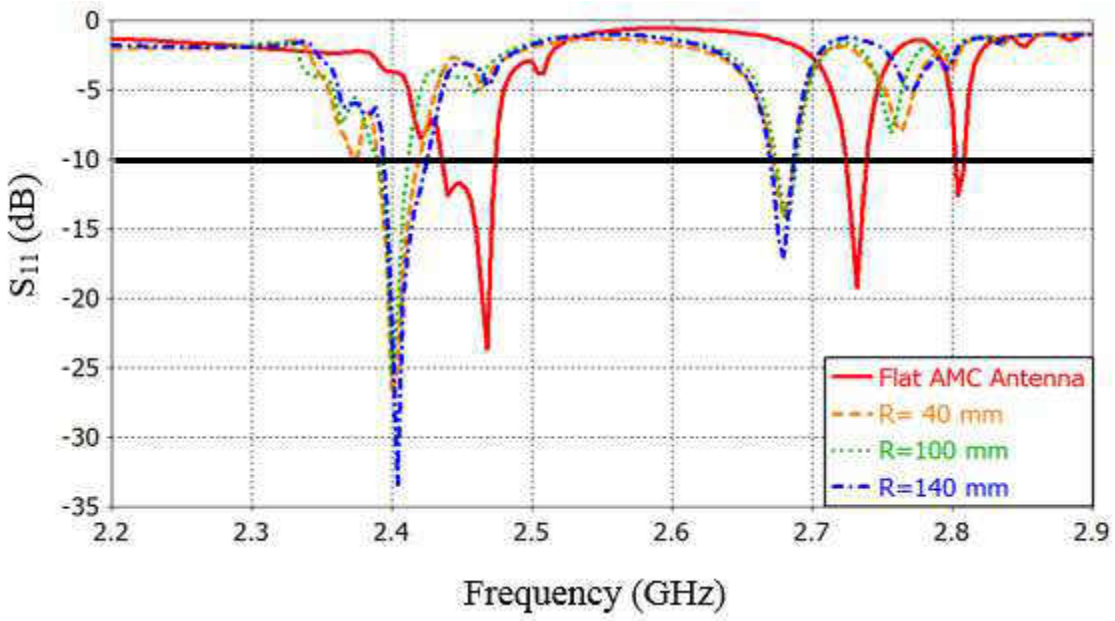

Figure 43: Simulated S_{11} of AMC antenna bent with different radii in E-plane.

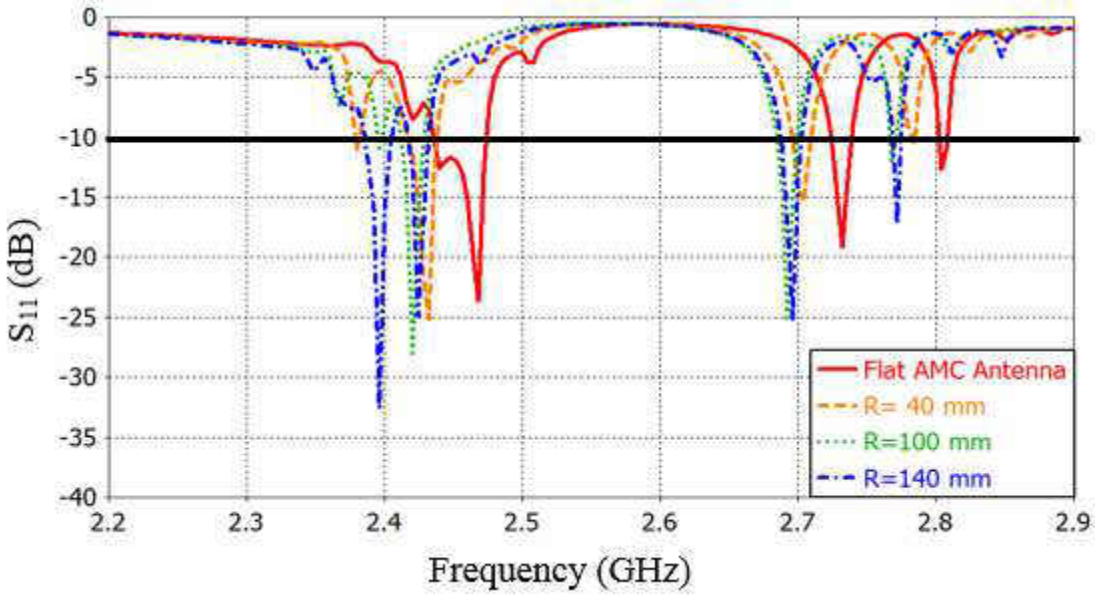

Figure 44: Simulated S_{11} of AMC antenna bent with different radii in H-plane.

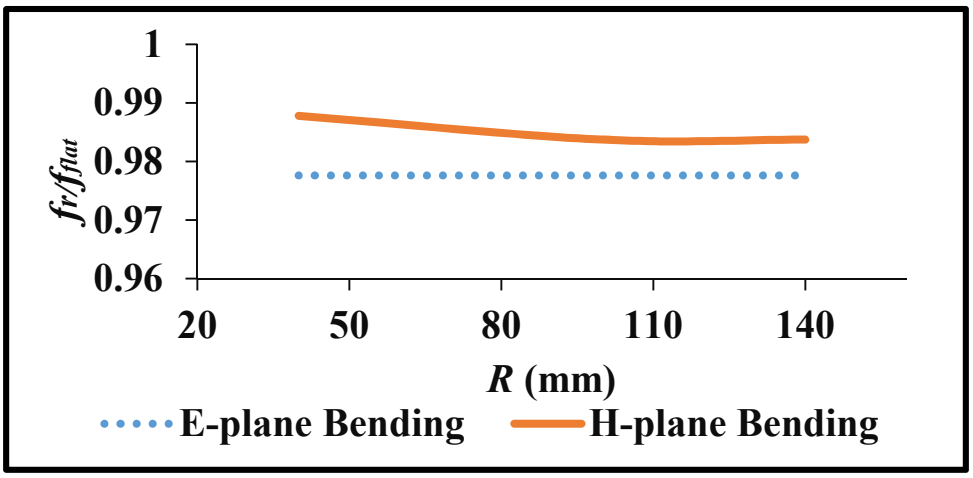

(a)

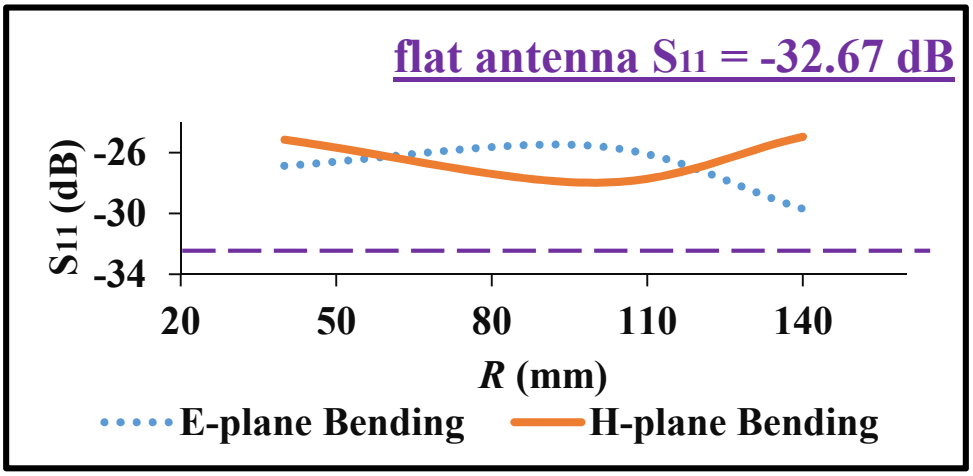

(b)

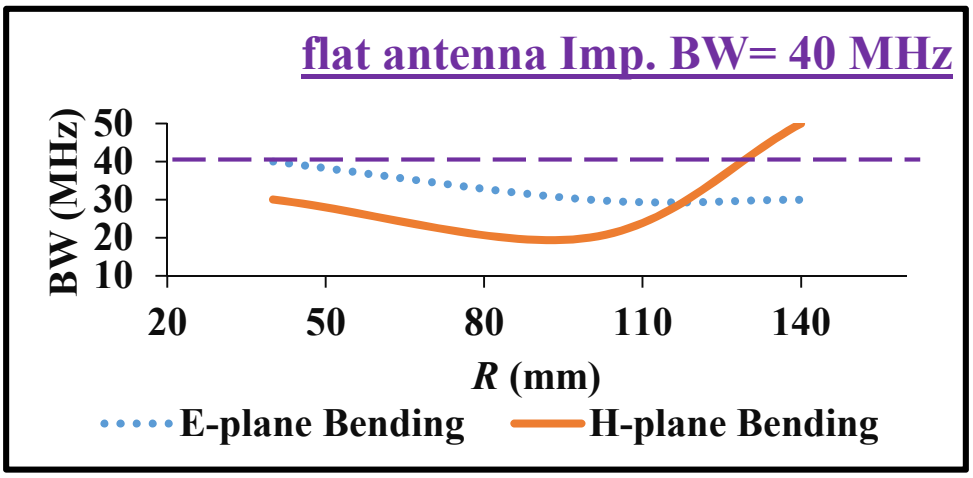

(c)

Figure 45: Effect of antenna bending on (a) resonance frequency, (b) reflection coefficient, and (c) impedance bandwidth.

4.3.2 Radiation Characteristics Results under Bending Conditions

Deviations of AMC antenna gain, directivity, FBR and total efficiency at the resonance frequency of AMC antenna due to bending conditions in both E-plane and H-plane are summarized in Figure 46 and Figure 47. Radiation patterns at the resonance frequency of the AMC antenna are presented for two orthogonal bending planes, E-plane and H-plane, in Figure 48. Patterns in E-plane and H-plane of the AMC antenna are provided for both bent and flat condition at the resonance frequency to compare the variations in pattern shape.

In general, it can be observed that as the AMC antenna is bent more and more (bending radius gradually decreased), the antenna gain and directivity are decreased due to both E-plane and H-plane bending conditions. Due to E-plane bending, a reduction in the antenna gain is noticed for R= 40 mm bending case while enhancement in the gain is obtained for R=100 mm and R=140 mm bending cases as compared to the flat antenna. On the other hand, a reduction in the antenna gain is observed due to H-plane bending in all bending cases with the least value of 3.4 dB obtained for R=100 mm bending case. The power level of the cross-pol components has been increased under bending conditions in H-plane, while less deformation achieved due to bending in E-plane, as shown in the radiation patterns figures.

Moreover, due to E-plane bending, FBR was increased for R=100 mm and R=140 mm bending cases while dropped for R=40 mm bending case. However, H-plane bending has an opposite impact on the obtained FBR values. An improvement in the antenna efficiency is obtained due to E-plane bending while it remains comparable to the flat antenna efficiency for H-plane bending. Thus, it can be concluded that H-plane bending

puts a limit on the performance of this antenna and for better results it must be ensured that antenna is not bent too much along this plane.

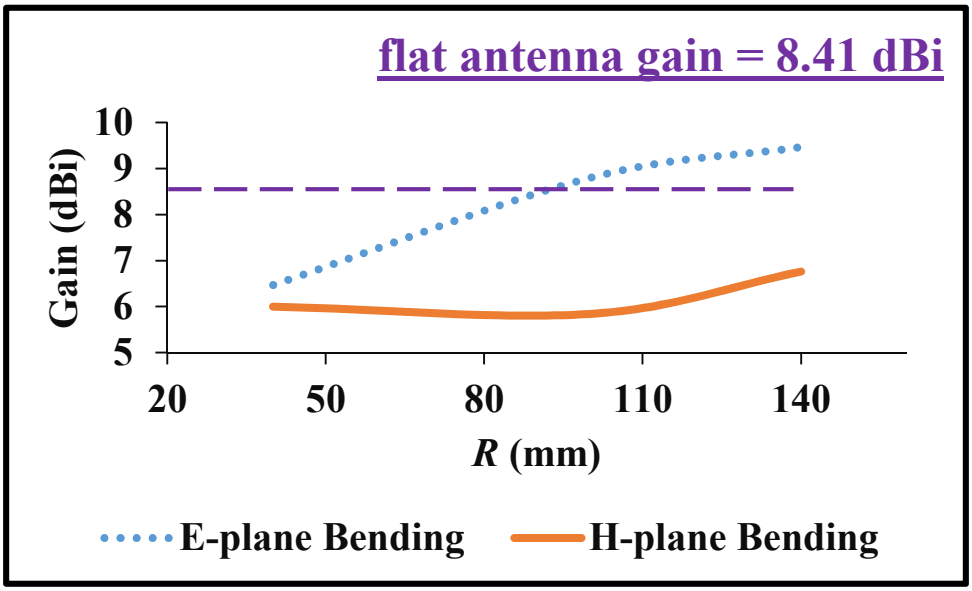

(a)

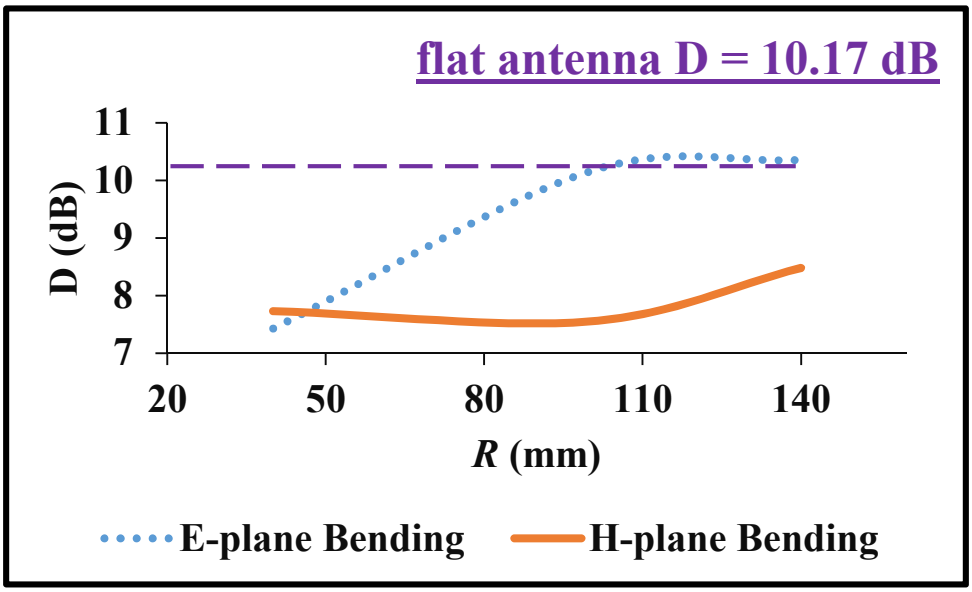

(b)

Figure 46: Effect of AMC antenna bending on antenna (a) gain, and (b) directivity at f_r.

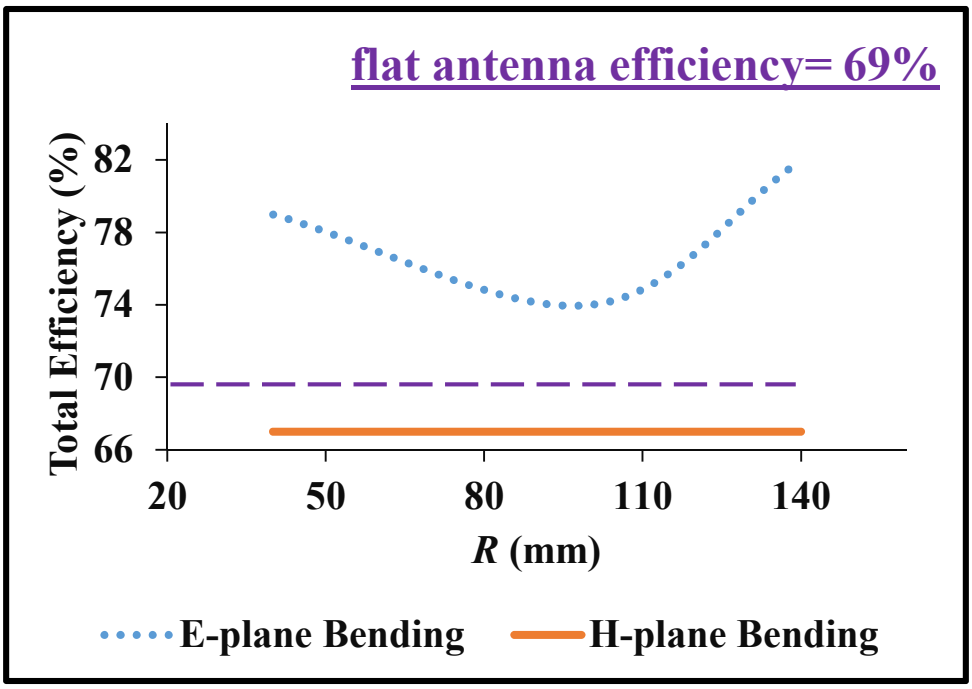

(a)

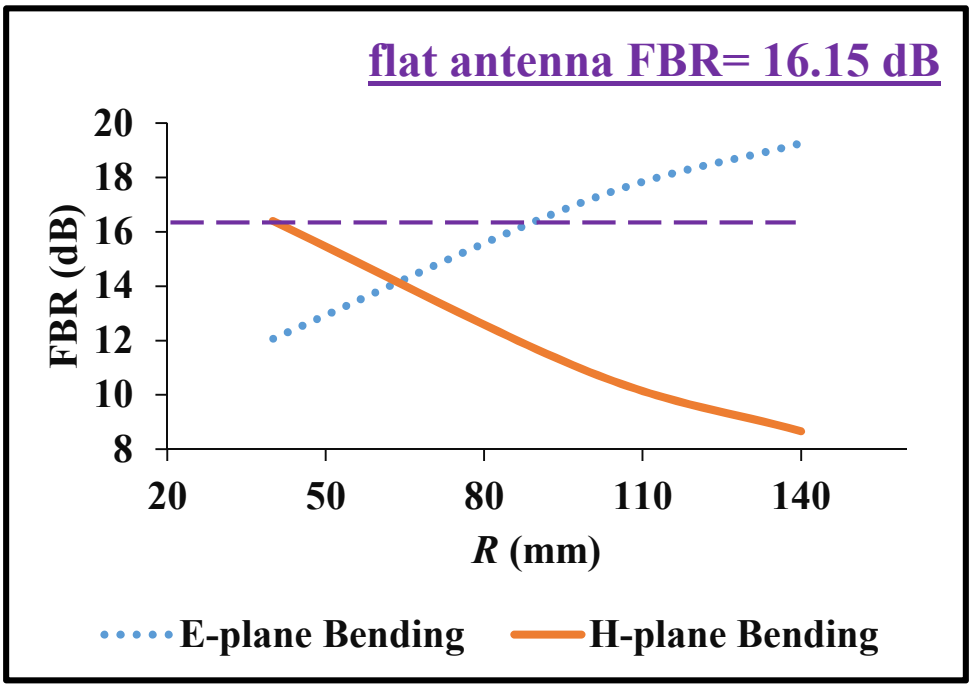

(b)

Figure 47: Effect of AMC antenna bending on antenna (a) efficiency, and (b) FBR at f_r.

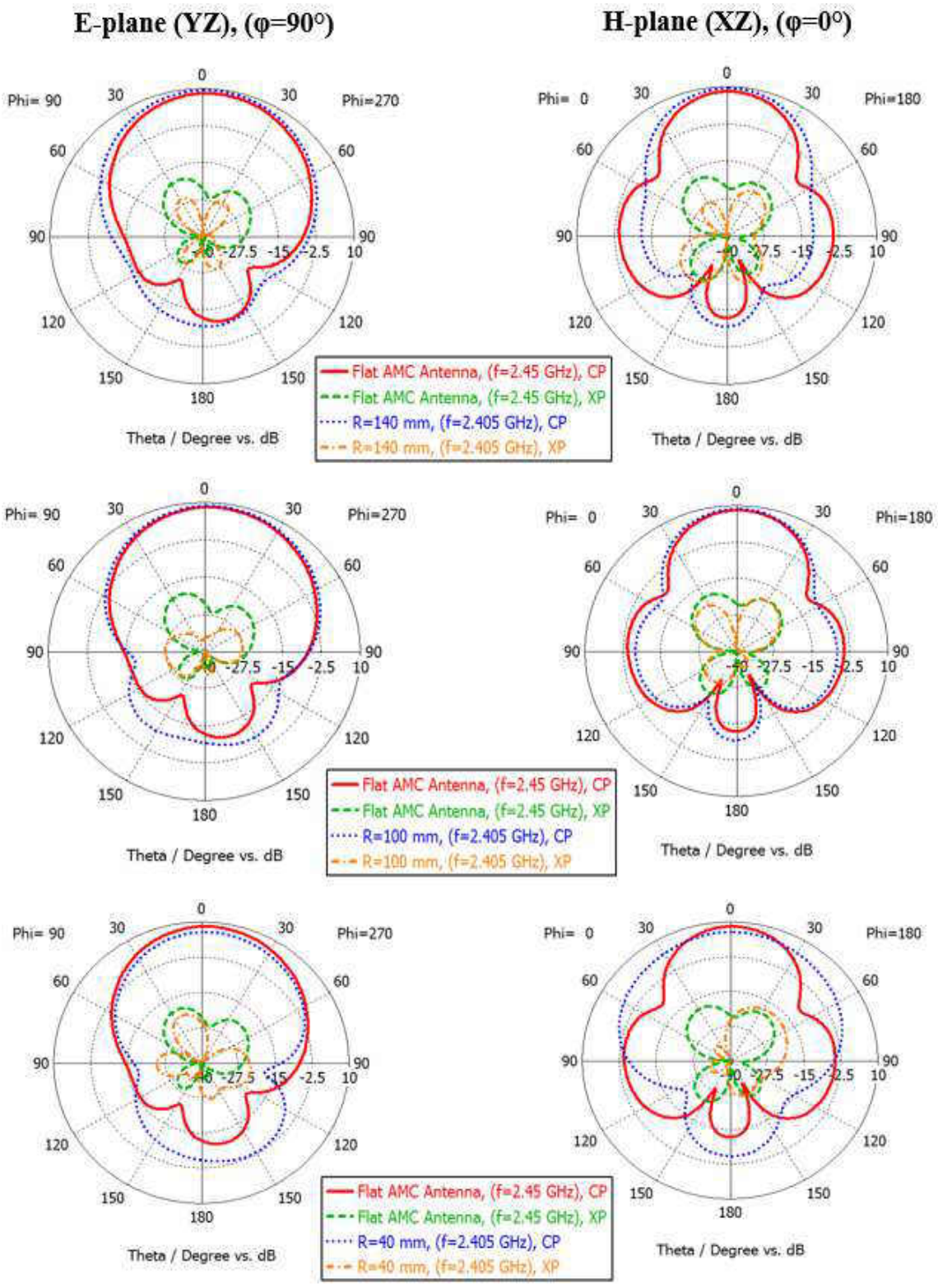

Figure 48: Simulated radiation patterns of AMC antenna bent along Y-axis at f_r: (left) E-plane and (right) H-plane; Co Polarization (CP) and Cross Polarization (XP).

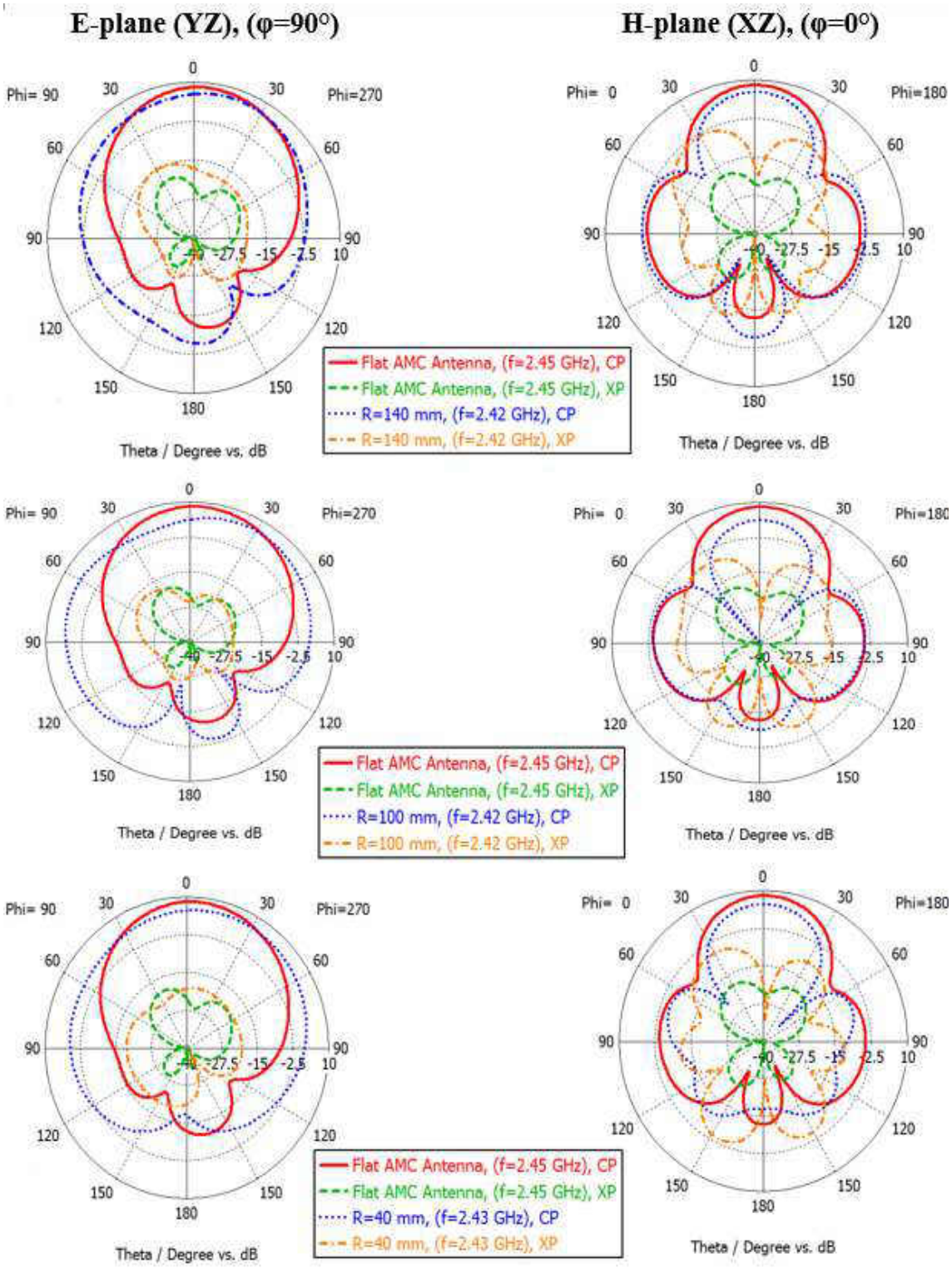

Figure 49: Simulated radiation patterns of AMC antenna bent along X-axis at f_r: (left) E-plane and (right) H-plane; Co Polarization (CP) and Cross Polarization (XP).

CHAPTER 5

PERFORMANCE OF WEARABLE ANTENNAS UNDER CRUMPLING CONDITIONS

5.1 Introduction

In practical situations for wearable antenna integrated on a textile or flexible substrate for on-body communication applications, the antenna will be subject to several shape distortion forms, which is due to the uncertain and varying form of garment surface during wearer's daily activities. Bending is a fundamental shape distortion for wearable antennas. However, the antenna shape distortion will be more complicated in practical situation. For example, as a person takes up various positions, the antenna not only will bend but also will crumple, particularly near joints. Thus, the general properties of antenna crumpling will be potential particularly with respect to any change in resonance frequency, gain, and impedance matching characteristics. Performance of CPW-fed monopole textile and AMC antennas is studied under crumpling conditions. Simulations were carried out in CST Microwave Studio software.

5.2 Performance of Monopole Antenna under Crumpling Conditions

In practical environment, many types of crumpling may take place. Four typical forms of crumpling are selected as the main investigation targets in this research into two

perpendicular planes of the antenna, namely XZ (H-plane) and YZ (E-plane) planes. Antenna performance, specifically S_{11} and impedance bandwidth results under crumpling conditions will be presented. Moreover, radiation characteristics and radiation patterns in the orthogonal planes of the antenna, namely E-plane and H-plane, under crumpling conditions will be presented, as well, to observe the changes in the radiation characteristics of the antenna and the limitations for any crumpling plane.

5.2.1 Monopole Antenna Crumpling in E-plane

Figure 50 presents four typical crumpling cases that are selected for investigation in E-plane of the antenna. Crumpling profile is defined by: crumple depth *N*, and crumple period *M*. A central part of the antenna of 0.5 mm is kept flat for the feeding requirements imposed by the simulation program.

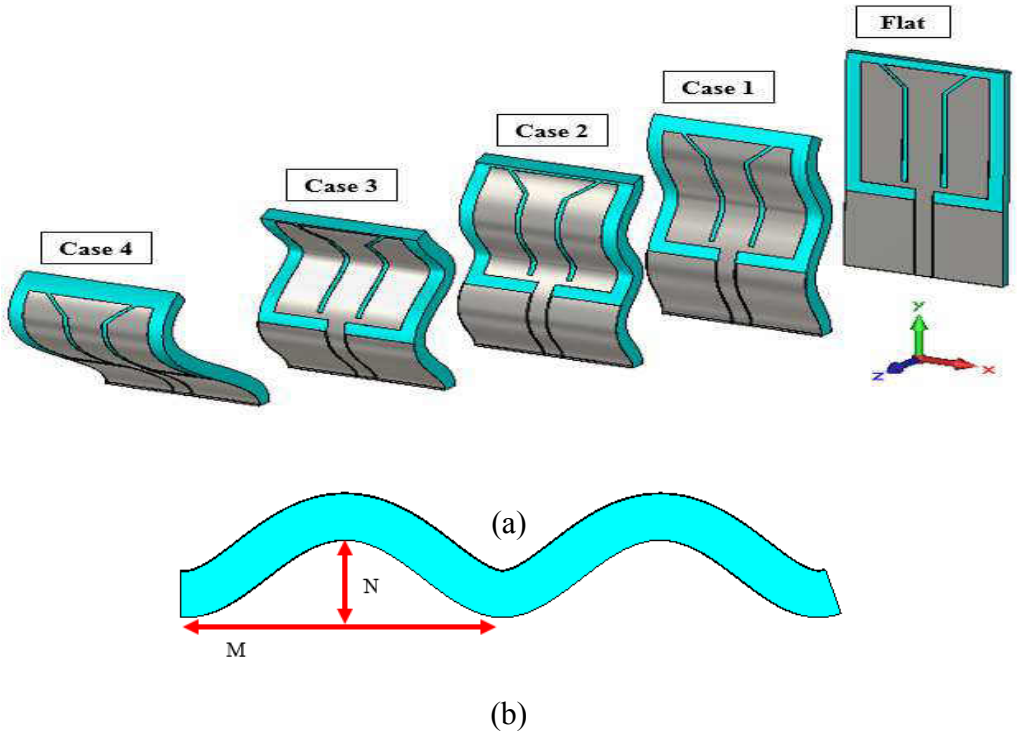

Figure 50: CPW-fed monopole antenna crumpled in E-plane, (a) crumpling cases, and (b) crumpling profile.

In crumpling Case 1, antenna aperture is reduced from 57×32.1 mm^2 (flat) to 54.37×32.1 mm^2, with *M* and *N* values of 6 mm and 31 mm, respectively. In Case 2 a further reduction in the antenna aperture is obtained to 50.25×32.1 mm^2, where *M* value is reduced to 24 mm, while in Case 3 *N* value is increased to 11 mm to result in a further reduction in the antenna aperture to 44.92×32.1 mm^2. Moreover, antenna aperture of 44.92×32.1 mm^2 is achieved in crumpling Case 4, which shows the least reduction in the antenna aperture, where *M* and *N* values are 60 mm and 35 mm, respectively. On human body, Cases 1 and 2 are typical for general clothing distortion most likely to appear when the antenna is placed on the chest or the back of the wearer. Crumpling cases 3 and 4 are to be observed near the knee or the elbow joints. Dimensions of the antenna in each crumpling case are described in Figure 51 and Table 6.

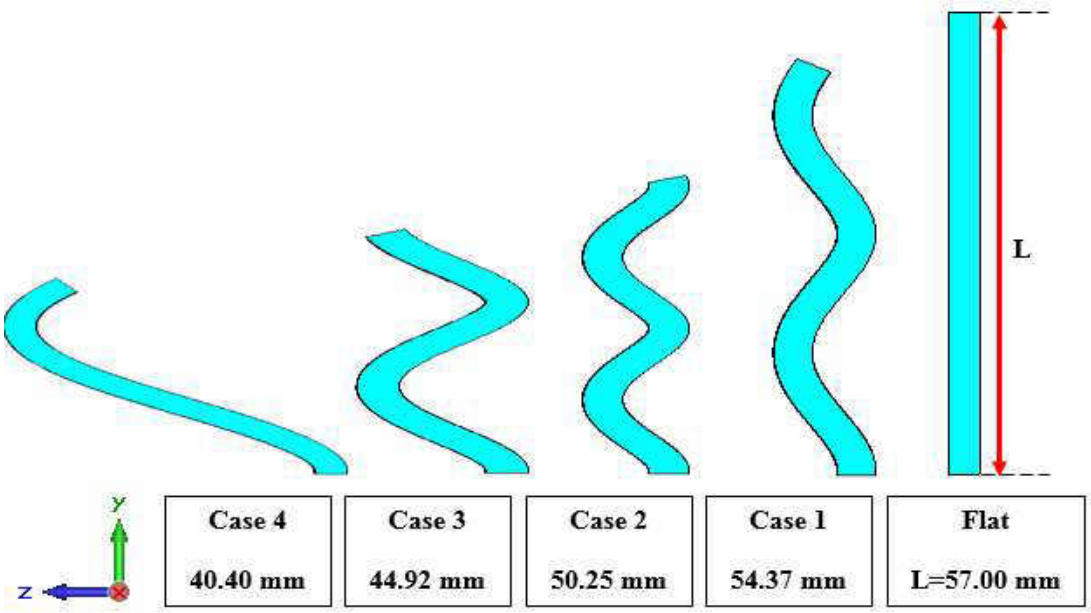

Figure 51: Side view of a crumpled CPW monopole antenna (Y- axis).

Table 6: Dimensions of the crumpled monopole antenna in YZ plane.

	Antenna Length (mm)	*N* (mm)	*M* (mm)
Flat	57.00	-	-
Crumpling Case 1	54.37	6.00	31.00
Crumpling Case 2	50.25	6.00	24.00
Crumpling Case 3	44.92	11.00	31.00
Crumpling Case 4	40.40	35.00	60.00

5.2.1.1 Input Impedance Matching Results under Crumpling Conditions in E-plane

Figure 52 shows the deviations of the resonance frequency, input matching and impedance bandwidth due to antenna crumpling in E-plane along with the antenna in flat form. It can be observed that the antenna resonance frequency is shifted up under different crumpling conditions. Crumpling in Case 3 shows the most significant shift in the resonance frequency out of the designed ISM-2.45 GHz band from 2.16 GHz (flat) to 3.13 GHz. However, acceptable matching in terms of the return loss being under -10 dB is obtained within the designed band under different crumpling conditions.

It's worth mentioning that although the antenna is bent almost 90° in crumpling Case 4, the impedance bandwidth is only slightly reduced with the resonance frequency shifting up by just 58 MHz, while the obtained impedance bandwidth under in crumpling Cases 1, 2, and 3 remains comparable with that obtained when antenna is flat.

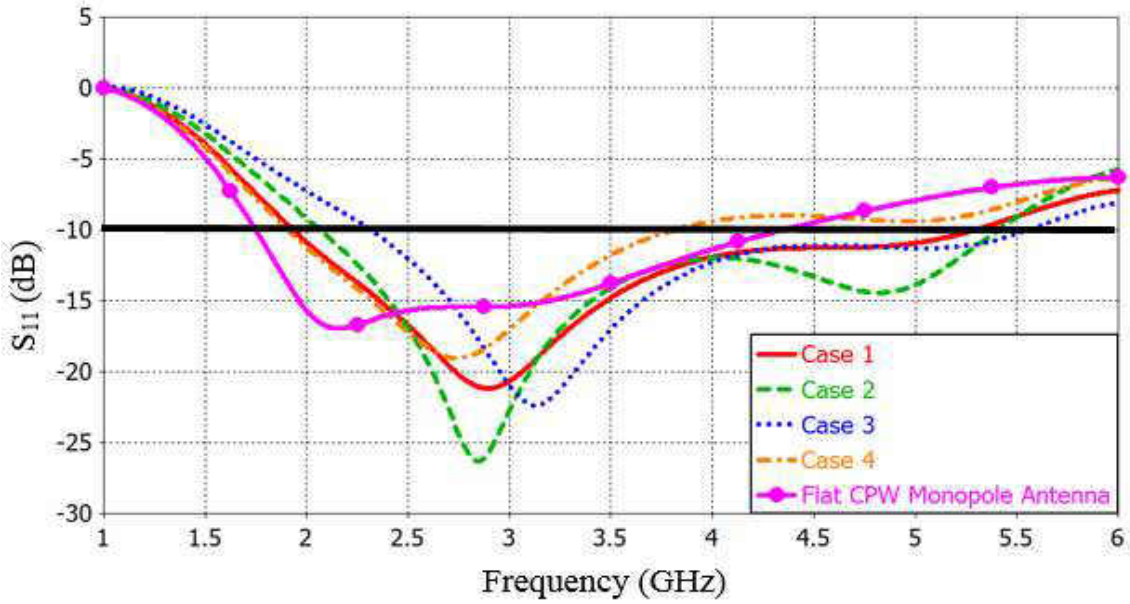

Figure 52: Simulated S_{11} of CPW monopole antenna crumpled in E-plane.

5.2.1.2 Radiation Characteristics under Crumpling Conditions in E-plane

Radiation characteristics in terms of antenna gain, directivity, and total efficiency at 2.45 GHz are summarized in Table 7 under crumpling conditions, which shows that the overall antenna performance remains acceptable and comparable with the antenna in flat form.

Table 7: Radiation characteristics summary of the crumpled monopole antenna in E-plane.

	Gain (dBi)	Directivity (dB)	Efficiency (%)
Flat	2.45	2.67	95
Crumpling Case 1	2.45	2.66	95
Crumpling Case 2	2.32	2.50	96
Crumpling Case 3	2.21	2.58	92
Crumpling Case 4	2.32	2.50	96

Figure 53 and Figure 54 show the radiation patterns in E-plane and H-plane of the antenna at 2.45 GHz under four E-plane crumpling cases. Patterns of the antenna in flat form are also presented to compare the variations in the radiation patterns. For E-plane patterns, crumpling shows changes in the pattern shape, showing increase in the beamwidth with a slight reduction in the forward direction power level. In Case 4, E-plane pattern shows some distortions, primarily by rotation of the main lobe direction by 60°. For H-plane patterns, crumpling increases the radiated power level of the cross-pole components by about 29.16 dB in the most severe crumpling Case 4.

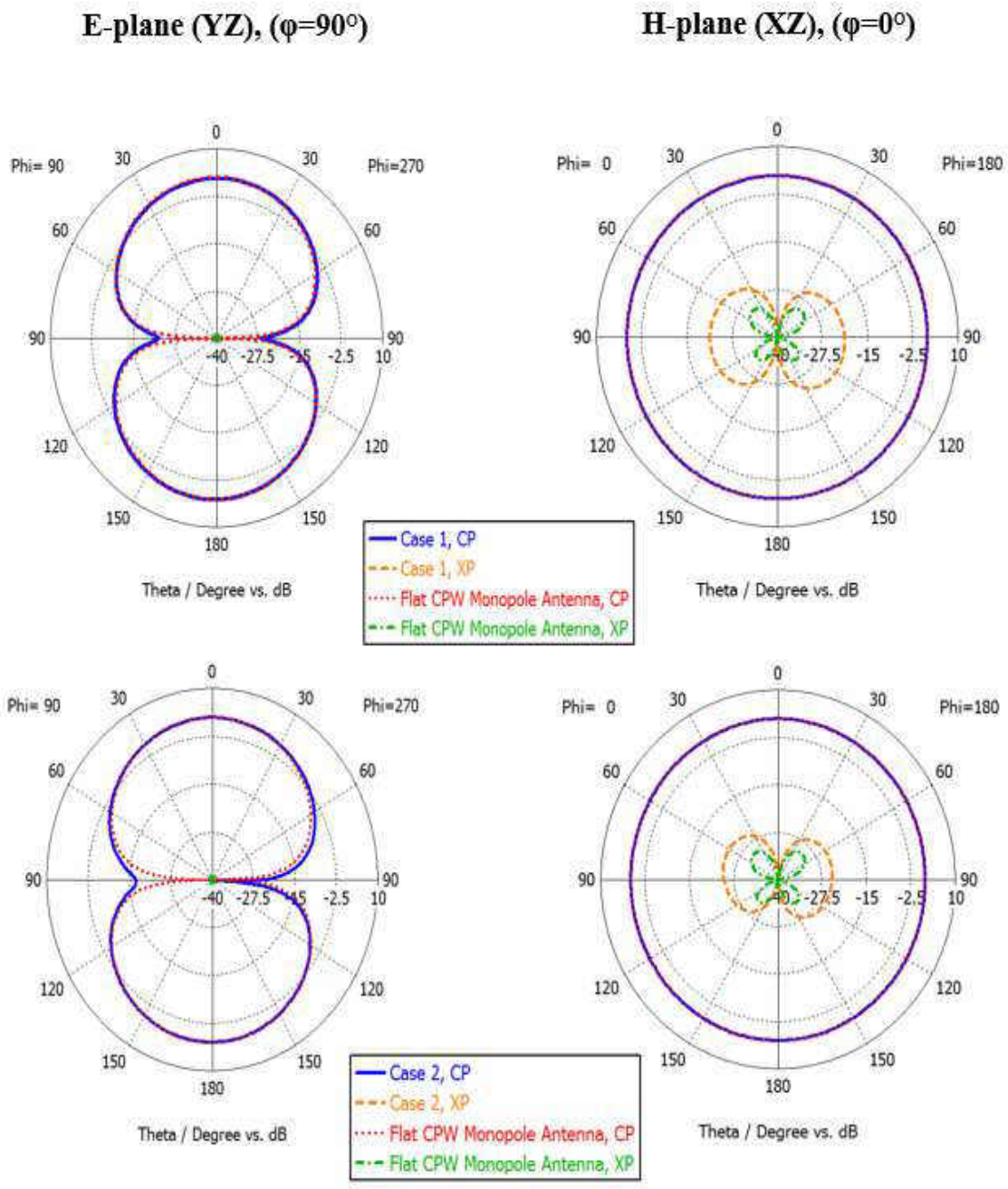

Figure 53: Simulated radiation patterns of monopole antenna crumpled along Y-axis for Cases 1 and 2 at 2.45 GHz: (left) E-plane, and (right) H-plane; Co Polarization (CP), and Cross Polarization (XP).

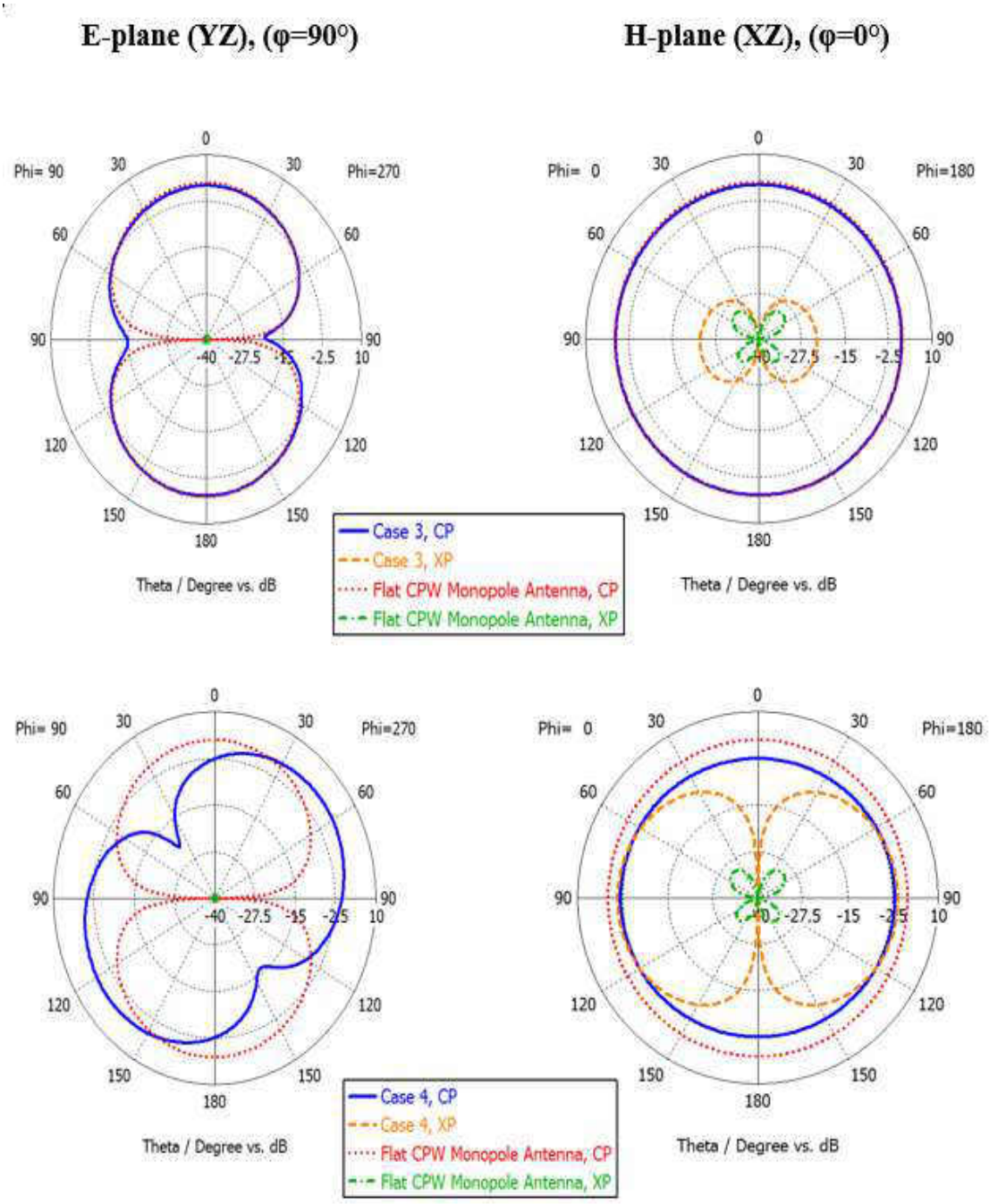

Figure 54: Simulated radiation patterns of monopole antenna crumpled along Y-axis for Cases 3 and 4 at 2.45 GHz: (left) E-plane, and (right) H-plane; Co Polarization (CP), and Cross Polarization (XP).

5.2.2 Monopole Antenna Crumpling in H-plane

Figure 55 shows four cases of antenna crumpling, similar to those chosen for crumpling investigation in E-plane, along with the same definition of the crumpling profile. Antenna crumpling starts from the center of the feeding line for H-crumpling. In Case1, antenna aperture is reduced from 57×32.1 mm^2 when flat, to 57×30 mm^2. As the crumpling length reduces to 24 mm in Case 2 the antenna aperture measures 57×31 mm^2, then further reduced to 57×27.13 mm^2 in Case 3. The antenna is sharply bent in Case 4 with aperture size of 57×25.70 mm^2.

On human body, Cases 1 and 2 are typical for general clothing distortions most likely to appear when the antenna is placed on the chest or the back of the wearer. Crumpling Cases 3 and 4 are to be observed near the knee or the elbow joints. Dimensions of the antenna in each crumpling Case are described in Figure 56 and Table 8.

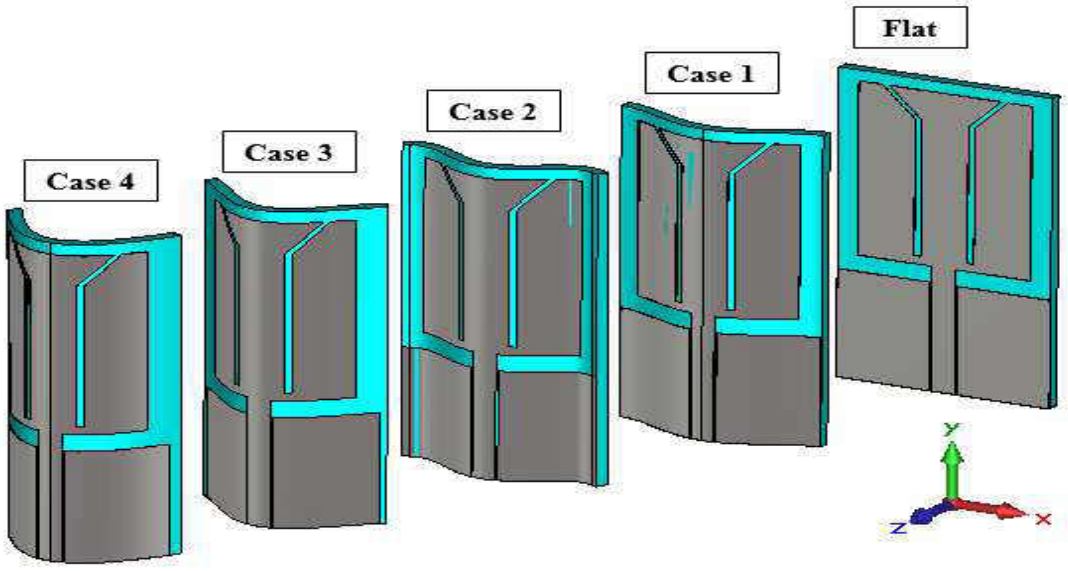

Figure 55: CPW-fed monopole antenna crumpled in H-plane.

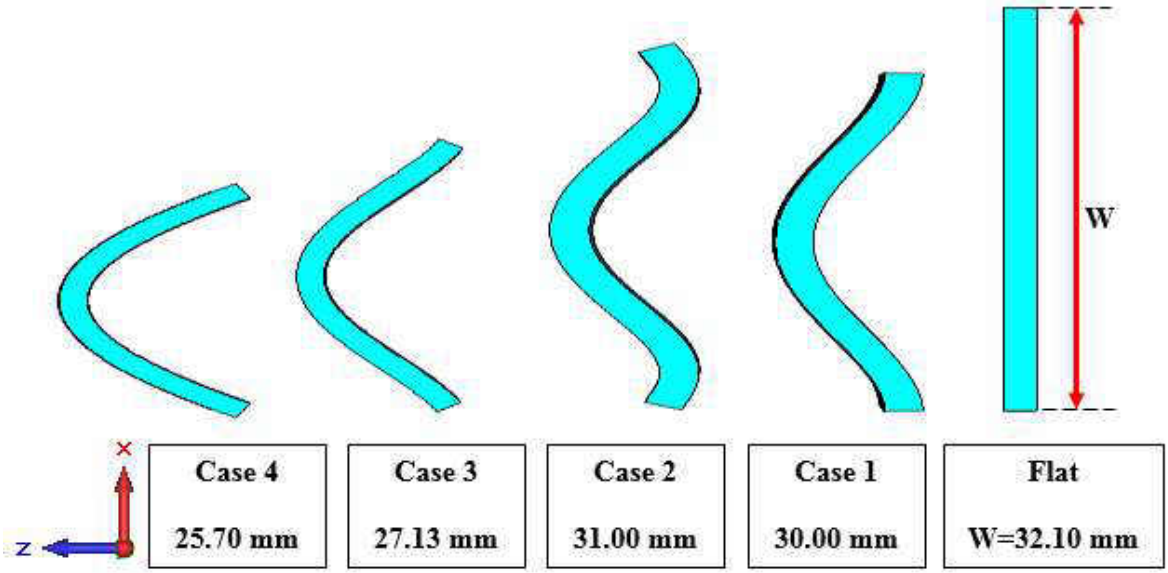

Figure 56: Side view of crumpled CPW monopole antenna (X- axis).

Table 8: Dimensions of the crumpled antenna in H-plane.

	Antenna Width (mm)	*N* (mm)	*M* (mm)
Flat	32.10	-	-
Crumpling Case 1	30.00	6.00	31.00
Crumpling Case 2	31.00	6.00	24.00
Crumpling Case 3	27.13	11.00	31.00
Crumpling Case 4	25.70	35.00	60.00

5.2.1.3 Input Impedance Matching Results under Crumpling Conditions in H-plane

Reflection coefficient results of antenna crumpling in H-plane is illustrated in Figure 57. In general, effect of antenna crumpling on the antenna input matching characteristics is variant among different crumpling cases. Changes in the antenna resonance frequency are much more significant and variant due to crumpling in H-plane than crumpling in E-plane, as discussed earlier. In Case 2, the resonance frequency moved

from 2.16 GHz (for flat antenna) to 5.12 GHz while it moved down in Case 3, to 1.51 GHz. Impedance bandwidth is increased in crumpling Cases 1, 2, and 3 with the maximum value obtained in Case 2 to cover from 1.67 GHz to 5.65 GHz while the flat antenna covers from 1.76 GHz to 4.35 GHz. On the other hand, impedance bandwidth is halved in Case 4 as compared with the antenna in flat form. However, acceptable matching, where the reflection coefficient being below -10 dB, is obtained within the ISM-2.45 GHz band in all crumpling cases.

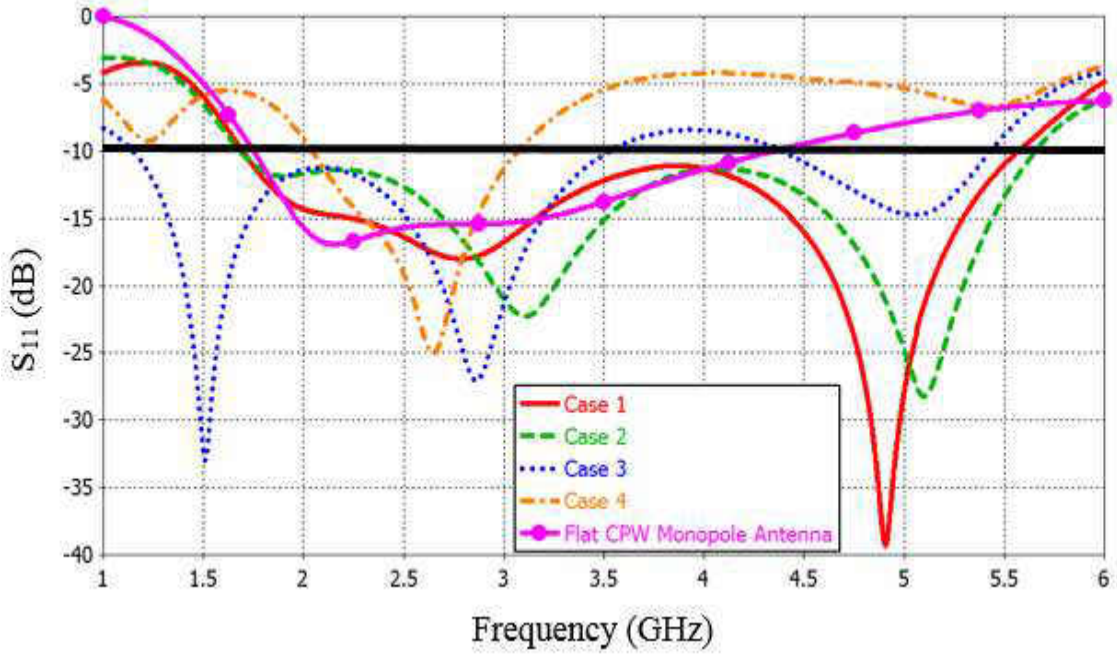

Figure 57: Simulated S_{11} of CPW monopole antenna crumpled in H-plane.

5.2.1.4 Radiation Characteristics under Crumpling Conditions in H-plane

Radiation characteristics in terms of antenna gain, directivity, and total efficiency at 2.45 GHz are summarized in Table 9 under crumpling conditions. Also, Figure 58 and Figure 59 show the radiation patterns in E-plane and H-plane of the antenna at 2.45 GHz

for four crumpling cases in H-plane. Radiation patterns of the antenna in flat form are also presented to compare the variation in radiation patterns.

Crumpling in Case 3 shows a high reduction in the total efficiency down, from 95% for the flat antenna to just 82%. Also, it was shown through the impedance matching results that Case 4 had a poor reflection coefficient at 2.45 GHz, which reflected in a total efficiency of just 61%. Moreover, Case 4 is suffering from a reduction in the antenna gain. Antenna gain is 72% less than of that obtained when the antenna is flat, which can be seen through the radiation pattern results. Radiation patterns of Cases 1 and 2 were affected much less than the other cases. A part of the increase in the power level of the cross-pole components, antenna forward gain remained close to the flat antenna.

Table 9: Radiation characteristics summary of the crumpled monopole antenna in H-plane.

	Gain (dBi)	Directivity (dB)	Efficiency (%)
Flat	2.45	2.67	95
Crumpling Case 1	2.53	2.85	93
Crumpling Case 2	2.62	2.85	95
Crumpling Case 3	2.00	2.86	82
Crumpling Case 4	0.69	2.86	61

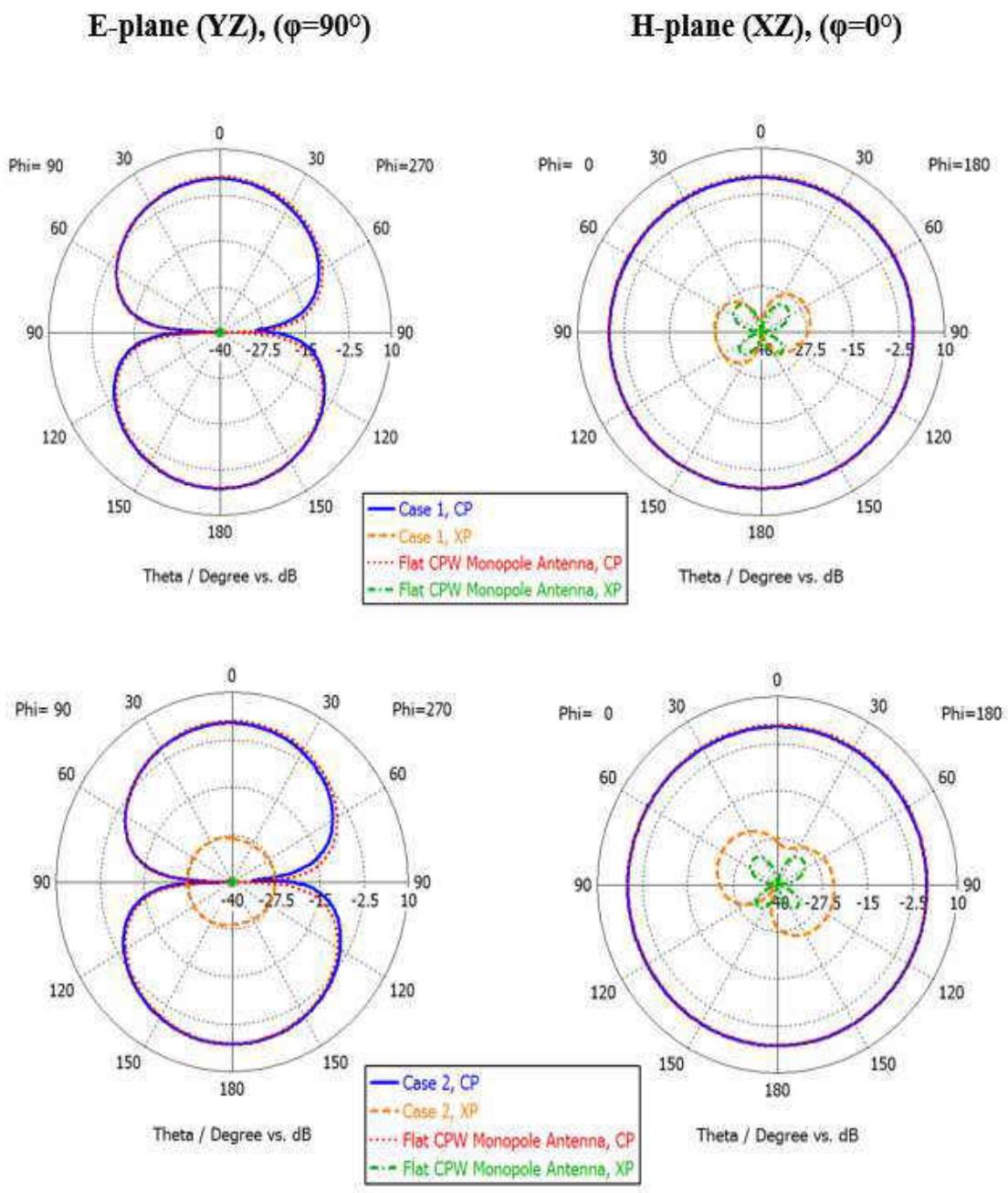

Figure 58: Simulated radiation patterns of monopole antenna crumpled along X-axis for Cases 1 and 2 at 2.45 GHz: (left) E-plane, and (right) H-plane; Co Polarization (CP), and Cross Polarization (XP).

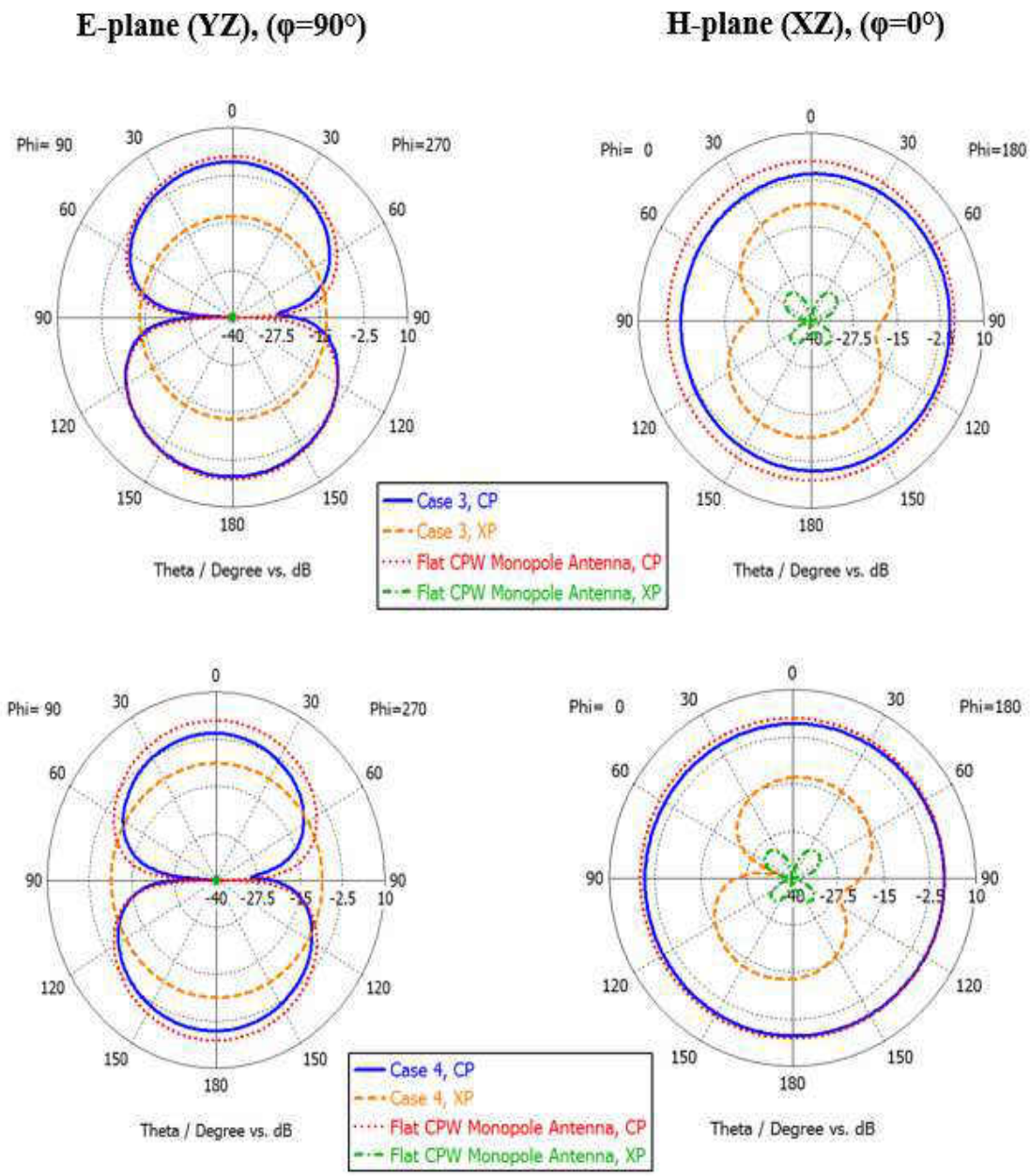

Figure 59: Simulated radiation patterns of monopole antenna crumpled along X-axis for Cases 3 and 4 at 2.45 GHz: (left) E-plane, and (right) H-plane; Co Polarization (CP), and Cross Polarization (XP).

5.3 Performance of AMC Antenna under Crumpling Conditions

Because of the limitations imposed by the simulation program to build a crumpled AMC antenna structure due to the total thickness of the structure and the feeding requirements to keep a distance of the feeding line in a flat form, performance of AMC antenna under crumpling conditions has been studied only in E-plane. The crumpling profile is defined in the same manner as mentioned earlier in this chapter, where *M* is the crumpling periodic length and *N* is the crumpling depth. A parametric study on the effects of change in crumpling profile parameters on the performance of AMC antenna has been carried out.

AMC antenna crumpling is investigated for two series. Series 1 has a three crumpling cases where *M* is 30 mm and *N* is chosen to have 5 mm, 6 mm, and 7 mm values. In Series 2, *M* is chosen to be 31 mm while *N* has the same values as in Series 1. It is worth mentioning that because of the simulation software limitations, we were limited in these crumpling profiles. Dimensions of the AMC antenna in both crumpling series are defined in Table 10. AMC antenna aperture is reduced from 124×124 mm^2 (flat) to a minimum value of 111.60×124 mm^2 obtained when $M = 30$ mm and $N = 7$ mm.

A typical crumpling Case of 31 mm crumpling length and 6 mm crumpling depth for general clothing distortion most likely to appear when the antenna is placed on the chest or the back of the wearer is shown in Figure 60 along with the AMC antenna in flat condition.

Table 10: Dimensions of the crumpled AMC antenna in E-plane.

Series 1: Crumpling Periodic Length (*M*=30 mm)		
Case	Antenna Length (mm)	*N* (mm)
Flat	124.00	-
Crumpling Case 1: 30_5	116.78	5.00
Crumpling Case 2: 30_6	114.25	6.00
Crumpling Case 3: 30_7	111.60	7.00
Series 2: Crumpling Periodic Length (*M*=31 mm)		
Case	Antenna Length (mm)	*N* (mm)
Flat	124.00	-
Crumpling Case 1: 31_5	117.48	5.00
Crumpling Case 2: 31_6	114.97	6.00
Crumpling Case 3: 31_7	111.89	7.00

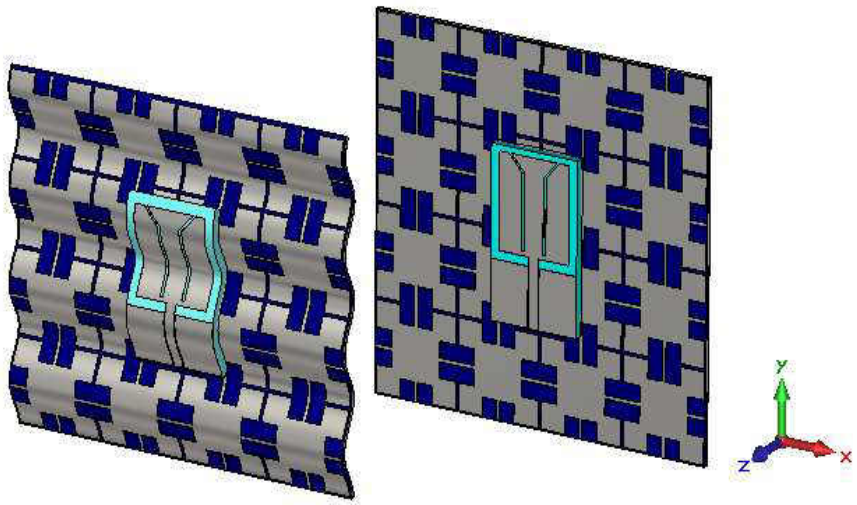

Figure 60: Geometry of crumpled AMC antenna along with the antenna in a flat form.

5.3.1 Input Impedance Matching Results under Crumpling Conditions

Reflection coefficient results are depicted due to crumpling conditions in Series1 and Series 2 in Figure 61 and Figure 62, respectively. The effect of changing *M* value from 30 mm to 31 mm on the input impedance matching characteristics of the AMC antenna can be seen as a shift in the resonance frequency, in a range of MHz, toward higher values. On the other hand, it can be concluded that changing *N* value has less impact on the AMC antenna performance. Crumpling in Series 2 showed a better matching within the frequency range of interest (ISM-2.45 GHz), where the return loss being less than -10 dB, as compared with crumpling in Series 1. The impedance bandwidth has been reduced dramatically under crumpling condition as compared with the AMC antenna in flat form.

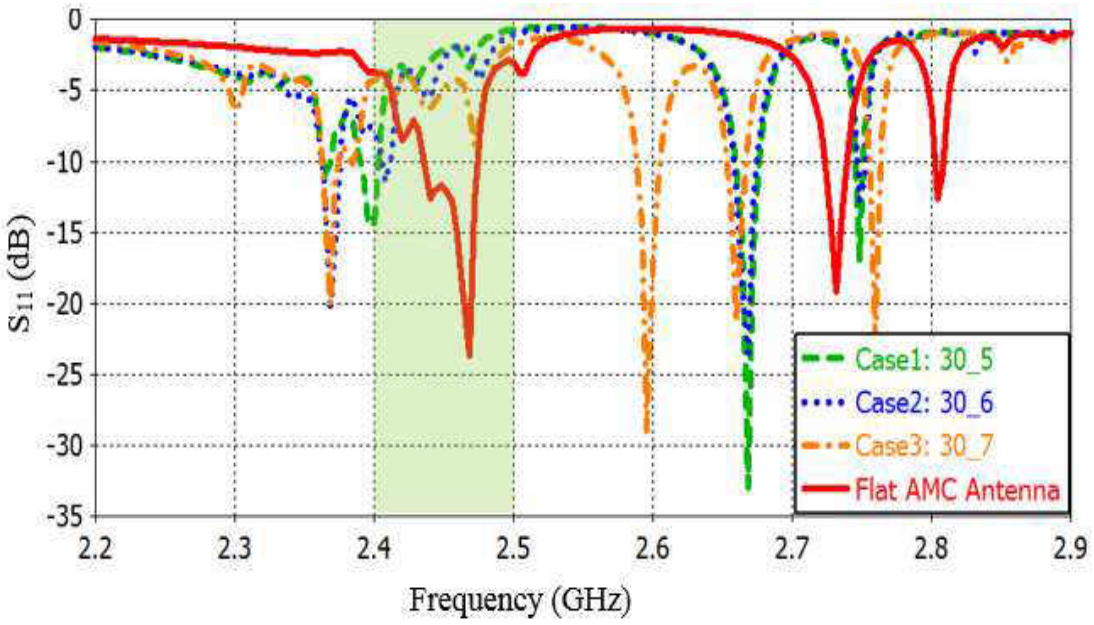

Figure 61: Simulated S_{11} of AMC antenna crumpled in E-plane [Series 1].

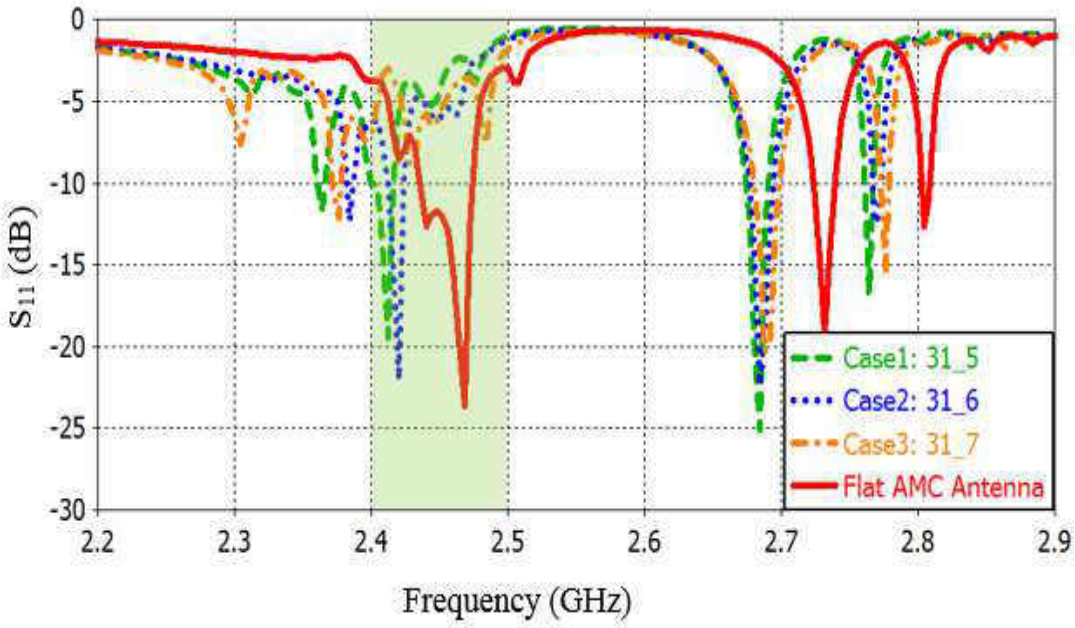

Figure 62: Simulated S_{11} of AMC antenna crumpled in E-plane [Series 2].

5.3.2 Radiation Characteristics Results under Crumpling Conditions

Radiation characteristics in terms of antenna gain, directivity, and total efficiency at the resonance frequency of the AMC antenna and at 2.45 GHz are summarized in Table 11 for both crumpling series. It's worth mentioning that for the cases in which AMC antenna experience a multi-resonance behavior, the resonance that is chosen for investigation is the closest to the operating band of the AMC structure, which is within the ISM-2.45 GHz band.

Radiation characteristics of the AMC antenna at the resonance frequency are comparable with those obtained when the antenna is flat for crumpling Cases 1 and 2 in both series, while a degradation in the antenna performance is noticed due to crumpling conditions in Case 3 at the resonance frequency that is being shifted out of the ISM-band. On the other hand, the most noticeable crumpling effect at 2.45 GHz being a significant

reduction in the antenna gain and efficiency of 6.69 dB and 41%, respectively, in the worst crumpling conditions of Case 2 in Series 1. Crumpling in Case 3 in Series 2, which represents the typical crumpling case that may take place in reality, shows acceptable performance as compared with the flat antenna.

Table 11: Radiation characteristics summary of AMC antenna under crumpling conditions.

Series 1: Crumpling Periodic Length (M=30 mm)							
Case	f_r (GHz)	Gain at f_r (dBi)	Directivity at f_r (dB)	Efficiency at f_r (%)	Gain at 2.45 (dBi)	Directivity at 2.45 (dB)	Efficiency at 2.45 (%)
Flat	2.46	8.55	10.17	70	8.41	9.86	71
Crumpling Case1: 30_5	2.40	7.27	9.43	61	1.72	7.34	30
Crumpling Case 2: 30_6	2.41	7.46	9.60	61	3.50	8.35	33
Crumpling Case 3: 30_7	2.36	2.01	6.07	40	6.23	8.86	55
Series 2: Crumpling Periodic Length (M=31 mm)							
Case	f_r (GHz)	Gain at f_r (dBi)	Directivity at f_r (dB)	Efficiency at f_r (%)	Gain at 2.45 (dBi)	Directivity at 2.45 (dB)	Efficiency at 2.45 (%)
Flat	2.46	8.55	10.17	70	8.41	9.86	71
Crumpling Case1: 31_5	2.41	7.29	9.57	59	3.75	7.49	42
Crumpling Case 2: 31_6	2.41	7.41	9.28	65	6.80	9.15	58
Crumpling Case 3: 31_7	2.70	5.33	6.61	74	5.64	8.16	56

CHAPTER 6

FUTURE WORK AND CONCLUSIONS

6.1 Introduction

This thesis focused on the design and fabrication of a textile wearable antenna integrated with flexible AMC. Design cycle of wearable antennas including material selection, AMC synthesis, integration of AMC with wearable antenna and finally the antenna performance evaluation under bending and crumpling conditions were explained. In this chapter, the significance of the research work of this thesis and conclusions based on the results will be presented. Finally suggestions for future work that can be done in this area will be given.

6.2 Conclusions

The thesis has demonstrated a wearable CPW-fed monopole antenna integrated with AMC ground plane that operates at ISM-2.45 GHz band for wireless communication. AMC structure consists of 4×4 cells, which measures 124×124 mm^2. As the antenna is intended to be integrated with the human body, thus, the absorption of the back radiation by the human body causing a problem. A small AMC structure is proposed and the overall design has relatively low back radiation. FBR was improved from 0.05dB obtained by the conventional antenna to 16.15dB obtained by the AMC antenna.

In addition AMC structure has improved the antenna gain by about 61% to enhance the communication performance. SAR analysis using a three layered rectangular body model shows that AMC ground plane reduces SAR values by factors of up to 50 and 57 for 1 g and 10 g tissues, respectively. Overall, performance of AMC antenna is superior to that of the conventional monopole antenna in terms of gain, FBR and SAR obtained values.

Effects of antenna bending on monopole and AMC antennas characteristics were investigated in two perpendicular planes. Three bending cases were used for investigations that were corresponding to different parts of human body. An improvement in FBR results was noticed due to monopole antenna bending in both E-plane and H-plane to result in a maximum value of 95% when the antenna bent in H-plane. On the other hand, AMC antenna suffers a reduction in FBR due to H-plane bending while remains comparable due E-plane bending with the obtained values, when the AMC antenna is flat.

In general it was found that the more the antenna is bent, no matter which bending plane is chosen, the more reduction in antenna gain will take place. Gain reduction is more notable for H-plane bending conditions to result in a reduction by up to 2.71dB obtained when R=40 mm. Therefore it can be concluded that for on body placement like arm based AMC wearable antenna performs better when its H-plane is aligned along the sleeve length. It is worth mentioning that performance of AMC antenna was unstable due to bending conditions, however it remains better than that obtained using conventional monopole antenna in terms of input impedance matching and radiation characteristics.

Crumpling of CPW-fed monopole antenna was investigated in two perpendicular planes for four cases of crumpling in each plane that corresponding to those that might be

found on clothing distortion. Performance of the antenna under crumpling conditions is very dependent on the plane of the crumple and its severity. Simulation results have demonstrated that H-plane crumpling substantially degrades the reflection coefficient and detunes the antenna so that the resonance peak shifts out of the ISM-2.45 band.

The most severe crumpling conditions chosen for monopole antenna performance evaluation resulted in a reduction in the antenna gain by 72% and 6% due to crumpling in H-plane and E-plane, respectively. Moreover, the total efficiency for the flat antenna was 95%, the efficiency was decreased due to H-plane crumpling by up to 34%, but remained comparable due to E-plane crumpling. Hence, for better results it must be ensured that antenna is not crumpled too much in H-plane.

On the other hand, crumpling conditions showed significant changes on the radiation characteristics of AMC antenna compared to the conventional monopole antenna. A comparison is carried out in Table 12 for monopole and AMC antennas under the same E-plane crumpling conditions defined by 31 mm crumpling periodic length and 6 mm crumpling depth. It can be seen that AMC antenna suffers a reduction in the antenna efficiency of 13% and almost 1 dB in the antenna gain, while the monopole antenna remains robust against crumpling conditions.

Table 12: Performance summary of monopole and AMC antennas.

	Planer CPW monopole antenna	Crumpled CPW monopole antenna	Planer AMC antenna	Crumpled AMC antenna
f_r (GHz)	2.45	2.45	2.46	2.42
Bandwidth	2.57 GHz	3.87 GHz	50.00 MHz	20.00 MHz
S_{11} at f_r (dB)	-15.80	-16.10	-23.50	-21.00
Gain at f_r (dBi)	2.45	2.43	8.55	7.41
Efficiency at f_r (%)	95	93	71	58

6.3 Future Work

The research work introduced in this thesis has investigated wearable antenna design cycle, however there is still an enormous amount of research and development that needs to be performed. CPW-fed monopole antenna design was carried out based on fabrics, however, the AMC structure was deigned based on a flexible material, which caused a lot of limitations on the flexibility of the proposed AMC antenna. Therefore, there is still need for a study on material selection of the proposed AMC antenna in order to achieve a higher degree of flexibility to further facilitate antenna's integration into clothing. Also, AMC structure based on fabric material instead of flexible one is of interest to extend the investigation of AMC antenna performance under wet and stretching conditions.

Bending and crumpling conditions have been investigated based on simulation results, however measurements of antenna performance based on a real experiment set up considering the surrounding environment can be carried out as a future research idea. Moreover, the interaction between the proposed AMC wearable antenna and human body can be never avoided as it will be placed in very close proximity to the body and therefore,

it requires further investigations. On body measurements are of interest and they are potentially important in order to further validate the antenna design for wearable antenna application.

REFERENCES

[1] S. Sankaralingam and B. Gupta, "Determination of dielectric constant of fabric materials and their use as substrates for design and development of antennas for wearable applications," *IEEE Trans. Instrum. Meas.,* vol. 59, no. 12, pp. 3122-3130, Dec. 2010.

[2] Y. Ouyang, E. Karayianni, and W. J. Chappell, "Effect of fabric patterns on electrotextile patch antennas," in *Proc. IEEE AP-S Int. Symp.*, Washington DC, Jul. 2005, vol. 2B, pp. 246-249.

[3] P. Salonen, Y. Rahmat-Samii, H. Hurme, and M. Kivikoski, "Effect of conductive material on wearable antenna performance: a case study of WLAN antennas," in *Proc. IEEE AP-S Int. Symp.*, 2004, pp. 455-458.

[4] S. Velan, E. Sundarsingh, M. Kanagasabai, A. Sharma, C. Raviteja, and R. Sivasamy, "Dual-band EBG integrated monopole antenna deploying fractal geometry for wearable applications," *IEEE Antennas Wireless Propag. Lett.,* vol. 14, pp. 249-252, 2015.

[5] H. R. Raad, A. I. Abbosh, H. M. Al-Rizzo, and D. G. Rucker, "Flexible and compact AMC based antenna for telemedicine applications," *IEEE Trans. Antennas Propag.,* vol. 61, no. 2, pp. 524-531, Feb. 2013.

[6] P. Salonen, F. Yang, Y. Rahmat-Samii, and M. Kivikoski, "WEBGA-wearable electromagnetic band-gap antenna," in *Pro. IEEE AP-S Int. Symp.*, Monterey, CA, Jun. 2004, pp. 451-454.

[7] S. Kim, Y.-J. Ren, H. Lee, A. Rida, S. Nikolaou, and M. M. Tentzeris, "Monopole antenna with inkjet-printed EBG array on paper substrate for wearable applications," *IEEE Antennas Wireless Propag. Lett.,* vol. 11, pp. 663-666, 2012.

[8] S. Zhu and L. Liu, "Dual band body worn antenna," in *Antennas and Propagation Conference*, Loughborough, 2007, pp. 137-140.

[9] D. Sievenpiper, L. Zhang, R. F. Broas, N. G. Alexopolous, and E. Yablonovitch, "High-impedance electromagnetic surfaces with a forbidden frequency band," *IEEE Trans. Microwave Theory Tech.,* vol. 47, pp. 2059-2074, Nov. 1999.

[10] F. Yang and Y. Rahmat-Samii, *Electromagnetic band gap structures in antenna engineering*: ser. Cambridge RF Microw. Eng. Cambridge, U.K.: Cambridge Univ. Press New York, 2009.

[11] F. Yang and Y. Rahmat-Samii, "Reflection phase characterizations of the EBG ground plane for low profile wire antenna applications," *IEEE Trans. Antennas Propag.,* vol. 51, no. 10, pp. 2691-2703, Oct. 2003.

[12] H. Nakano, S. Okuzawa, K. Ohishi, H. Mimaki, and J. Yamauchi, "A curl antenna," *IEEE Trans. Antennas Propag.,* vol. 41, pp. 1570-1575, Nov. 1993.

[13] F. Yang and Y. Rahmat-Samii, "A low-profile circularly polarized curl antenna over an electromagnetic bandgap (EBG) surface," *Microwave Opt. Technol. Lett.,* vol. 31, no. 3, pp. 165-168, 2001.
[14] R. E. Collin, *Field theory of guided waves*. 2nd ed. New York: IEEE Press, 1991.
[15] R. Waterhouse, *Microstrip Patch Antennas: A Designer's Guide: A Designer's Guide*. Norwell, MA: Kluwer, Jan. 2003.
[16] M. T. Islam and M. S. Alam, "Compact EBG structure for alleviating mutual coupling between patch antenna array elements," *Progress In Electromagnetics Research,* vol. 137, pp. 425-438, 2013.
[17] Q. Li, A. Feresidis, M. Mavridou, and P. Hall, "Miniaturized double-layer EBG structures for broadband mutual coupling reduction between UWB monopoles," *IEEE Trans. Antennas Propag.,* vol. 63, no. 3, pp. 1168-1171, Mar. 2015.
[18] R. Coccioli, F.-R. Yang, K.-P. Ma, and T. Itoh, "Aperture-coupled patch antenna on UC-PBG substrate," *IEEE Trans. Microwave Theory Tech.,* vol. 47, pp. 2123-2130, Nov. 1999.
[19] F. Yang, A. Aminian, and Y. Rahmat-Samii, "A novel surface-wave antenna design using a thin periodically loaded ground plane," *Microw. Opt. Technol. Lett.,* vol. 47, pp. 240-245, Nov. 2005.
[20] G. Goussetis, A. P. Feresidis, and J. C. Vardaxoglou, "Tailoring the AMC and EBG characteristics of periodic metallic arrays printed on grounded dielectric substrate," *IEEE Trans. Antennas Propag.,* vol. 54, no. 1, pp. 82-89, 2006.
[21] R. Kshetrimayum and L. Zhu, "EBG design using FSS elements in rectangular waveguide," *ACES Journal,* vol. 21, pp. 149-154, 2006.
[22] E. Özbay, A. Abeyta, G. Tuttle, M. Tringides, R. Biswas, C. Chan*, et al.*, "Measurement of a three-dimensional photonic band gap in a crystal structure made of dielectric rods," *Phys. Rev. B, Condens. Matter,* vol. 50, pp. 1945-1951, 1994.
[23] C. Soukoulis, "The history and a review of the modelling and fabrication of photonic crystals," *Nanotechnology,* vol. 13, pp. 420-423, 2002.
[24] V. Radisic, Y. Qian, R. Coccioli, and T. Itoh, "Novel 2-D photonic bandgap structure for microstrip lines," *IEEE Microwave Guide Wave Lett.,* vol. 8, pp. 69-71, Feb. 1998.
[25] A. Aminian, F. Yang, and Y. Rahmat-Samii, "Bandwidth determination for soft and hard ground planes by spectral FDTD: a unified approach in visible and surface wave regions," *IEEE Antennas Wireless Propag.,* vol. 53, no. 1, pp. 18-28, Jan. 2005.
[26] T. Mandal and S. Das, "Design of a microstrip fed printed monopole antenna for bluetooth and UWB applications with WLAN notch band characteristics," *International Journal of RF and Microwave Computer-Aided Engineering,* vol. 25, pp. 66-74, 2015. [Online]. Avaliable: John Wiley & Sons. [Accessed: January, 2015].
[27] R. Singh, G. K. Pandey, M. Agarwal, H. S. Singh, P. K. Bharti, and M. K. Meshram, "Compact planar monopole antenna with dual band notched characteristics using T-shaped stub and rectangular mushroom type electromagnetic band gap structure for UWB and bluetooth applications," *Wireless Pers Commun,* vol. 78, pp. 215-230, Apr, 2014. [Online]. Avaliable: Springer Science+Business Media. [Accessed: January, 2015].

[28] L. Peng and C.-L. Ruan, "UWB band-notched monopole antenna design using electromagnetic-bandgap structures," *IEEE Trans. Microwave Theory Tech.,* vol. 59, no. 4, pp. 1074-1081, 2011.

[29] N. M. Mohamed-Hicho, E. Antonino-Daviu, M. Cabedo-Fabres, and M. Ferrando-Bataller, "A novel low profile high-gain UHF antenna using high-impedance surfaces," in *8th European Conference on Antennas and Propagation (EuCAP2014)*, Apr. 2014, pp. 919-922.

[30] D. Elsheakh, H. Elsadek, E. Abdallah, H. Elhenawy, and M. Iskander, "Enhancement of microstrip monopole antenna bandwidth by using EBG structures," *IEEE Antennas Wireless Propag. Lett.,* vol. 8, pp. 959-962, 2009.

[31] F. Yang, C.-S. Kee, and Y. Rahmat-Samii, "Step-like structure and EBG structure to improve the performance of patch antennas on high dielectric substrate," in *Proc. IEEE AP-S Dig.*, July 2001, pp. 482-485.

[32] S. D. Assimonis, T. V. Yioultsis, and C. S. Antonopoulos, "Design and optimization of uniplanar EBG structures for low profile antenna applications and mutual coupling reduction," *IEEE Trans. Antennas Propag.,* vol. 60, no. 10, pp. 4944-4949, Oct. 2012.

[33] A. M. Soliman, D. M. Elsheakh, E. A. Abdallah, and H. El-Hennawy, "Design of planar inverted-F antenna over uniplanar EBG structure for laptop mimo applications," *Microwave and Optical Technology Letters,* vol. 57, no. 2, pp. 277-285, Feb. 2015. [Online]. Avaliable: John Wiley & Sons. [Accessed: January, 2015].

[34] R. Gonzalo, P. De Maagt, and M. Sorolla, "Enhanced patch-antenna performance by suppressing surface waves using photonic-bandgap substrates," *IEEE Trans. Microwave Theory Tech.,* vol. 47, no. 11, pp. 2131-2138, Nov. 1999.

[35] R. Coccioli and T. Itoh, "Design of photonic band-gap substrates for surface waves suppression," in *Proc. IEEE MTT-S 1998 Symp.*, 1998, pp. 1259-1262.

[36] M. Fallah-Rad and L. Shafai, "Enhanced performance of a microstrip patch antenna using a high impedance EBG structure," in *Proc. IEEE AP-S Int. Symp.*, Jun. 2003, pp. 982-985.

[37] C. Chiau, X. Chen, and C. Parini, "A microstrip patch antenna on the embedded multi-period EBG structure," in *Proc. 6th Int. Symp. Antennas, Propag., EM Theory*, Oct.-Nov. 2003, pp. 96-99.

[38] G. Guida, A. De Lustrac, and A. C. Priou, "An introduction to photonic band gap (PBG) materials," *Progress In Electromagnetics Research,* vol. 41, pp. 1-20, 2003.

[39] N. Engheta and R. W. Ziolkowski, *Metamaterials: physics and engineering explorations*. Hoboken, NJ: Wiley-IEEE Press, 2006.

[40] M. Qiu and S. He, "High-directivity patch antenna with both photonic bandgap substrate and photonic bandgap cover," *Microw. Opt. Technol. Lett.,* vol. 30, no. 1, pp. 41-44, July 2001.

[41] M. A. R. Osman, M. K. Abd Rahim, M. Azfar Abdullah, N. A. Samsuri, F. Zubir, and K. Kamardin, "Design, implementation and performance of ultra-wideband textile antenna," *Progress In Electromagnetics Research B,* vol. 27, pp. 307-325, 2011.

[42] L. Josefsson and P. Persson, *Conformal array antenna theory and design*. Hoboken, NJ: Wiley-IEEE Press, 2006.

[43] S. Bashir, "Design and synthesis of non uniform high impedance surface based wearable antennas," Ph.D. thesis, Loughborough University, 2009.
[44] A. Tsolis, W. G. Whittow, A. A. Alexandridis, and J. Y. C. Vardaxoglou, "Embroidery and Related Manufacturing Techniques for Wearable Antennas: Challenges and Opportunities," *Electronics,* vol. 3, pp. 314-338, 2014.
[45] N. Rais, P. J. Soh, F. Malek, S. Ahmad, N. Hashim, and P. Hall, "A review of wearable antenna," in *Proc. LAPC*, Loughborough, U.K., 2009, pp. 225-228.
[46] P. Salonen, L. Sydanheimo, M. Keskilammi, and M. Kivikoski, "A small planar inverted-F antenna for wearable applications," in *3rd Int. Symp. on Wearable Computers Digest*, 1999, pp. 95-100.
[47] P. Salonen and J. Rantanen, "A dual-band and wide-band antenna on flexible substrate for smart clothing," in *IEEE Ind. Electr. Soc. Conf.*, 2001, pp. 125-130.
[48] M. Tanaka, "Wearable microstrip antenna for satellite communications," *IEICE Trans. Communications,* vol. 87, no. 8, pp. 2066-2071, Aug. 2006.
[49] N. Noury, P. Barralon, and D. Flammarion, "Preliminary results on the study of smart wearable antennas," in *Proc. 2005 IEEE Eng. Med. Biol. 27th Annu. Int. Conf.*, 2005, pp. 3814-3817.
[50] J.-Y. Park and J.-M. Woo, "Miniaturization of microstrip line monopole antenna for the wearable applications," in *Proc. Asia-Pacific Microwave Conf.*, 2008, pp. 1-4.
[51] H. Nurul, F. Malek, P. Soh, G. Vandenbosch, V. Volski, S. Ooi*, et al.*, "Evaluation of a wearable hybrid textile antenna," in *Loughborough Antennas and Propagation Conference (LAPC)*, 2010, pp. 337-340.
[52] P. Salonen, Y. Rahmat-Samii, M. Schaffrath, and M. Kivikoski, "Effect of textile materials on wearable antenna performance: a case study of GPS antennas," in *Proc. IEEE Antennas Propag. Soc. Int. Symp.*, 2004, pp. 459-462.
[53] S. Sankaralingam and B. Gupta, "Development of textile antennas for body wearable applications and investigations on their performance under bent conditions," *Progress In Electromagnetics Research B,* vol. 22, pp. 53-71, 2010.
[54] S. Sankaralingam and B. Gupta, "Effects of bending on impedance and radiation characteristics of rectangular wearable antenna utilizing smart clothes," *Microw. Opt. Technol. Lett.,* vol. 54, no. 6, pp. 1508-1511, 2012.
[55] K. Koski, E. Koski, T. Bjorninen, A. A. Babar, L. Ukkonen, L. Sydanheimo*, et al.*, "Practical read range evaluation of wearable embroidered UHF RFID tag," in *Proc. IEEE AP-S Int. Symp.* , July 2012, pp. 1-2.
[56] S. J. Boyes, P. J. Soh, Y. Huang, G. A. Vandenbosch, and N. Khiabani, "Measurement and performance of textile antenna efficiency on a human body in a reverberation chamber," *IEEE Trans. Antennas Propag.,* vol. 61, no. 2, pp. 871-881, Feb. 2013.
[57] D. Psychoudakis, G.-Y. Lee, C.-C. Chen, and J. L. Volakis, "Military UHF body-worn antennas for armored vests," in *Proceedings of the Fourth European Conference on Antennas and Propagation (EuCAP)*, Barcelona, Spain, Apr. 2010, pp. 1-4.

[58] D. L. Paul, H. Giddens, M. G. Paterson, G. S. Hilton, and J. P. McGeehan, "Impact of body and clothing on a wearable textile dual band antenna at digital television and wireless communications bands," *IEEE Trans. Antennas Propag.,* vol. 61, no. 4, pp. 2188-2194, 2013.

[59] P. Salonen and L. Hurme, "A novel fabric WLAN antenna for wearable applications," in *Proc. IEEE AP-S Int. Symp*, 2003, pp. 700-703.

[60] C. Hertleer, H. Rogier, L. Vallozzi, and F. Declercq, "A textile antenna based on high-performance fabrics," in *Proc. Eur. Conf. Antennas Propag.*, Edinburgh, U.K., Nov. 2007, pp. 11-6.

[61] C. Hertleer, H. Rogier, and L. Van Langenhove, "A textile antenna for protective clothing," in *Proc. IET Seminar on Antennas and Propag. Body-Centric Wireless Commun.*, Apr. 2007, pp. 44-46.

[62] Z. N. Chen, *Antennas for portable devices*. Hoboken, NJ: John Wiley & Sons, 2007. [Online]. Avilable: 10: 0470030739.

[63] W. Scanlon, G. Conway, and S. Cotton, "Antennas and propagation considerations for robust wireless communications in medical body area networks," in *IET Seminar on Antennas and Propagation for Body-Centric Wireless Communications*, 2007, p. 37.

[64] E. C. Fear, S. C. Hagness, P. M. Meaney, M. Okoniewski, and M. A. Stuchly, "Enhancing breast tumor detection with near-field imaging," *IEEE Microwave Mag.,* vol. 3, no. 1, pp. 48-56, Mar. 2002.

[65] T. F. Kennedy, P. W. Fink, A. W. Chu, N. J. Champagne, G. Y. Lin, and M. A. Khayat, "Body-worn E-textile antennas: the good, the low-mass, and the conformal," *IEEE Trans. Antennas Propag.,* vol. 57, no. 4, pp. 910-918, Apr. 2009.

[66] T. Peter and R. Nilavalan, "Study on the performance deterioration of flexible UWB antennas," in *Antennas and Propagation Conference Loughborough (LAPC'09)*, Loughborough, Nov. 2009, pp. 669-672.

[67] M. Klemm and G. Troester, "Textile UWB antennas for wireless body area networks," *IEEE Trans. Antennas Propag.,* vol. 54, no. 11, pp. 3192-3197, Nov. 2006.

[68] M. A. R. Osman, M. K. Abd Rahim, N. A. Samsuri, H. A. M. Salim, and M. F. Ali, "Embroidered fully textile wearable antenna for medical monitoring applications," *Progress In Electromagnetics Research,* vol. 117, pp. 321-337, 2011.

[69] M. Koohestani, N. Pires, A. K. Skrivervik, and A. A. Moreira, "Bandwidth enhancement of a wearable UWB antenna near a human arm," *Microw. Opt. Technol. Lett.,* vol. 55, no. 12, pp. 2965-2967, 2013.

[70] M. Klemm, I. Locher, and G. Troster, "A novel circularly polarized textile antenna for wearable applications," in *Proc. 34th Eur. Microw.Week*, Oct. 2004, pp. 137-140.

[71] J. Carter, J. Saberin, T. Shah, P. Sai Ananthanarayanan, and C. Furse, "Inexpensive fabric antenna for off-body wireless sensor communication," in *Proc. IEEE AP-S Int. Symp.*, July 2010, pp. 1-4.

[72] I. Locher, M. Klemm, T. Kirstein, and G. Troster, "Design and characterization of purely textile patch antennas," *IEEE Trans. Adv. Packaging,* vol. 29, no. 4, pp. 777-788, Nov. 2006.

[73] P. Salonen, M. Keskilammi, and L. Sydanheimo, "A low-cost 2.45 GHz photonic band-gap patch antenna for wearable systems," in *IEEE 11th Int. Conf. Antennas Propag. (ICAP'01)*, Manchester, U.K., 2001, pp. 719-723.

[74] S. Velan, E. Sundarsingh, M. Kanagasabai, A. Sharma, C. Raviteja, and R. Sivasamy, "Dual-band EBG integrated monopole antenna deploying fractal geometry for wearable applications," *IEEE Antennas Wireless Propag. Lett.,* vol. 14, pp. 249-252, Feb. 2014.

[75] S. Zhu and R. Langley, "Dual-band wearable textile antenna on an EBG substrate," *IEEE Trans. Antennas Propag.,* vol. 57, no. 4, pp. 926-935, 2009.

[76] Z. Duan, D. Linton, W. Scanlon, and G. Conway, "Using EBG to improve antenna efficiency in proximity to the human body," *Proc. Wideband, Multiband Antennas and Arrays for Defense or Civil Applications IET Seminar,* pp. 173-180, 2008.

[77] C. A. Balanis, *Antenna Theory, Analysis and Design*. New Jersey: John Wiley & Sons, 2012.

[78] M. Mantash, A.-C. Tarot, S. Collardey, and K. Mahdjoubi, "Investigation of flexible textile antennas and AMC reflectors," *International Journal of Antennas and Propagation,* vol. 2012, 2012, article ID 236505, 10 pages http://dx.doi.org/10.1155/2012/236505.

[79] *CST Microwave Studio,* visited December 2013.

[80] J. R. Sohn, H. S. Tae, J.-G. Lee, and J.-H. Lee, "Comparative analysis of four types of high-impedance surfaces for low profile antenna applications," in *Proc. IEEE AP-S Int. Symp. (Digest) Antennas Propag. Society*, 2005, pp. 758-761.

[81] M. Klemm and G. Troester, "EM energy absorption in the human body tissues due to UWB antennas," *Progress in Electromagn. Res.,* vol. 62, pp. 261-280, 2006.

[82] J. Gemio, J. Parron, and J. Soler, "Human body effects on implantable antennas for ISM bands applications: Models comparison and propagation losses study," *Progress In Electromagnetics Research,* vol. 110, pp. 437-452, 2010.